POLITECNICO DI TORINO

Master's Degree in Biomedical Engineering

Development and characterization of an Electrolytic-Gated Organic Field-Effect Transistor for biosensing applications

Candidate: Elena Camilli 263755

Supervisor: Dr. Francesca Frascella

Co-supervisor: Dr. Simone Marasso

Academic Year: 2020-2021

Abstract

Over the past decades Electrolyte-Gated Organic Field-Effect Transistors (EGOFETs) have gained attention for fast and disposable sensors development, thanks to their many avantages as low-voltage operation, high sensitivity, and easy and low cost fabrication.

This thesis is focused on the testing and electrical characterization of a sensor for biological molecules detection, based on an EGOFET device. The purpose of the work is to investigate thoroughly the operation of the transistor, testing it in several conditions in order to evaluate its performance and prospect of use.

The measurement setup includes a probe station and a microfluidic system, which allows a continuous flow of aqueous solution inside the EGOFET chamber. In this configuration, the target solution flows in the system and reaches the surface previously functionalized, that may be either the gate electrode or the polymer surface. Being the EGOFET highly sensitive to surface changes, the binding between the target and the recognition element results in a current signal change. Moreover, the setup allows real time current measurements at a fixed voltage operating point during the entire period of the protocol. This is a distinctive choice compared to the most common type of test , in which usually the characterizations of the device are compared only before and after exposure to the target.

The sensor has proved to be versatile, responding to several different molecules. Depending on the target, different kinds of surface functionalization have been performed and tested. The reference targets object of this thesis were Angiopoietin-2 and Tetracycline antibiotic.

In EGOFET fabrication one of the most crucial element is the organic material. In this project it was used and investigated the poly(3-carboxypenthylthiophene) (P3CPT), a derivative of poly(3-hexylthiophene) (P3HT). Despite the latter is widely used and studied in literature, P3CPT has the advantage to expose carboxyl groups in the lateral chains, which allows a direct functionalization of the material.

Currently, the obtained results have shown that it has not yet been possible to obtain a specific sensing by a direct functionalization of the polymer. Instead, the most promising result has been achieved with the gold gate functionalized with Anti-Angiopoietin-2 antibodies or with aptamers designed for Tetracycline, and bare P3CPenT. Having obtained the specific sensing with the gate functionalization and not with the polymer functionalization, could mean that in this configuration the gate capacitance dominates over the polymer one.

Table of Contents

Chapter 1

Introduction

The core element of this work is an electrochemical biosensor based on an Electrolyte Gated Organic Field Effect Transistor (EGOFET), with the aim of detection of biological molecules. In particular EGO FET-based sensors have the intent to be part of a new frontier of sensing devices, in the contest of point-of-care (POC) applications. In fact, the high performance and low cost fabrication processes that characterize EGOFETs, make them promising for the development of an affordable and portable sensor, for the detection of diseases biomarkers at low concentration, also with a single-use purpose.

1.1 Biosensors

According to the IUPAC (International Union of Pure and Applied Chemistry), a biosensor can be defined "as a device that uses specific biochemical reactions mediated by isolated enzymes, immunosystems, tissues, organelles, or whole cells to detect chemical compounds usually by electrical, thermal, or optical signals" [1]. Thus, a biosensor is an integrated receptor-transducer device capable of providing selective quantitative or semi-quantitative analytical information using a biological recognition element [2]. The operation of a biosensor relies on the coupling between an active biological system and a transducer, that converts the chemical signal in a physical one.

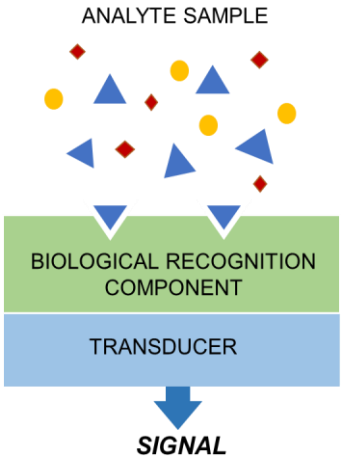

Figure 1 – Block diagram of biosensor principal components

A common classification is based on the biological recognition component, rather than on the analyte, because on it relies the specificity and the sensibility of the sensor. Here some existing typologies of biosensors are listed.

- *Enzymatic Biosensors* are the first developed biosensors, and widely spread in the market. The biological components are enzymes, proteins that act as biological catalysts. Considering that enzymes are characterized by an extreme biological specificity with the substrate, these sensors are highly specific, and with a sensibility to low target concentration. [3]
- *Immunosensors*: the biological elements are antibodies that interact with the corresponding antigens through a non-covalent but specific and strong binding. Accordingly, the sensor has high specificity between the recognition element and analyte. [4]
- *Biosensors based on nucleic acids*: these sensors owe their selectivity and specificity to the strong pair-base affinity between complementary strands. This typology of biosensors may rely on the use of DNA or RNA strands as biological recognition elements. They may also exploit aptamers, which are artificial and short single stranded DNA or RNA sequences, used to bind a variety of targets, including drugs. [5]
- *Biosensors based on cells or tissue:* they rely on the detection of physiological signals caused by the metabolic activity of the living cells (both entire cell and cellular component) or tissue. [6]

Another possible way to categorize biosensors is based on the transducer element, namely the unit that provides the measurable output signal, in response to the input quantity [1]. The main categories of biosensors, referring to the nature of the transduction mechanism, are [6]:

1. *Electrochemical biosensors,* that rely on the operation on the chemical reaction between the bio-recognition element and the analyte, that produces a change in the electrical properties of the solution within the device. Sensors included in this category are: amperometric, potentiometric, conductometric and ion sensitive field effect transistors (ISFETs) [2].
2. *Optical biosensors* measure the adsorption, the emission, and the scattering of the light, that is the transduced signal. Often these sensors are fluorescence-based.
3. *Piezoelectric biosensors* are based on quartz crystals which vibrational frequency is mass-sensitive.
4. *Calorimetric biosensors* incorporate a temperature sensor that measures the heat of the analyte-receptor reaction.

Biosensors can be promising and useful tools in different fields of application, like biomedical and healthcare [7], environment [8], or food industry [9]. The main characteristics of a biosensor are [10]:

- Specificity: capability of detecting and measuring only the biochemical species of interest.
- Sensitivity: the capability to discriminate small differences in analyte concentration. Two parameters connected with this concept are: the limit of detection (LOD), the minimum concentration of the analyte that the sensor is able to detect, and the limit of quantification (LOQ), the lowest concentration of the analyte that can be quantified with a certain precision [10].
- Reproducibility: the ability to produce the same results in the repeated use when the sensor is employed in the same conditions.
- Stability: it represents the susceptibility of the sensor to ambient disturbances that may affect the accuracy of the results.

The interest of this work is a smart and disposable sensor to be employed in clinical analysis, ideally for point-of-care (POC) application, with the intent to allow an

immediate and practical clinical test for patients [11]. From this perspective, an ideal biosensor should be characterized by: high selectivity and stability, short response time, low limit of detection, ease of use, low cost, and scalability.

In this regard electrochemical sensors based on low cost technologies represent a valid option to implement an everyday life device. Moreover, electrochemical sensors are attractive means thanks to the direct conversion of the detection of the target into an electronic signal. Sensors based on electrochemical transduction have been implemented through different techniques, including various field-effect transistor-based methods [12]. In particular Organic field-effect transistors (OFETs) may represent good candidates as smart and disposable sensors, thanks to the high sensitivity, low costs, and portability.

1.2 From Inorganic to Organic FETs

Field-effect transistors (FET) are three terminal devices based on semiconductive materials. Transistors are key electronic components, used in a multitude of different applications, from signal amplification to logical gates and memories [13].

A MOSFET is composed of three electrodes, *source* (S), *drain* (D) and *gate* (G) on a substrate of a semiconductor material, usually silicon. The gate electrode is insulated from the semiconductor by a thin layer of silicon dioxide (typically 1-10 nm). The working principle relies on the modulation of the current flowing between source and drain by applying a voltage to the gate electrode. In recent years, FETs have been intensively studied for biosensing applications, thanks to their already well established miniaturization and integration into portable electronic devices, and due to their high sensitivity to changes in surface potential [14]. The metal-oxide-semiconductor FET (MOSFET) is the most widespread architecture in both digital and analog electronics .

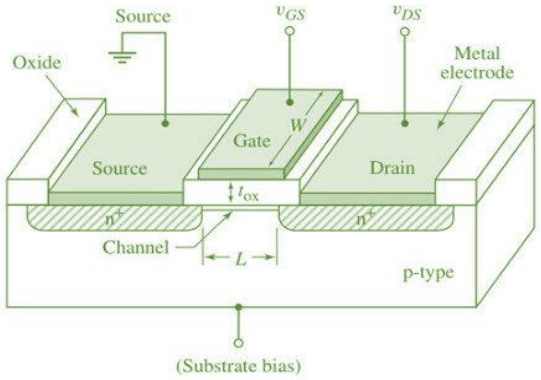

Figure 2 – A metal-oxide-semiconductor (MOSFET) schematic representation

The main drawback of silicon-based transistors are the expensive fabrication and miniaturization processes that make them unsuitable for disposable sensors. To overcome this limitation, during the last decades different configurations of transistors devices have been developed, including organic thin film transistors (OTFTs), characterised by an organic semiconducting material as the active layer of the transistor, instead of the inorganic silicon. In particular the OTFTs that rely on the operation on the field-effect are defined as organic field-effect transistors (OFETs). Different configurations of OFET exist depending on how the semiconductor and the three electrodes are reciprocally placed, as represented in Figure 3.

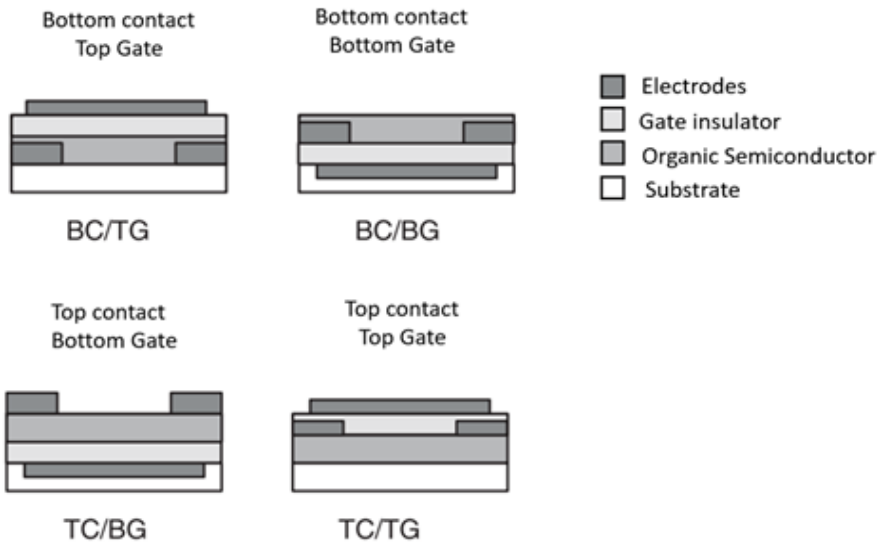

Figure 3 - Different configuration for OFETs. Adapted from [39]

The transition from inorganic to organic electronics in biosensing application has been driven by the possibility to lower the production costs. This feature is possible thanks the use of organic polymers as semiconductive material, that are often solution processable, and thus suitable for a large number of low-cost fabrication processes, such as printing techniques and a variety of deposition methods [15]. These methods employ not expensive machines that can support large-scale production.

Moreover, the low-temperature processes allow to employ a variety of different substrates, also temperature-sensible, cheap, and recyclable, meaning a slighter impact on the environment with respect to silicon based transistors. Furthermore, these substrates may be mechanically flexible, intriguing features for different applications in wearable and light biosensors. Another advantage in OFET is the possibility to choose biocompatible organic materials, that make possible the direct contact of the biological compounds with the elements of the sensor. Anyhow, referring to the performances OFETs cannot compete with MOSFET, in terms of stability, carrier mobility, switching frequency and miniaturization.

One of the main constraints of a biological detection is that the device is often required to work with low operating voltages and in an aqueous environment, which is not possible to achieve with standard OFETs. For these reasons, a particular configuration of OFETs was developed, in which the dielectric material is substituted with an electrolyte, that can be either liquid or solid. This configuration is called Electrolyte-Gated Organic Field Effect Transistor (EGOFET). The novelty of this type of device is that the presence of the electrolyte increases dramatically the capacitance at the semiconductor interface, allowing a consequent reduction of the operating voltage below 1V. The EGOFET architecture, depicted in Figure 4, comprises the source and drain electrodes isolated from the electrolyte by the organic semiconductor layer. The electrolyte is placed on the semiconductor, and the gate is immersed in it.

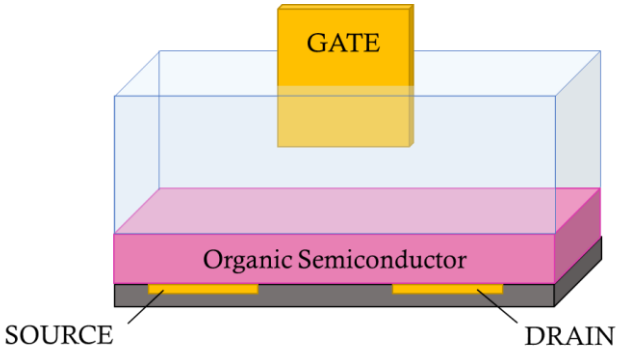

Figure 4 – Schematic representation of Electrolyte-Gated Organic Field Effect Transistor in bottom contact/top gate configuration

The possibility to work in aqueous media and the extremely high sensitivity, make EGOFETs ideal candidates for a new generation of biosensors.

1.3 Purpose and outline of this work

This thesis project has been carried out between the Nanoscience Laboratory and the *Chilab*, of the DISAT department of Politecnico di Torino.

The work is focused on the testing of an EGO FET-based sensor, previously developed in precedent studies. The principal object of this thesis is to test the sensor, by means of several electrical characterisation of the transistor and real-time current measurements. The purpose is to better understand the performance of the device, evaluate the sensitivity, deepen the stability issue that characterizes this type of sensor, with the intention to understand its potentialities and enhance a future optimization.

In particular, here the main configurations in which the EGOFET-based device has been tested are listed:

- Two different organic semiconductor polymers have been used: poly(3-hexylthiophene) (P3HT) and a derivative, poly[3-(5-carboxypentyl) thiophene-2,5-diyl] (P3CPenT). The latter has been investigated more specifically.
- Surface functionalization with bioreceptors has been performed and tested both on gold gate electrode and polymer.

- Different designs of interdigitated source and drain electrodes of the transistor, and two different gate electrodes (gold and Ag/AgCl).

Moreover, the trials comprised multiple target species, mainly a protein, Angiopoietin-2, at different concentrations, and antibiotics (Oxytetracycline Hydrochloride, Sulfadimethoxine). The choice of these targets was driven by the two main projects within this work . In particular the protein detection is linked with the *DEFLeCT* project (Digital tEchnology For Lung Cancer Treatment), with the aim of developing a biosensor for early diagnosis and treatment of lung cancer, through the detection of tumor biomarkers. The antibiotic detection instead concerns a *Food Drug Free* project, with the aim of the detection of antibiotic traces in food samples.

After an introduction to the contest in which the EGOFET technology is inserted (Chapter 1), the theoretical background will be deepened (Chapter 2), facing the different physical and chemical phenomena on which functioning of EGOFET relies. Thus an overview of the operation of conventional MOSFETs is presented, followed by a description of how organic transistors differ from inorganic ones. Then are depicted the characteristics of the electric-double layer formation and features, with a focus on the sensing mechanism of the device. Finally the organic semiconductor polymers are discussed. In the Chapter 3 are shown both the sensor and the sensing set-up, with a detailed description of each element, including the fabrication of the components and the bio-functionalization procedure. Moreover, the different electrical characterization and test protocols are described. Finally in Chapter 4, the most relevant obtained results are illustrated and discussed.

Chapter 2

Theoretical Background

In recent years Electrolyte-gated organic field-effect transistors (EGOFETs) have been investigated with much attention thanks to the low voltage operation, compared with classical OFETs [14]. As anticipated previously, the main structural difference from OFETs is that in EGOFETs the gate is separated from the semiconductor by an electrolyte, that may be solid or liquid. The device used in this work is characterised by an aqueous liquid electrolyte, in which the gate is immersed. Considering a p-channel EGOFET, the imposition of a negative voltage to the gate electrode (V_{GS}) implies a redistribution of the ions within the liquid electrolyte: the cations are attracted to the gate/electrolyte interface, while the anions migrate and accumulate on the semiconductor/electrolyte one, generating on both interfaces an electrical double layer (EDL). The accumulation of negative charges on the semiconductive layer is compensated by the accumulation of holes in a thin topmost layer of the organic semiconductor, that become conductive.

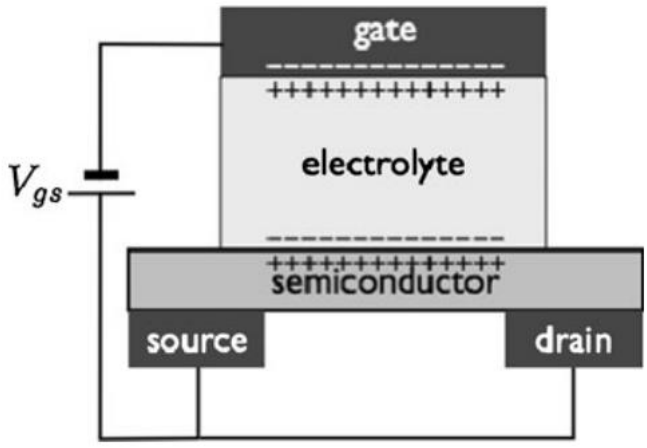

Figure 5 - Formation of the conductive channel in an EGOFET. Reprinted form [3]

In this type of device the sensing mechanism is governed by capacitance, because in FET the field-effect is strictly related to the capacitance, and this is very sensitive to

surface changes. A change in the capacitance on one of the interfaces results in a variation on the conductance of the channel [16]. The presence of the EDLs is a key feature of the operation of EGOFETs, because implies higher capacitance (on the order of tens of $\mu F/cm^2$ [16]) compared to OFET with solid dielectrics (tens of nF/cm^2 [17]), and that allows lower operating voltages.

As said already, one strong suit in EGOFETs is the possibility to work in aqueous solutions. Many different electrolytes may be used, and thanks to the work of Kegoat et al. [18], it was demonstrated that also water is a suitable liquid for gating a P3HT-based EGOFET. The aqueous environment allows the possibility to implement an in-situ sensing of molecules in a biocompatible media. Moreover, the bio-detection can be specific thanks to a proper functionalization of an active surface in contact with the electrolyte, that may be the gate electrode [19] or the semiconductor layer [20].

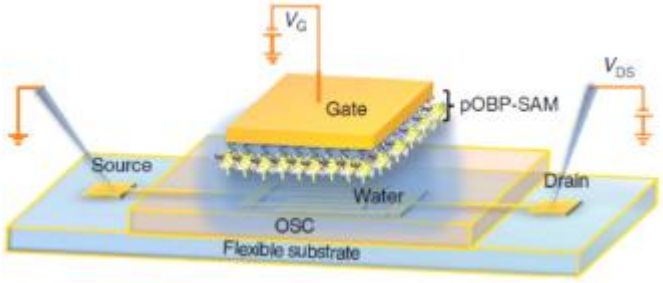

Figure 6 - Schematic view of an pBTTT-C14-based EGOFET with the gate functionalized with a SAM of odorant binding protein [19]

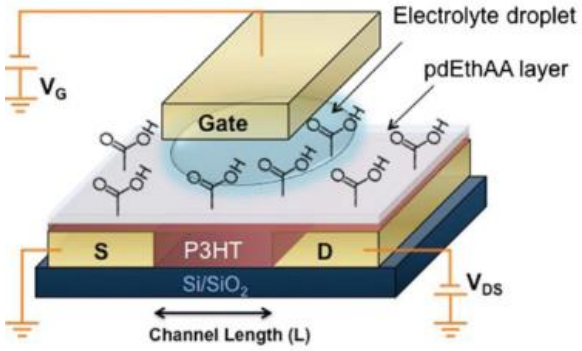

Figure 7 - Schematic view of an P3HT-based EGOFET with a plasma deposited ethylene/acrylic acid (pdEthAA) coating on the P3HT layer [20]

EGOFETs are complex devices in which different physical phenomena coexist, both field-effect related, and electrochemical related. In the following paragraphs the theoretical background of device operation will be deepened, starting from the electrical description, useful to read and understand the results, then EDL formation and finally the structure of the organic semiconductor.

2.1 Field-effect Transistors

To better understand how EGOFETs work, it is convenient to introduce the field-effect transistors theory, whose main results can be applied in a first approximation to quantitatively describe the device behaviour. The application of the MOSFET models [13] [21] is still a valid solution for the EGOFET dissertation, given that a complete and unique model for OFETs has not been developed, yet.

MOSFETs exploit semiconductors, which are materials with an intermediate conductivity behaviour between conductors and insulators, which can be controlled through an external voltage. By far, the most popular and the most used semiconductor is silicon, which may be doped with specific impurities in the crystalline structure in order to increase the number of free electrons (n-type doped silicon) or free holes (p-type doped silicon). As already said, the interesting features of those devices is the possibility to modulate the number charge carriers inside the semiconductor through the application of an external bias applied at the so-called gate electrode. Those charges are then accelerated through another voltage applied between the other two terminals of the MOSFET, that is to say the drain and source.

Considering a pMOS, the substrate is a n-type semiconductor, thus with a high number of free electrons. If a negative gate bias (V_{GS}) is applied, with drain and source connected to ground, the free electrons move away from the area of the substrate in the proximity of the gate, the so-called channel region, while positive free charges are attracted. The accumulation of positive charges induces the formation of a channel, that connects drain and source, and if the applied $|V_{GS}|$ overcomes the threshold value (V_t), the number of charged carriers is enough to make the channel conductive.

The channel region and the gate form a parallel plate capacitor, with the insulator in between as dielectric. An electric field (in the vertical direction) is generated, which modulates the carrier density, and consequently the value of the current in the channel.

The carrier charges quantity within the channel is:

$$|Q| = C_{ox}(WL)(V_{GS} - V_t) \quad (1)$$

In the formula W is channel width and L is channel length, whereas C_{ox} (oxide capacitance, referring to MOSFET) is the parallel plate capacitor capacitance per unit area (F/m^2). Typical values of channel dimensions are L between 0.03 and 1 μm, W between 0.1 and 100 μm, while the C_{ox} is in the order of magnitude of femto Farad [13].

When the gate voltage reaches the threshold ($|V_{GS}| \geq |V_t|$), the behaviour of the device depends on the applied V_{DS}:

- Low V_{DS} ($|V_{DS}| \ll |V_{GS}|$): the tension along the channel is neglected, the section is considered constant, and the current behaviour follows the Ohm's law (I_{DS} proportional to V_{DS} according to the channel resistance). This is the linear regime. Increasing V_{GS} value, will increase carrier density and consequently the current. To determine the value of the current (Eq. 3), the channel charge per unit length is multiplied for the drift velocity of the charge carriers (Eq. 2), which is their mobility (μ_p for hole, μ_n in case of electrons) times the electric field generated by V_{DS}:

$$s_p = \mu \frac{V_{DS}}{L} \quad (2)$$

$$I_{DS} = \left[(\mu C_{ox})\left(\frac{W}{L}\right)(V_{GS} - V_t)\right] V_{DS} \quad (3)$$

The current-voltage ($I_{DS} - V_{DS}$) curve (fig 6) is linear:

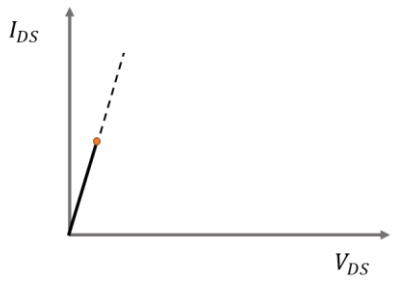

Figure 8 – Representation of the linear regime.

- Higher V_{DS} ($|V_{DS}| < |V_{GS}|$): the voltage drop along the channel cannot be neglected anymore, and increases from 0 at the source, to V_{DS} at the drain. Thus, the tension between gate and channel decreases from source to drain. Being the thickness of the channel proportional to V_{GS}, the section is not constant any longer. The section reduction leads to the resistance increase, that implies that the $I_{DS} - V_{DS}$ characteristic does not proceed with a linear trend, but sub-linear (the curve bends):

$$I_{DS} = (\mu C_{ox}) \left(\frac{W}{L}\right) \left[(V_{GS} - V_t)V_{DS} - \frac{1}{2}V_{DS}^2\right] \quad (4)$$

The current behaviour until this point is called the *triode operating* region.

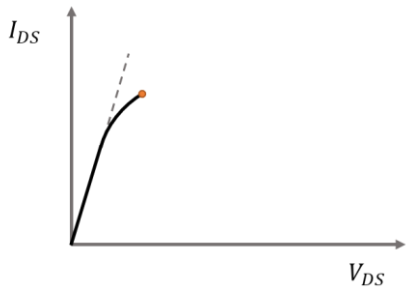

Figure 9 – Sublinear trend of the drain current.

- $|V_{DS}| \geq |V_{GS}| - |V_{DS}|$: the section decrease leads to the pinch-off of the channel (triangular section). In first approximation, increasing V_{DS} over $(V_{GS} - V_t)$ does not affect anymore the current flowing in the channel, which remains constant to the value reached for $V_{DS} = |V_{GS}| - |V_{DS}|$. This is the saturation region, and the current is:

$$I_{DS} = \frac{1}{2}(\mu C_{ox}) \left(\frac{W}{L}\right) (V_{GS} - V_t)^2 \quad (5)$$

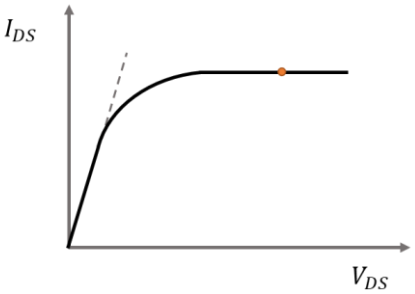

Figure 10 – The current reaches the saturation regime. This complete curve represents the $I_{DS} - V_{DS}$ characteristic.

The $I_{DS} - V_{DS}$ characteristic, referred to as output characteristic, represents the drain current as drain voltage function, at different values of V_{GS}, and it is possible to distinguish the linear and the saturation region:

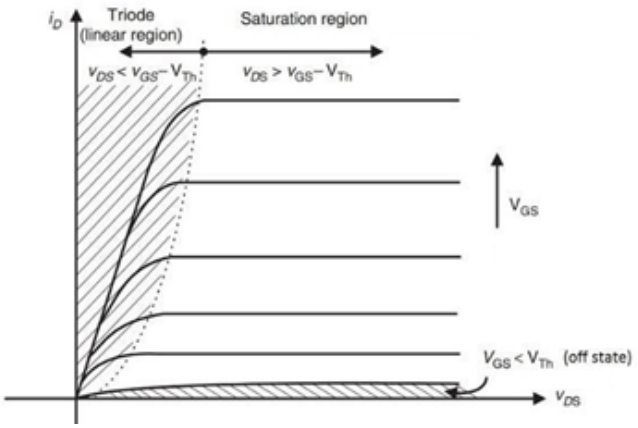

Figure 11 – Output characteristic: $I_{DS} - V_{DS}$ curve of MOSFET for different V_{GS} value [55].

From the current equations is possible to extract charge carrier mobility μ, that is a crucial parameter of FETs performance, considering that determines the channel resistance, and so the channel current.

Along with the output characteristic another key representation is the $I_{DS} - V_{GS}$ curve, namely the transfer characteristic (Figure 12). This curve illustrates the behaviour of the transistor in the linear or in the saturation regime. In the latter the I_{DS}, independent from V_{DS}, is quadratically dependent from V_{GS}. Consequentially, $\sqrt{I_{DS}}$ is linearly dependent from V_{GS} with a slope proportional to the mobility (Eq. 5). This is a key point, because from the $\sqrt{I_{DS}} - V_{GS}$ characteristic, it is possible to extract a crucial figure of merit, that is the threshold voltage V_t. The V_t may be extrapolated from the intersection of $\sqrt{I_{DS}}$ linear fit with the x-axis [22]. Equivalently, V_t may be extrapolated as a linear fit of the $I_{DS} - V_{GS}$ curve in the linear regime.

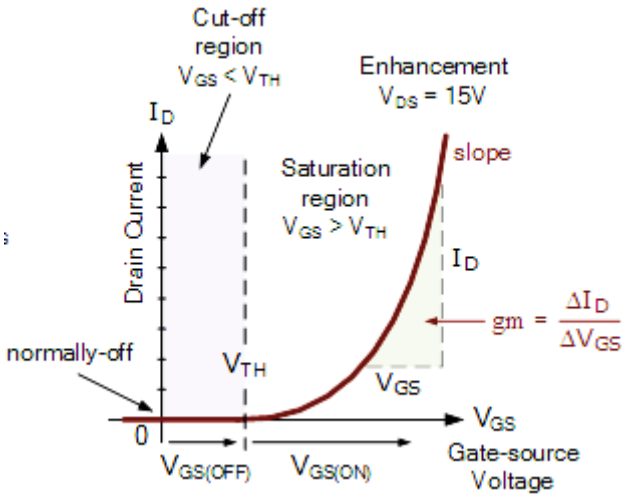

Figure 12 - Transfer characteristic: $I_{DS} - V_{GS}$ curve of MOSFET [56]

The threshold voltage from an operational point of view represents the V_{GS} value at which the transistor turns from an off state to an on state. For p-type transistor this value is negative.

Another useful figure of merit is the transistor transconductance g_m, that can be derived from linear (Eq. 3) and saturation (Eq. 5) current regime, taking into account that the transconductance is defined as $g_m = \frac{\partial i_{DS}}{\partial v_{GS}}$, and therefore resulting respectively:

$$g_m = (\mu C_{ox}) \left(\frac{W}{L}\right) (V_{DS}) \tag{6}$$

$$g_m = (\mu C_{ox}) \left(\frac{W}{L}\right) (V_{GS} - V_t) \tag{7}$$

The channel transconductance is the slope of the transfer characteristic in the saturation region (Figure 12). At an operational level, g_m gives a measure of how much the modulation of the channel current, I_{DS}, is sensible to the variation of the gate voltage, V_{GS}.

Finally, another figure of merits in FETs is I_{ON}/I_{OFF}, namely the ratio between the current when the FET is turned on, and the current at $|V_{GS}| < |V_t|$ when the FETs are off-state. This parameter should be as large as possible.

The MOSFET depiction can be useful to have a well-defined electrical description in terms of figure of merits, characteristics, and formulas. Anyhow, the mechanism that allows the conductivity of the channel is different. In fact, while the MOSFETs operate in inversion mode (the p-channel takes place in the n-type semiconductor), the OFETs operate in accumulation mode [23]. It means that, employing a p-type semiconductor, if a negative gate bias is applied (Figure 13), the positive charges in the OSC will be attracted to the insulator interface, in the channel region, because the gate and the organic semiconductor are capacitively coupled through the insulator.

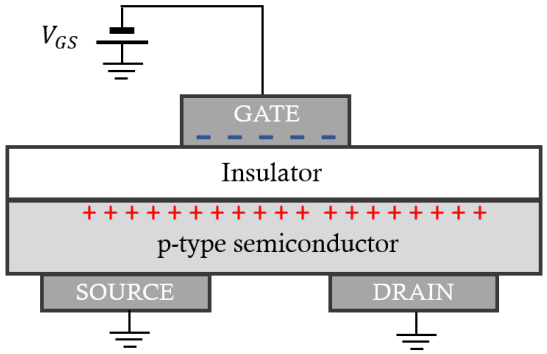

Figure 13 – Formation of the conducting channel in a OFET. Adapted from [5]

When V_{GS} is over the threshold voltage, and a negative V_{DS} is applied, the holes are injected from the source, and the I_{DS} current flows inside the channel [14]. The current can be controlled by regulating the charge density at the OSC/insulator interface, varying the gate voltage.

2.2 From OFETs to EGOFETs

In EGOFETs the crucial additional element is the liquid electrolyte that interfaces gold electrode and semiconductor, with ions inside completely free to move, instead of fixed charges in standard OFETs dielectric. When the gate is negatively polarized, cations are drawn towards the electrolyte-gate interface, and anions towards the electrolyte-semiconductor interface. The anions accumulation produces accumulation of free holes in the topmost layer of the semiconductor, and that allows the channel to become conductive. When a negative voltage is applied between source and drain, current flows inside the channel. The accumulation of ions and charges results in the formation of an electrical double layer (EDL) at both interfaces

[14][16]. The EDL formation is affected by the electrode potential as well as the chemical properties and polarity of the electrolyte. The factor that mainly dominates the charging kinetics is the ion migration through the electrolyte and considering that ions mobility is usually lower than electrons, the EDL formation takes a few milliseconds. The switching speed may be lowered in case of high gate voltage, that may cause the electrochemical doping, a phenomenon in which ions from the electrolyte penetrate in the semiconductor, affecting the semiconductor electrical properties and the robustness of the device. The electrical doping is the main cause of EGOFET performance degradation upon use.

According to the analytical description of the channel current, it is clear the strict relation with the dielectric capacitance. A great advantage of EGOFETs is that they display a much higher capacitance per unit area since the double layer holds a very high capacitance (*ca.* 10 $\mu F/cm^2$), being the thickness of the EDL on a sub-nanometric scale. This is a critical difference with MOSFET, in which the capacitance is constrained to the thickness of the oxide that cannot be lowered under a technological limit [24]. So, the capacitance value one order of magnitude higher in EGOFETs, significantly lowers the operational voltage (under 1V versus over 10V in conventional FETs).

In EGOFETs, the presence of a dynamic liquid environment influences the figure of merit because of stability issues. Regarding the threshold voltage, the value of V_t depends on many effects related with the semiconductor and the dielectric used. During a repeated use of an organic transistor, threshold voltage may change, and that causes hysteresis in back and forth scan of transfer curves measurements. The lower mobility with respect to the one in MOSFETs is due the different transport mechanism, diffusion in the inorganic semiconductor, hopping in the organic semiconductor. Finally about the I_{ON}/I_{OFF} ratio, this value has to be as high as possible. The off-current should be ideally zero, but this does not happen because of many unwanted factors, like semiconductor doping or gate electrode leakage [22].

The potential of EGOFETs as biosensors resides right in the connection between field effect and capacitance, and the latter is very sensitive to surface changes. This means that, as instance, the presence of a target species over one of the interfaces (gate/dielectric or dielectric/semiconductor) would result in a change in the

gate/semiconductor capacitance, and consequently in the output current. [16][25][23].

2.3 Theory of the EDL

The basic phenomenon behind the working principle of an EGOFET device is the formation of the so-called Electrical Double Layer (EDL), whose relatively high capacitance per unit area is the reason why EGOFETs can operate at such low voltage. Indeed, it is also the main cause of the ultrasensitive interface properties of these devices [12].

Considering an electrolyte between two electrodes, when an external voltage is applied, (charging process) the charged ions in the electrolyte move towards the opposite charged electrode. The space that comprises cations/anions and the electrons/holes constitutes the EDL. One EDL is formed on each electrode/electrolyte interface (Figure 14).

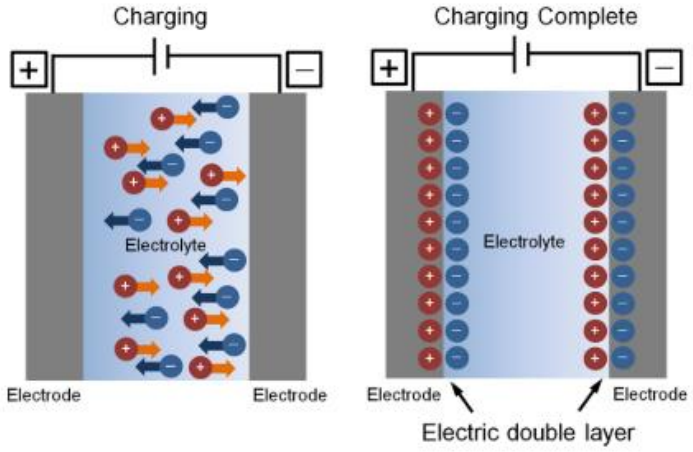

Figure 14 – Scheme of the formation of an electrical double layer on charged electrodes. Reprinted from [26]

The EDL concept was firstly used for electrical double layer capacitors, with the capacitance proportional to the surface area of the EDL [26].

Three models have been adopted to picture the ionic environment next to a charged surface. The first one was developed by Herman von Helmholtz in 1853, who stated that no charge transfer happens between the ions in the electrolyte and the electrode, and that the EDL takes place because a single ion layer arranges on the electrode

surface to balance the charge. He assumed that the charge drop is limited to the region that comprises the ions [27], and that the stored charge depends linearly on the applied voltage. Moreover, the capacitance is assumed constant from the charge density, and consequently from the voltage [28]. This model was later modified by Louis Georges Gouy and David Leonard Chapman in 1910', who observed that the capacitance depends on applied voltage and on the ionic concentration. Furthermore, with respect to the Helmholtz model, they considered the diffusion/mixing of ions in the solution and stated that the charge distribution of ions is a function of the distance from the electrode, and so the potential decreases exponentially with the distance. Because the Gouy-Chapman model was not suitable for highly charged EDL, in 1924 Otto Stern modified it, proposing a combination of the previous two [12][26], assuming that the electrostatic interactions are in competition with Brownian motion, and thus considering ions both adherents on the electrode surface, and a diffused in a layer of solution. Other modifications did follow during the years, but the Stern Model is an option solid and widely adopted.

The Stern Model consists of three layers (Figure 15):

1. The compact layer, or Helmholtz plane: ions are strongly adsorbed at the electrode surface. This layer is divided in an inner Helmholtz plane (IHP) and an outer Helmholtz plane (OHP), that refer to the distance of specifically adsorbed ions and non-specifically adsorbed ions. In this region the potential has a linear drop.
2. The diffuse layer, or Gouy-Chapman layer, extended from the OPH to the electrolyte bulk. It contains mobile ions. In this region the potential decreases exponentially.
3. The bulk solution: in this area the potential is constant, and the ions are no more accelerated.

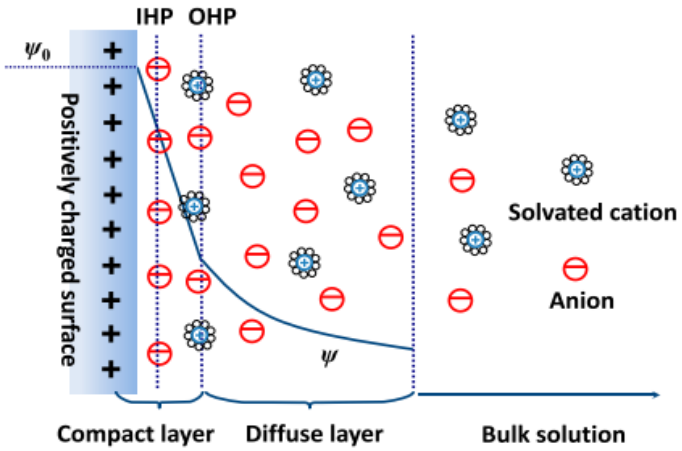

Figure 15 –Stern model of the electrical double layer formation on a positively charged electrode surface. Reprinted from [29]

At steady-state, the applied electrode potential mostly drops across the EDL: the potential ψ in the electrolyte is maximum at the interface, and quickly decreases within the compact layer and the diffuse layer. That means that in an EDL-based transistor, theoretically the ionic current from the gate to the source is near zero, being the driving force for ion migration in the bulk deleted [30].

The characteristic thickness of the EDL is the Debye length μ, that is the distance over which mobile ions screen out the electric fields in the solution [31], and thus the limit over a charge is shielded by the ions of the electrolyte. In the application of EGOFETs as biosensor, the Debye length represents the limit into which the interaction between the analyte and the bioreceptor has to happen, because over this distance, the binding events are not detected. The Debye length is inversely proportional to the square root of ionic strength of the solution, and that is an important factor in the choice of the electrolyte: an increase in electrolyte concentration leads to a less thick Debye length. Thus a compromise is needed between a large enough thickness of the EDL (larger with diluted ionic strength solution) and a suitable solution for the maintenance of biomolecules activity and the binding affinity (better environment for proteins in highly concentrated solutions). As instance, the Debye length in a physiological salt environment such as PBS 1x results ≈0.7 nm, less than the size of a regular IgG antibody (5~10 nm) [32]. Instead, in PBS 0.1x the Debye length is 2.4 nm, while in PBS 0.01x it is 4 nm [33].

In the electrical double layer model, the Helmholtz plane and the diffusive layer are considered as two capacitances in series [29][30]. The capacitance per unit area of each EDL can be estimated by the Helmholtz equation:

$$C = \frac{\varepsilon_0 \varepsilon_r}{\lambda} A$$

with ε_0 the vacuum permittivity, ε_r the electrolyte dielectric constant, A the electrode specific surface area accessible to the ions, and λ the Debye length (in the order of 1 nm). With λ on the order of 1 nm, and $\varepsilon_r \sim 10$, values above 1 $\mu F/cm^2$ are achievable that is an order of magnitude larger than with conventional OFETs. [31]. Assuming the two capacitances equal ($C = C_1 = C_2$), and considering them in series, the total capacitance is the half of C:

$$\frac{1}{C_{tot}} = \frac{1}{C_1 + C_2} \rightarrow C_{tot} = \frac{C}{2}$$

However, the total EDL capacitance is typically governed by the capacitance Helmholtz plane, having a thickness of only a few Angstroms (1 Å=1×10^{-10} m).

2.4 Sensing principle

As it might be clear, the operation of EGOFETs relies on the formation of the electrical double layers at the two interfaces, gold/electrolyte, and OSC/electrolyte. In the application as biosensor, in the electrolyte is injected the target spices, that adsorbed specifically on the properly functionalized surface, that may be the gate electrode or the semiconductor. The interaction between the analyte and the receptor causes a change in the local electrostatic potential [12], and the variation of the surface potential depends on the binding affinity. The phase that follows the sensing is the transduction, in which the change of the potential at the interface entails a variation in the channel conductivity and thus in the channel current.

- When the sensing surface is the gate electrode, the adsorption of charged species imply the polarization of the electrode, and the V_{GS} changes, and consequently this is reflected in a variation of the threshold voltage, V_t [12].
- When the sensing surface is the semiconductor layer, the analyte is detected directly on the active channel, and necessarily when occurs the specific

adsorption, the conductivity of the channel is affected, as also the EDL capacitance and the carrier mobility.

In both cases the effects on the sensing surface are expressed in a change of the EDLs capacitance. In the EGOFET structure, the interfacial EDLs may be considered as capacitance in series [34]:

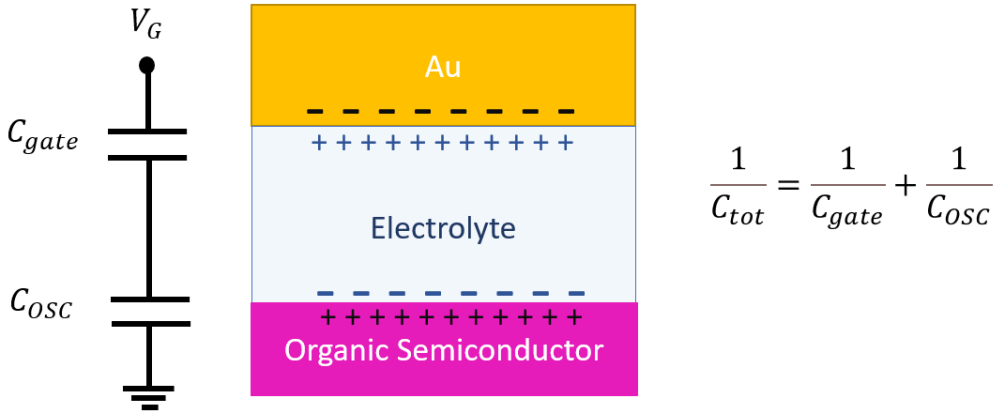

Figure 16 – Schematic depiction of the EDLs on the gold gate electrode/electrolyte and semiconductor/electrolyte interfaces, and the respective capacitance in an EGOFET.

2.5 Organic Semiconductor

A fundamental element not investigated yet is the thin layer of organic semiconductor over source and drain electrodes. In recent years organic semiconductors (OSCs) are gaining more and more attention in many technological applications such as displays [35] and solar cells [36]. OSCs show light weight, mechanical flexibility, availability, affordability, and easy production processes, all attractive properties compared to the equivalent inorganic ones [37]. For decades they have been studied in the exclusive view of insulator, until the discover of their conductivity properties: in 2000 Heeger, MacDiarmid, and Shirakawa won jointly the Nobel Prize in Chemistry for "the discovery and development of conducting polymers" [38].

As the name suggests, organic semiconductors are materials that bring together the properties of semiconducting materials, like adsorption/emission of light and electrical conductivity, and the properties of carbon based substances, like malleability and solubility. In inorganic semiconductors conductivity is due to low

band gaps that allows at room temperature the free charges to move from the valence band to the conduction band [39]. In contrast, in organic semiconductors the conductivity needs an external source, like charges injection [40].

Organic semiconductor materials, also known as conjugated polymers, consist of carbon and hydrogen based molecules with alternating single and double bonds, and with a sporadic presence of heteroatoms as sulphur, oxygen, and nitrogen. To better understand the phenomenon on the basis of the semiconductive properties of organic molecules, it is significant to go deep to the molecular level [39][41].

Considering the formation of a molecule by the bonding of two atoms, what determines the shape of the molecule is the configuration of each atom, that is the distribution of electrons within the energetic orbitals. When a binding between atoms is going to happen, in the central atom the isolated ground state atomic orbitals mix together, degenerating in hybrid atomic orbitals. That means new wave function with different electron densities and spatial orientations. Depending on what and how many atomic orbitals mix together, distinct type of orbital hybridization may happen. Ground state carbon electrons configuration is $1s^2 2s^2 2p_x^1 2p_y^1$. In hydrocarbons formation, during the bonding with another carbon or a hydrogen, carbon atomic orbitals may mix together in several ways. The amount of hybrid orbitals and of p-orbitals remains unhybridized in the C atom is crucial for the number and the type of bonds it can form. For instance, in the formation of methane (Figure 17), all four valence electrons orbitals (including the empty $2p_z$) mix generating four half-filled sp^3 hybrid orbitals, able to bind with four hydrogens. The overlapping of hybrid orbitals and hydrogen 1s orbital lead to the formation of σ−bonds.

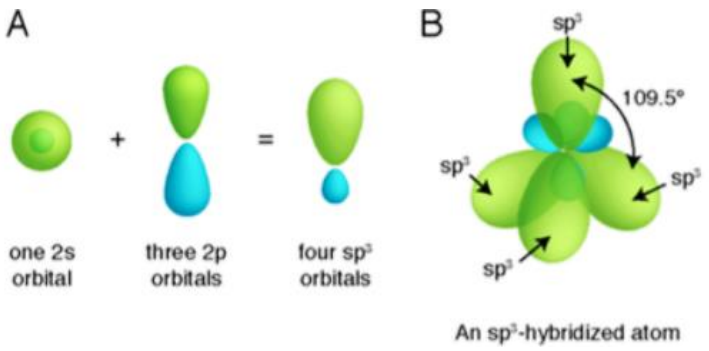

Figure 17 – Formation of the methane molecule, through the overlapping of four sp^3 hybrid orbitals and hydrogen 1s orbital.

Meanwhile, with the formation of a molecule with a double bond, like ethylene, carbon hybridization is sp^2, with p unhybridized orbitals in an orthogonal plane with respect to the sp^2 orbitals plane. A σ−bond occurs between the two carbons and between carbons and hydrogens. In addition, the p-orbitals of the two C overlap side-by-side, leading to a π− orbital: the electron cloud is delocalized between the two atoms, with the electron density distributed above and below the internuclear axis. Thus, a double bond consists of a σ− bond and a π-bond.

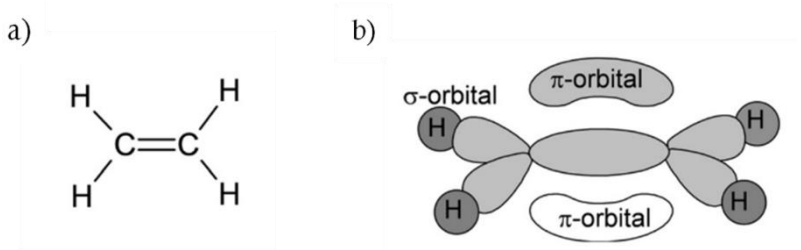

Figure 18 – Ethylene: a) chemical structure and b) illustration of orbital diagram. Reprinted from [42]

Following the molecular orbital theory (MO theory), the behaviour of electrons in a molecule is described, as well as in atoms, through the wave function. Moreover, molecular orbital may be studied through the method of the linear combination of atomic orbitals (LCAO). The combination of atomic orbital wave functions may lead to constructive interference, if the wave functions are in-phase, or destructive interference, if they are out-of-phase. Consequentially two types of molecular orbitals can raise: the in-phase combination leads to a lower energy molecular orbital, that promotes the nuclei to be close (bonding orbital), whereas the out-of-phase combination leads to a higher energy molecular orbital, and nuclei are driven apart (antibonding orbitals).

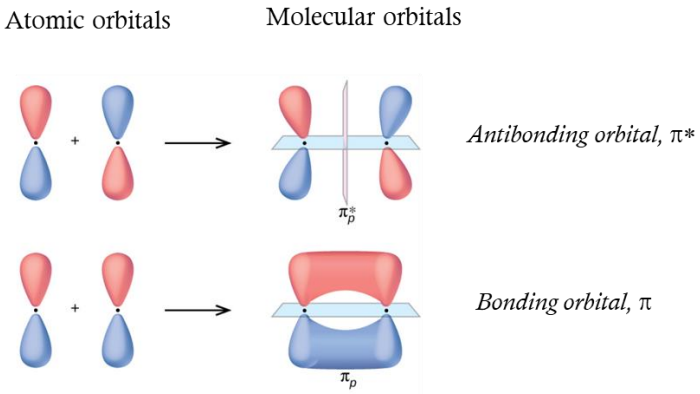

Figure 19 - Side-by-side p orbitals overlapping results in the formation of two π molecular orbital: antibonding (out-of-phase combination) or bonding (in-phase combination) orbitals. Adapted from [41]

Referring to the energy level diagram, is it possible to identify the highest occupied molecular orbital (HOMO) and the lowest unoccupied molecular orbital (LUMO), known as frontier orbitals.

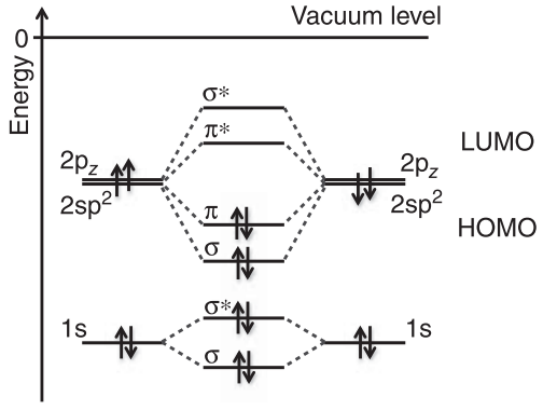

Figure 20 - Ethylene energy level diagram. Reprinted from [15]

The HOMO and LUMO energetical levels are crucial for the electrical behaviour of organic materials. In fact, the energy gap between the HOMO and LUMO is the needed energy to excite an electron in the molecule. A favourable condition is when the frontiers orbitals are π- orbitals rather than σ−orbitals, because of the lower energy gap. The low distance of π and π*-orbitals is the key element of the conductive capabilities in organic semiconductors. Moreover, a greater extent of the π-conjugation system means larger expansion of π - orbitals electrons delocalization and a decrease of energetic splitting between frontiers orbitals.

Two major categories of OSCs can be distinguished, depending on the molecular weight of the compounds [37],[39],[42]: small molecules, that can form crystal structures, and polymers. Polymers semiconductors are very large molecules formed by repeated structural units held together by covalent bonds. A carbon backbone, with alternating single and double bonds, may be enriched by aromatic and heteroaromatic rings, as well as side chains in order to make the polymer soluble in organic solvents. This molecular arrangement leads to an extension of π-electrons delocalization. In the microscopically disordered structure of the polymer, the charge transport that dominates is the intermolecular hopping transport between localized states. Thus, the hopping transport results strongly depend on the states availability: this transport mechanism explains the lower charges mobility compared to inorganic semiconductor crystals, in which dominates the band transport. To mimic the long-range carriers delocalization of inorganic materials, it is crucial to control structure morphology and crystallinity [43], in order to narrow states distribution. This aim can be firstly approached with widely ordered polymer chains, achievable with sufficiently high molecular weight or by pre-aggregation or external alignment. An additional favourable factor is a low energetic disorder, being related with a better accessibility of states for charge carriers.

Considering the role of ordered structure in the charge mobility, and hence conductivity, ordered π-stacks polymers are convenient. One of the most investigated conjugated polymers for p-type semiconductor applications is poly(3-hexylthiophene) (P3HT) (Figure 21-a).

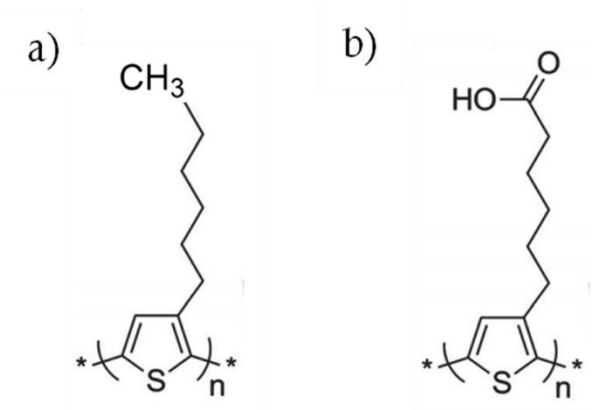

Figure 21 – Chemical structure of a) poly(3-hexylthiophene) (P3HT) and b) poly(3-carboxypentylthiophene) (P3CPT).

P3HT is so widely used thanks to its well-defined molecular architecture [37]. This feature is attainable when there is a high percentage of head-to-tail coupling in the thiophene ring in the polymer chain, because that leads to a regioregular structure [39].

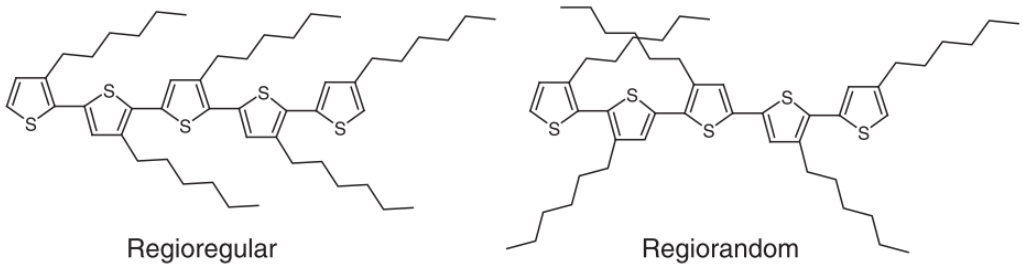

Figure 22 – When Thiophene rings are connected head-to-tail, the polymer structure results regioregular. Differently it is regiorandom. Reproduced from [39]

Regioregular polymer is a favourable configuration for the hopping transport, allowing the π− stacking that maximizes the electronic coupling within the stack. The lamellar organization formed by interchain stacking allows higher carrier mobility (0.1 cm^2/Vs) when the polymer backbone is orthogonal to the substrate while a 100 times lower mobility is achieved with the backbone parallel to the substrate [44].

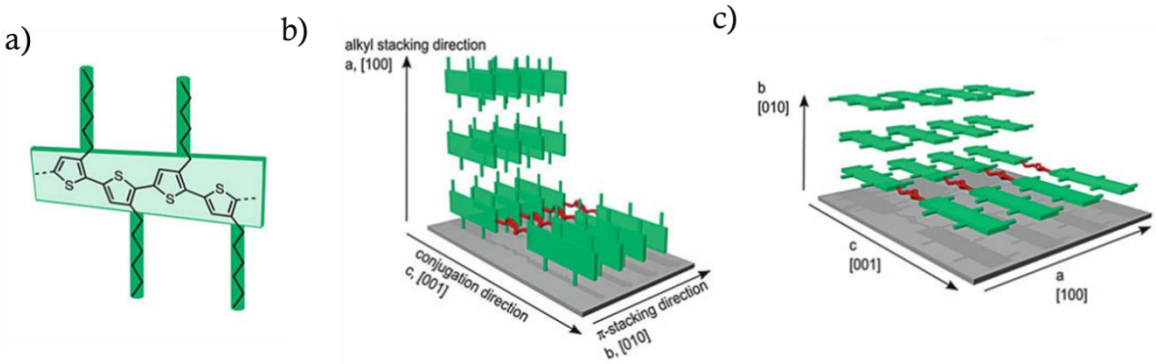

Figure 23 – a) Representation of the P3HT backbone constituted of thiophene rings and the lateral alkyl chains. Different disposition of the P3HT backbone: b) lamellar configuration normal c) parallel to the substrate. Reprinted from [44]

The polymer that has been used in nearly all cases is a P3HT derivate, poly(3-carboxypenthylthiophene) P3CPenT (Figure 21-b), as variation is characterized by a terminal carboxyl group (-COOH) in the side chain instead of the methyl group (-CH_3). In the application of EGOFET as a biosensor, the ending -COOH group is a

useful anchoring site for surface functionalization and allows to obtain the sensing surface on the organic semiconductor. In fact, the carboxyl group can be directly exploited to immobilize biomolecules of different nature. With respect of P3HT, that due to the exposed alkyl chain shows a hydrophobic behaviour (contact angle 105° [40]), P3CPT combines the hydrophobic π–conjugated backbone and the hydrophilic ionic side group [45] (contact angle 49° [40]).

With respect to P3HT, in which dominates the field effect doping (Figure 24 - Regime I), in P3CPT-based EGOFET may occur electrochemical doping when high gate voltages are applied [40] (|VGS|>1.5V [46]), and thus the ions penetrate in the interface (Figure 24 – Regime II) or in the bulk (Figure 24 – Regime III) of the semiconductor.

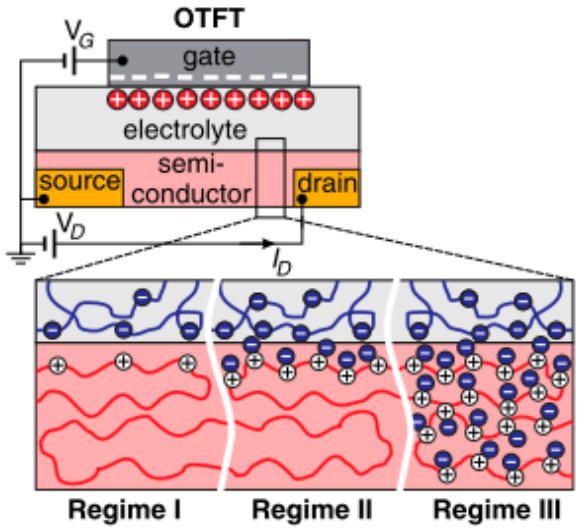

Figure 24 – Schematic representation of different possible behaviours of an organic semiconductor in a OFET with a negative gate bias. Regime I: field effect doping; Regime II: interfacial electrochemical doping; Regime III: bulk electrochemical doping. Reprinted from [40].

Moreover, in the point of view of the use as organic semiconductor in EGOFETs, a key feature of the polymers is the value of the capacitance of the electric double layer that takes place in the electrolyte/OSC interface. In particular, P3CPT has a higher capacitance value with respect to P3HT, and this may be due the propensity to electrochemical doping [40]. A critical point of the use of organic polymers as semiconductors, is that they are highly sensitive to oxygen and humidity, and that

induces degradation mechanisms in the material [15]. This feature must be taken into account, referring to the stability issue of EGOFET and OFET.

2.6 Target of interest

2.6.1 Angiopoietin-2

Angiopoietin-2 (Ang2) belongs to an important family of growth factors, whose activity is regulated by the tyrosine kinase receptors (Tie1 and Tie2), following the angiopoietin/Tie signaling pathway, a fundamental pathway in angiogenesis [47]. While Ang1 is a strong angiogenic growth factor, Ang2 role is context-dependent, and may behave both in antagonistic manner on Tie2 function (thus with a vascular disruptive role, inducing vascular permeability) and in agonist manner, playing a fundamental part in physiological processes [48]. Even if there is not an exact characterization of Ang2 expression, many studies have shown that Ang2 is up-regulated in several disease related to vascular permeability and angiogenesis. In fact, Ang2 expression may be triggered by inflammatory mediators, such as TNFa [49], and stressful environments, like hypoxia [50] and cancer [51]. So, considering the protein upregulation in these conditions, Ang2 has been proposed as a biomarker for inflammation and cancer.

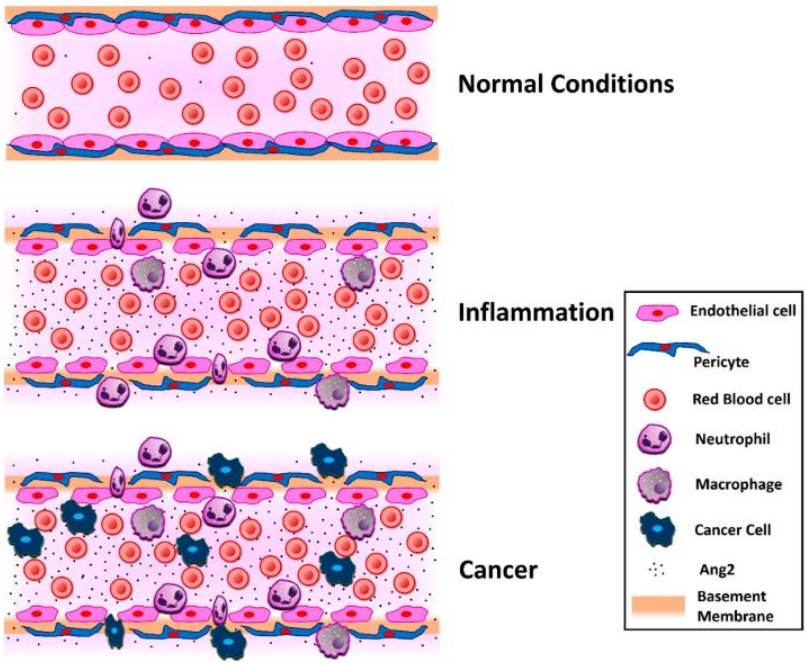

Figure 25 – Schematic illustration of the role of Ang2 on a blood vessel in normal condition, inflammation, and cancer. Reprinted from [47].

Considering these features, Ang2 has been chosen in this work as a target of primary interest.

2.6.2 Antibiotics

The antibiotics mostly used in this work are Tetracyclines, a family of broad-spectrum antibiotics, discovered in the 1940s, that exhibited action against a wide range of microorganisms, including gram-positive and gram-negative bacteria [52]. Their activity relies on interfering with the ability of a bacterium to produce a variety of vital proteins [53].

Tetracycline molecules consist of a linear fused tetracyclic nucleus, with addition a several lateral functional groups [52]. In particular two types have been tested as target molecules: Tetracycline (*Sigma-Aldrich*, Empirical Formula: $C_{22}H_{24}N_2O_8 \cdot xH_2O$) and Oxytetracycline hydrochloride (*Sigma-Aldrich*, Empirical Formula: $C_{22}H_{24}N_2O_9 \cdot HCl$).

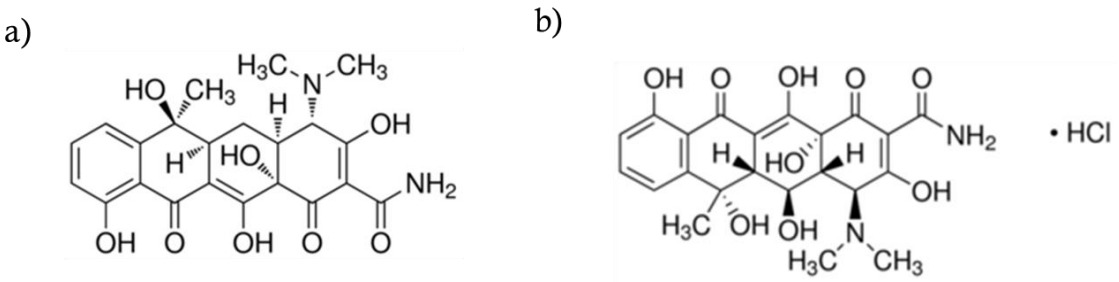

Figure 26 - Chemical structure of a) Tetracycline and b) Oxytetracycline hydrochloride

Another antibiotic used is Sulfadimethoxine (*Sigma-Aldrich*, Empirical Formula: $C_{12}H_{14}N_4O_4S$), an antibiotic usually used in veterinary medicine [54].

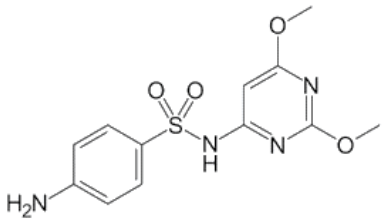

Figure 27 - Chemical structure of Sulfadimethoxine (4-Amino-N-(2,6-dimethoxy-4-pyrimidinyl)benzenesulfonamide)

Chapter 3

Materials and Methods

In this chapter each component of the sensor will be explored, starting from the description of features and fabrication of the different element, and proceeding with an overview of the setup measurement. After that, the electrical characterization and different protocol of measurements are depicted. Finally, the bio-functionalization procedure of the sensing surface is described.

3.1 Device overview

The sensing apparatus is overall composed of four main elements, briefly introduced here.

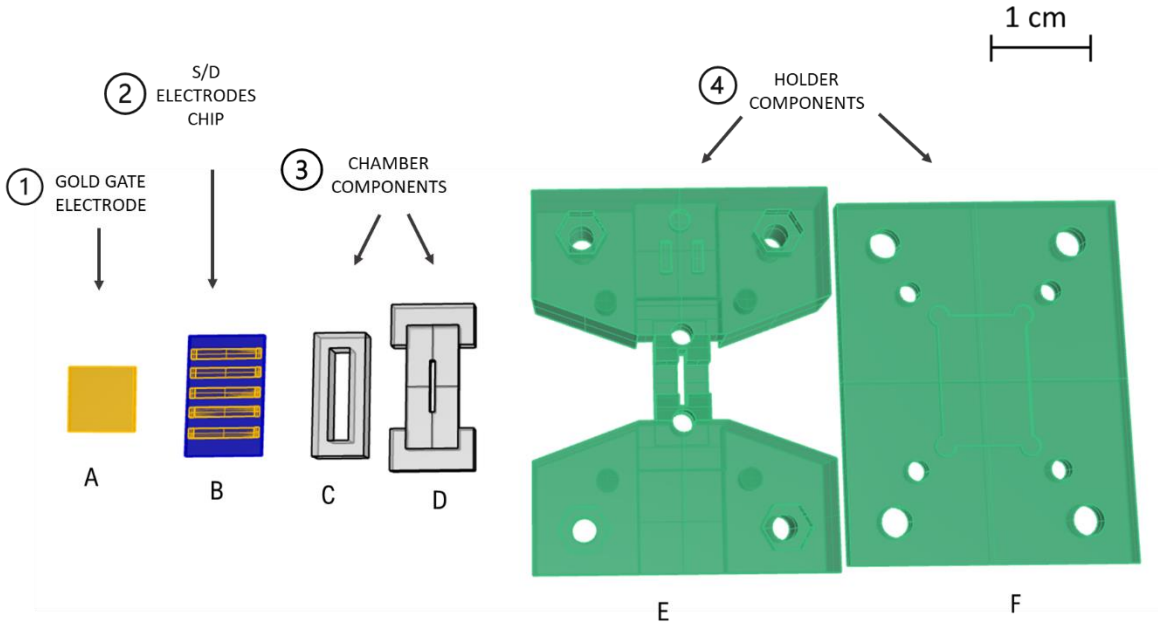

Figure 28 – CAD of all the single main elements of the device. Design by M. Segantini

1. Gate electrode: a 5x5mm squared gold electrode is exploited in almost the totality of experiment.
2. The chip (EGOFET) with five parallel interdigitated source and drain electrodes.
3. The microfluidic chamber is constituted by two complementary parts, made in PDMS: a hollow piece (Figure 28 - C), which is the actual chamber, and the cap (Figure 28 - D) which presents a narrow opening for the gate electrode and two holes for the fluidic inlet and outlet.
4. The holder is the rigid case that provides a solid support for all the other elements and guides their disposition. It consists of two parts, joined by four screws. The upper piece (Figure 28 - E) presents a slit for the gold gate insertion, while the bottom part (Figure 28 - F) houses the device.

3.2 Device fabrication

In this paragraph the fabrication method of each element will be discussed. All these processes are executed at the Chilab - Materials and Microsystems laboratory (DISAT, Politecnico di Torino). For what concerns the electrical components, they are fabricated following standard cleanroom processes in ISO-5/ISO-6 [57] environments.

3.2.1 Chip design

The starting substrate is a 4-inch silicon wafer, which presents a 1 μm of thermally grown silicon oxide (SiO_2) on top of it. On this substrate it will be designed more than 60 single chips of dimension 12.8x7.8 mm. Each chip in turn comprises five parallel source-drain interdigitate electrodes, characterised by W=9590 μm and L=10 μm, which are respectively the width and the length of the EGOFET channel.

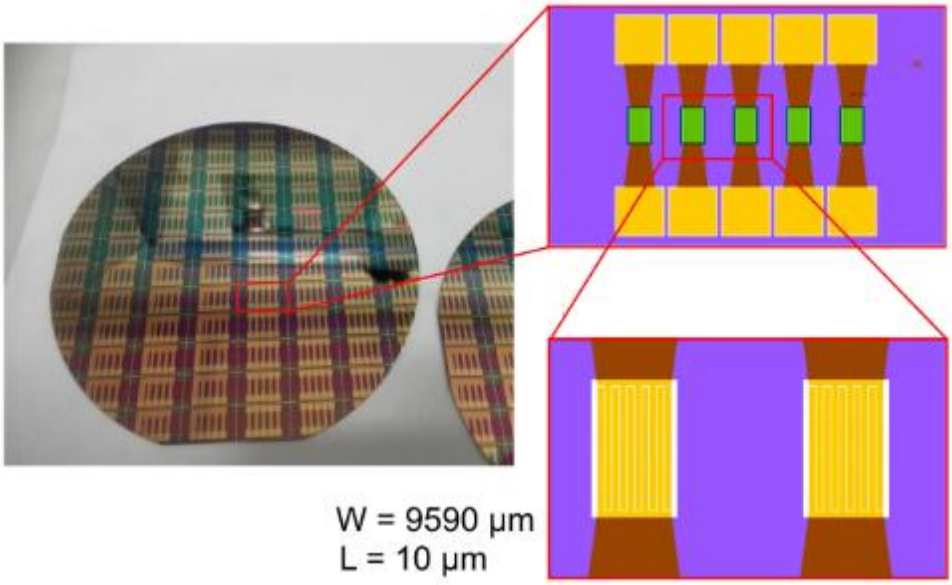

Figure 29 – a) The 4-inch wafer with patterned source/drain electrodes and passivation. b) Details of the chip containing five parallel devices. c) Detail of the interdigitated source/drain electrodes design. Reprinted from [58]

3.2.2 Fabrication of source and drain electrodes

The technological process used for the definition of the source and drain electrodes involves three main steps: metal deposition, UV-lithography and wet etching (Figure 30). Firstly, 10 nm of titanium (the adhesion layer) and then 100 nm of gold are deposited all over the substrate (Figure 30 – a), by means of an e-beam evaporator (ULVAC EBX-14D). A positive photoresist (AZ1518, MicroChemicals) is deposited through spin coating on the surface (5 seconds at 500 rpm, 30 seconds at 4000 rpm, for a final thickness of about 2 µm) (Figure 30 – b) and soft-baked (120 seconds, 110°C). The mask alignment and the UV-exposure are performed with the Neutronix Quintel NXQ-4006 Mask Aligner (Figure 30 – c). The mask used is a clear field mask, so the electrodes pattern is protected from UV light, while the exposed area of photoresist becomes soluble in the developer solution. After the UV-exposure for 5 seconds (power density 11mW/cm^2), the photoresist is developed (developer AZ400K, MicroChemicals) (Figure 30 – d) and the substrate is rinsed and post-baked. At this point, the last phase is the wet-etching, exploiting a gold etching solution (Techni Etch AC12, MicroChemicals GmbH), and a Ti-etch (HF based), in order to remove the un-protected metallic areas (Figure 30 – e).

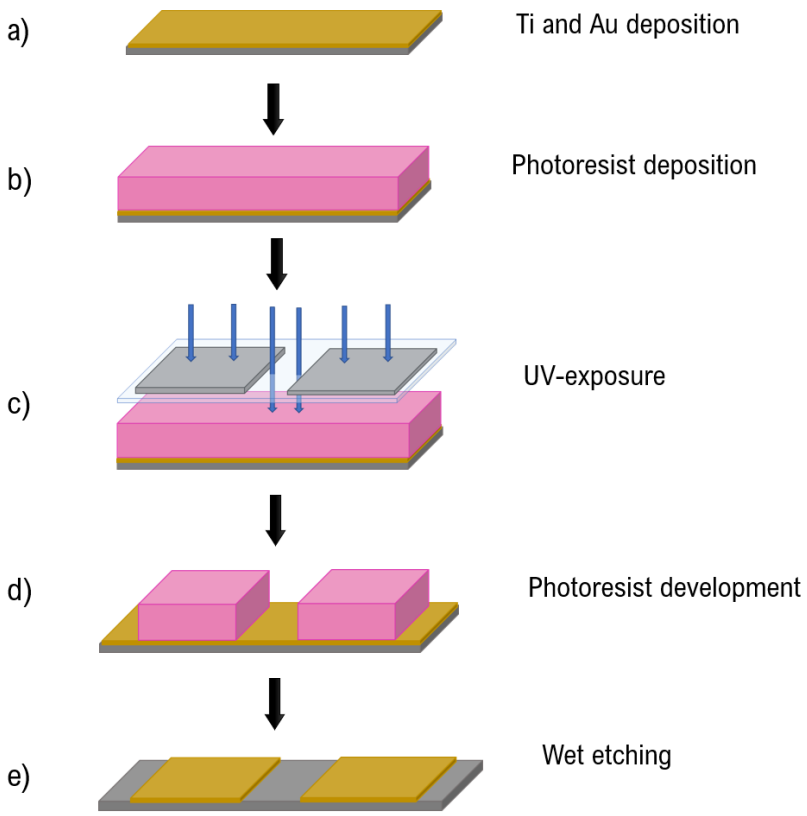

Figure 30 – The steps of fabrication of the source-drain electrodes on a Si substrate

So, the final result are the patterned gold electrodes on the substrate.

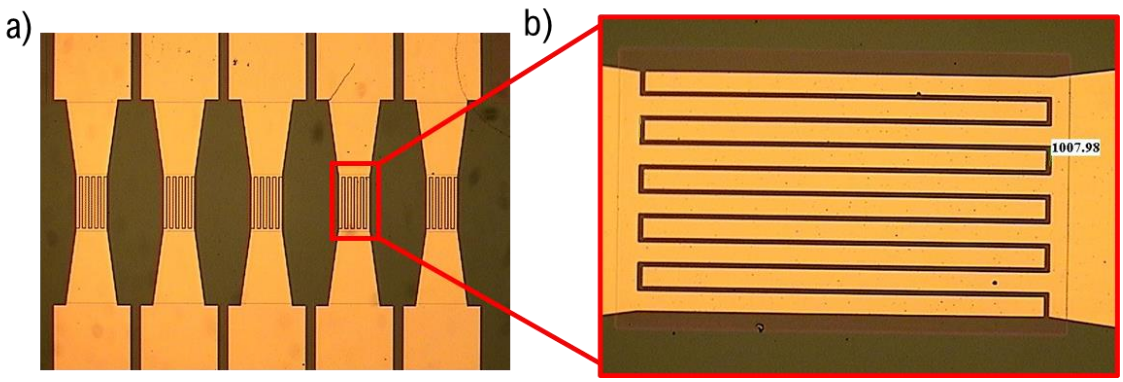

Figure 31 - Optical microscopy image of a) the single chip, which comprises an array of 5 parallel devices; b) a detail on the S/D interdigitation, with the length of the channel; the passivation window is noticeable

A passivation layer is then deposited with an e-beam evaporation of Al_2O_3 , and then patterned through UV-lithography following a lift-off process in DMSO. The

passivation has an opening (windows 690µm x 1110 µm) that leaves exposed the source-drain electrodes interdigitation, and the lateral contact pads.

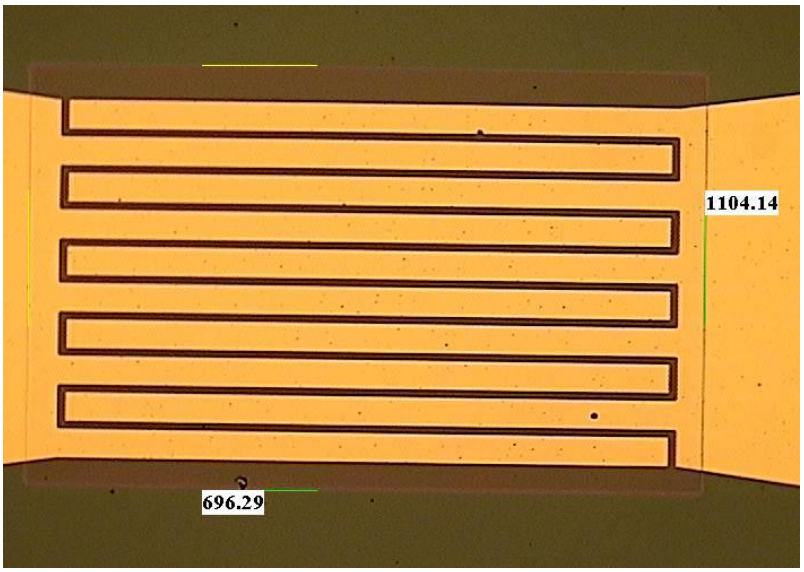

Figure 32 - Optical microscopy image of the passivation layer, with the dimensions.

After the deposition of a protective positive photoresist (AZ1518, MicroChemicals) the wafer is diced by Microla SRL, obtaining 12.8x7.8 mm chips (Figure 33).

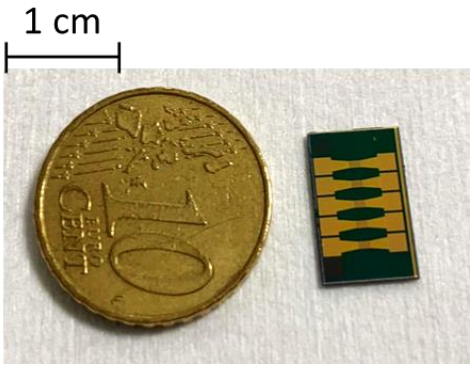

Figure 33 – Comparison between the size of the chip and a coin of ten cents.

The following step is the organic semiconductor deposition on each single chip. It is important to remark that the transistor figures of merit strongly depend on the thickness and uniformity of the deposited film of OSC on the electrodes. As already said, soluble organic materials permit inexpensive processing techniques. In literature several methods can be found, such as: vacuum thermal deposition [59] - preferred in case of deposition of thin films of organic small molecules [60] - inkjet printing [61] and spray deposition [61], preferentially employed in industrial application.

However, the most diffused techniques in laboratories are drop-casting and spin-coating [16].

Spin coating (Figure 34) is the method exploited for the sample fabrication in this work. With this process the achievable film thickness depends on solution concentration, spin speed and solvent evaporation rate. A great advantage of spin coating is that it does not need heating, avoiding thermal degradation for material whose decomposition temperature is lower than evaporation temperature [60] and furthermore the low temperatures allow the use of different substrates. In addition, spin coating is a quick and easy deposition method that does not need high-end machines. The main disadvantages are the material waste and the formation of beads defects and accumulation on the edges. Another limit in the use is that spin coating is exploitable only with soluble polymers.

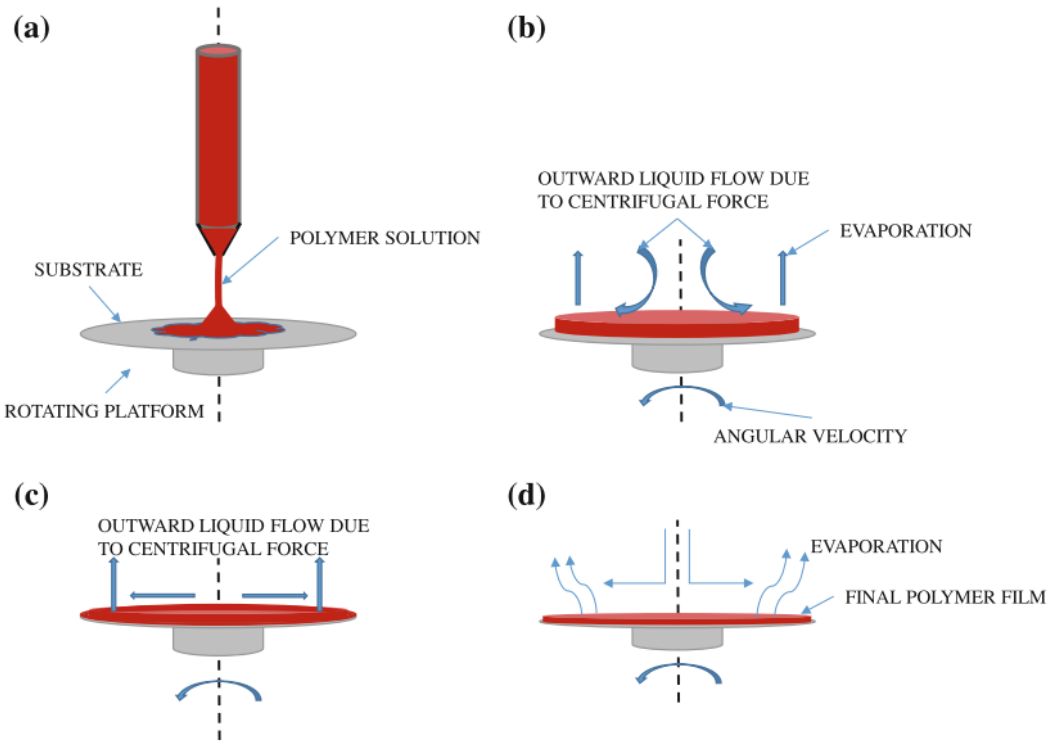

Figure 34 – Schematic representation of the spin coating process: (a) deposition of the polymer; (b) spin-up stage: the polymer flows radially due the centrifugal force; (c) spin-off: outward flow of the polymer in excess toward the edges, and ejection; (e) evaporation occurs throughout the entire process. Reprinted from [63]

Each phase of the process of OSC deposition and treatment is detailed below:

1) Preparation of the organic semiconductor polymer solution with an organic solvent: 2.5 mg/ml of P3CPT are dissolved in DMSO, at 60°C on a magnetic stirrer until the polymer is well blended and the colour is clear and uniform.
2) Pre-bake of the chip to remove any water trace, 120°C for 10 minutes on a hot plate.
3) Spin coating: the chip is placed on the platform inside the spin coater (SPIN 150i) and held in place through aspiration, which creates a vacuum that keeps the chip adherent to the base. Then, 25 µl of the solution are deposited on the centre of the sample and the protocol is started. The latter consists of 5 seconds at 500 rpm and 30 seconds at 2000 rpm. With the rotation, the solution is spread all over the sample and meanwhile the solvent evaporates. This procedure is repeated entirely a second time, in order to improve deposition homogeneity.
4) Samples are annealed for at least two hours at 75°C in a vacuum oven, in order to avoid oxygen exposure.
5) Once ready, the samples are preserved under vacuum and in a dark ambient to avoid light exposure.

For the deposition of P3HT, it is applied the same protocol as described above with a different solvent, which is in that case the 1,2-dichlorobenzene (oDCB).

3.2.3 Gate electrode

For the experiments, two different gate electrodes have been employed: a square gold electrode and an Ag/AgCl wire. This work is almost entirely focused on the former, in order to exploit the possibility to realize a surface functionalization on it. In fact the surface of the gold electrode may be exploited as a sensing surface, thanks to the elevated affinity between Au and thiol group (-SH). Thus, a self-assembled monolayer can be created, with -SH groups as anchoring points to the gold surface and an exposed functional group for the binding with a bio-receptor.

This gold gate electrode is produced from a silicon wafer, covered through e-beam evaporation (ULVAC EBX-14D) by 10 nm of titanium and 100 nm of gold. The wafer is diced obtaining 5x5mm square pieces.

When the Ag/AgCl electrode is employed, the device assembly is very similar to the one that employs the gold gate electrode, with the difference that the cap of the

chamber is full, and the top part of the holder has a round hole instead of the narrow slit. The Ag/AgCl electrode is realized by a standard protocol of chlorination of a silver wire. Unless otherwise specified, the configuration considered is always the one with the gold electrode, considering that almost the totality of the experiments employs it.

3.2.4 Chamber

The chamber components are made of PDMS, casted in a PMMA mould (fabricated with a milling machine), following a simple procedure:

- Sylgard 184 Silicone Elastomer Base and the curing agent are mixed together, proportioned 10:1. This solution is held for some minutes in vacuum to get rid of the air bubble trapped inside the viscous solution.
- Silicon is casted into the mould.
- Baking for around 2 hours at 65°C.
- The pieces are carefully extracted.

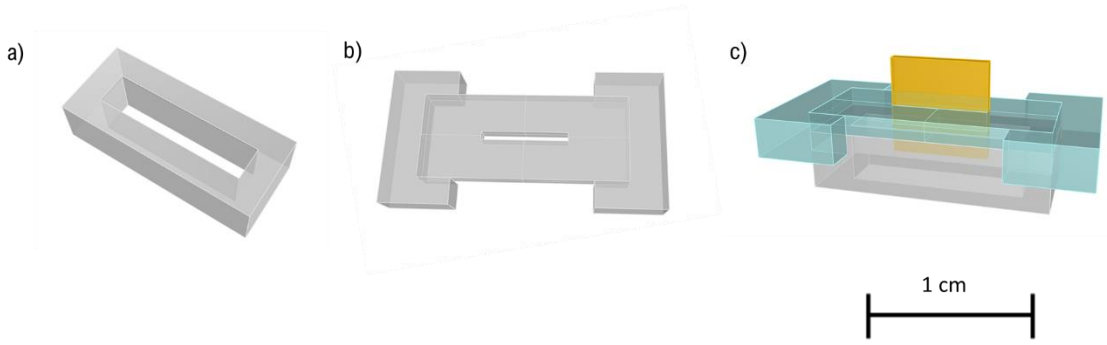

Figure 35 – CAD of (a) the chamber and (b) the lid, and (c) how the two pieces fit together, also with the gold gate electrode. Design by M. Segantini.

The volume of the chamber is 60 µl. In the centre of the lid there is a narrow opening for the gate insertion. Two additional holes are shaped piercing the PDMS lid, in order to create the fluidic inlet and outlet.

When the Ag/AgCl gate is employed a different lid is used, produced with a separate mould. The lid is completely full, without the central opening. A little hole is obtained by piercing the PDMS with a needle, and the wire is inserted from the side without the chlorination.

3.2.5 Holder

The PDMS elements are inserted in a rigid holder, that provides a solid support also for the fluidic tubes. The holder parts are created with a 3D printer, the Object 30 (*Stratasys*), employing the *VeroWhite* resin. This resin is a photosensitive polymer in liquid form, that polymerizes through UV light exposure, that occurs layer by layer. The un-polymerized resin remains soft and it is soluble in water, so after the elements are printed, they are cleaned and washed in order to remove all the residues, paying attention to the narrow parts. The material is resistant enough to allow the insertion of four nuts and the tightening with as many screws, in order to join the top and bottom elements. The two parts fit together thanks four little pillars on the top piece that get inserted in corresponding holes in the bottom piece.

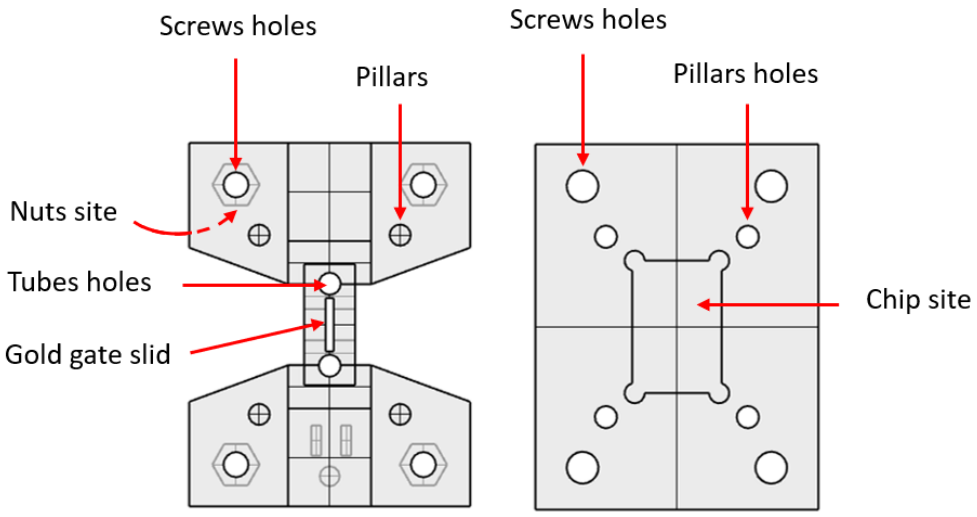

Figure 36– Top view of the top and bottom elements of the holder. Design by M. Segantini.

3.2.6 Assembly

Since the tests are executed with real-time measurements, the crucial feature of the assembly is to allow a continuous flow of the electrolyte from the inlet, inside the chamber and finally through the outlet, without liquid leakage.

The assembly follows some simple but delicate steps. First of all, the two holes for inlet and outlet are created on the PDMS chamber lid, using a pointed tool. Carefully with tweezers the gate is inserted in the central opening on the lid, that is then placed on the holder case. The gate is now slightly pulled in the lid, in order to be partially immersed in the electrolyte and partially come out from the top of the holder. Now,

the chamber hollow piece is fitted in the lid (, Figure 35-c, Figure 37– a). The chip is placed on the centre of the bottom holder (Figure Z- b)

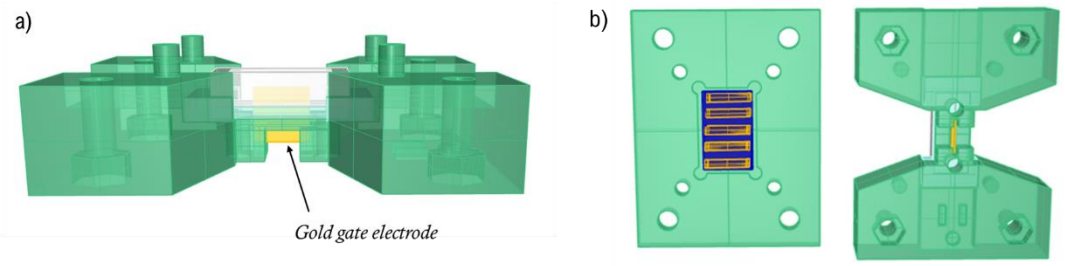

Figure 37 – CAD of: a) lateral view of the assembly of: top holder, chamber, and gate electrode; b) top view of the unassembled holder elements. Design by M. Segantini.

The two parts are then joined together, making sure that the PDMS chamber adheres on the median area of chip surface, so that the lateral contact pads remain accessible.

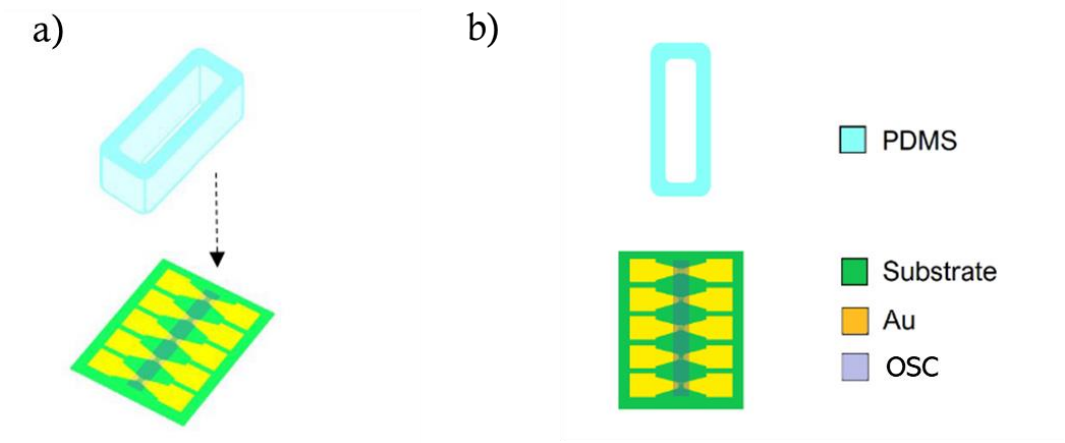

Figure 38 – Picture of the PDMS chamber and the chip, in perspective view (a) and from above (b). Reprinted form [64]

The top and bottom holder elements are fixed with four screws, tightened into the nuts (previously inserted in the dedicated hollows). Finally, few drops of fresh PDMS are deposited on the side of the external portion of the gold gate, with the aim of reducing the risk of leakage during the filling of the chamber.

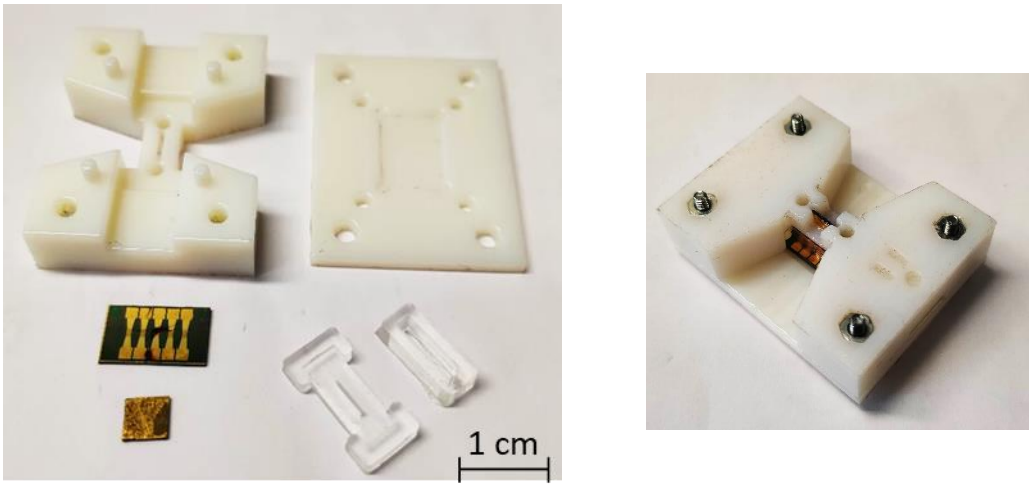

Figure 39 – Picture (a) of all the single elements and (b) of the assembled device

3.3 Measurements setup overview

The measurements setup used for the experiments is located in the *Nanoscience Lab* (DISAT, Politecnico di Torino). It comprises four main units: the probe station, the source/measure instrument, the controlling software, and the fluidic system.

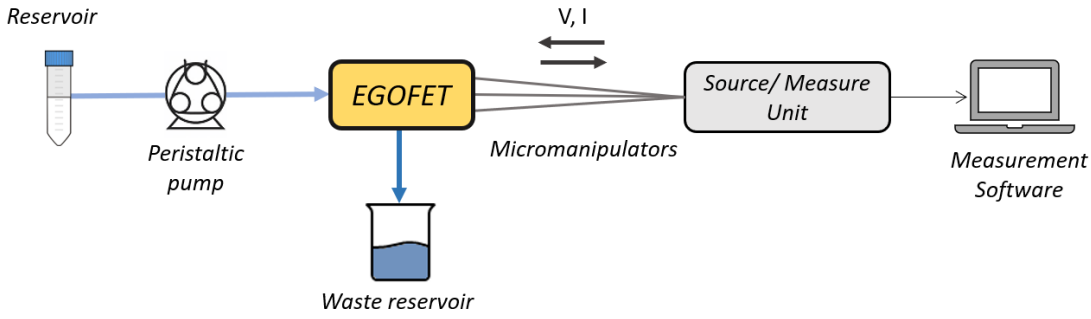

Figure 40 – Schematic representation of the measurement set up

3.3.1 Source/Measure Unit

First of all, a probe station with three micro-manipulators allows the contact of the three electrodes of the sensor: the source and drain lateral pads and the external portion of the gate electrode. The contacts are connected through triax cables to the

Keysight B2912A Precision Source/Measure Unit (SMU), *Keysight Technologies*. This high performance and versatile device allows to source and measure both voltage and current, without needing multiple instruments. It supports coverage of 210 V, 3 A DC/10.5 A pulse, and a minimum resolution of 10fA/100 nV. The SMU supports two channels, and each of them supplies the voltage while measuring voltage and current. Considering that the source is grounded, the drain and gate voltage are referred to the source. In this case the Channel 1 (CH1) is referred to V_{DS} and I_{DS}, while the Channel 2 (CH2) is referred to V_{GS} and I_{GS}. In the instrument is integrated a display of four quadrants with the voltage and current of each channel, useful to ease test and debug operation.

Figure 41 – Front view of the Keysight B2912A Precision Source/Measure Unit

The instrument is driven by the software Quick IV Measurement Software, provided by *Keysight Technologies*. The software supplies the interface that allows to configure the measurement and also to display the graphic of ongoing measure, in real time. It is possible to plot different quantities on the x and y axis, including current, voltage and time. For each measure the number of points to acquire and the scan rate can be set.

Figure 42 – Quick IV Measurement Software: example of the Setting interface

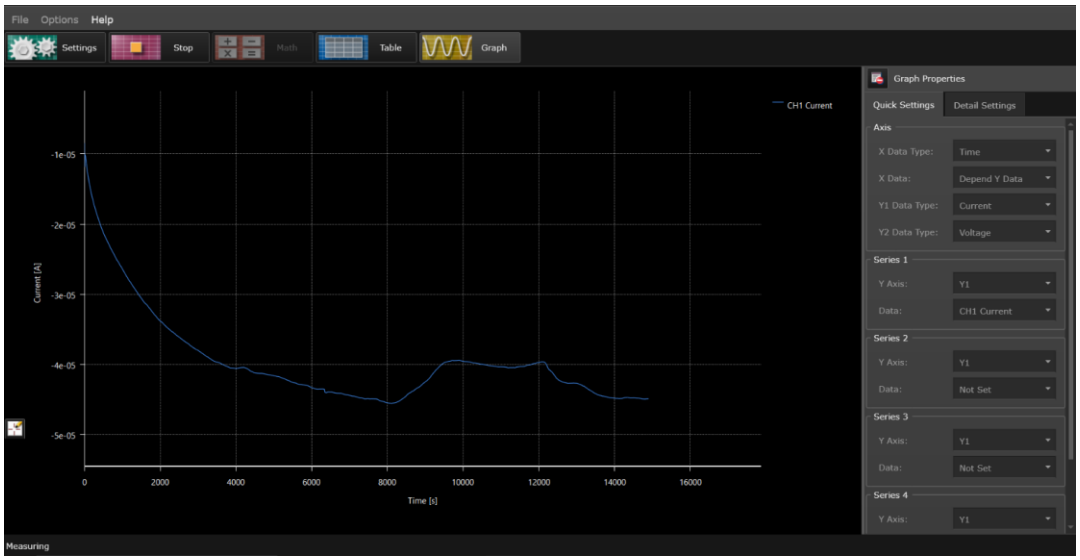

Figure 43 – Quick IV Measurement Software: example of the real time graph display

In the channel setting the source parameters are chosen, including the input functions trend and the compliance, that is the maximum output acquirable, fixed as a safe limit in order to not damage the device. Anyhow, the compliance value has to be comparable to the order of magnitude of the ongoing signal because it affects the resolution of the measure.

3.3.2 Microfluidic system

Concerning the microfluidic system, it comprises first of all a peristaltic pump and the correlated flexible tubes. This typology of pump has inside a rotor with two or

more rollers, that compresses the tube containing the fluid. As the rotor turns, the rollers force the fluid to be pumped through the tube and then transported, at ambient pressure, toward the pump outlet. Moreover, while the rollers rotate vacuum is formed in the tube, pulling inside more fluid.

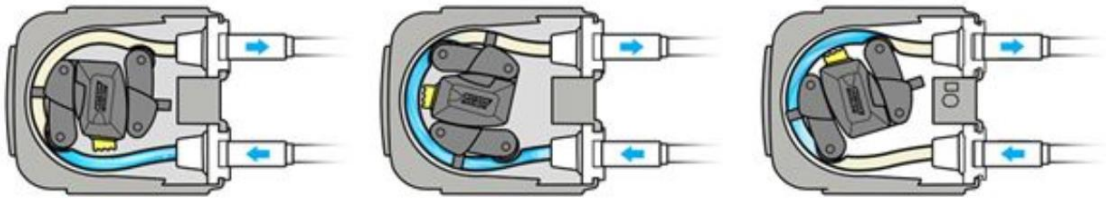

Figure 44 – Schematic representation of how a peristaltic pump works [65]

The pump used is the ISMATEC IPC, with 4 different channels. With the control panel on top, it is possible to set the flow rate (shown on a display), the flow direction and to start and stop the flux.

Figure 45 – Picture of the ISMATEC IPC 4 channels

For the scope of this work, the great advantage of the peristaltic pump is that it may run continuously without creating bubbles, and also that changing the solution is extremely easy, with low risk of air incorporation.

In practical terms, the measurement setup is prepared with the following steps:

1. The inlet tube (connected through the pump to the reservoir) and the outlet tube (connected to the waste reservoir) are inserted into the holes of the holder into the electrolyte chamber of the EGOFET.
2. The micro-manipulators, connected to the SMU, are placed on the gate (Channel 2 wires) and on the source and drain electrode of the first device of the sample (Channel 1).

3. The pump is turned on with a flow rate of 20 µl/min. The flow fills the chamber and goes through the outlet tube. When the first droplets come out from the tube, and it is sure that there is no liquid leakage, the system is ready for the measurement.

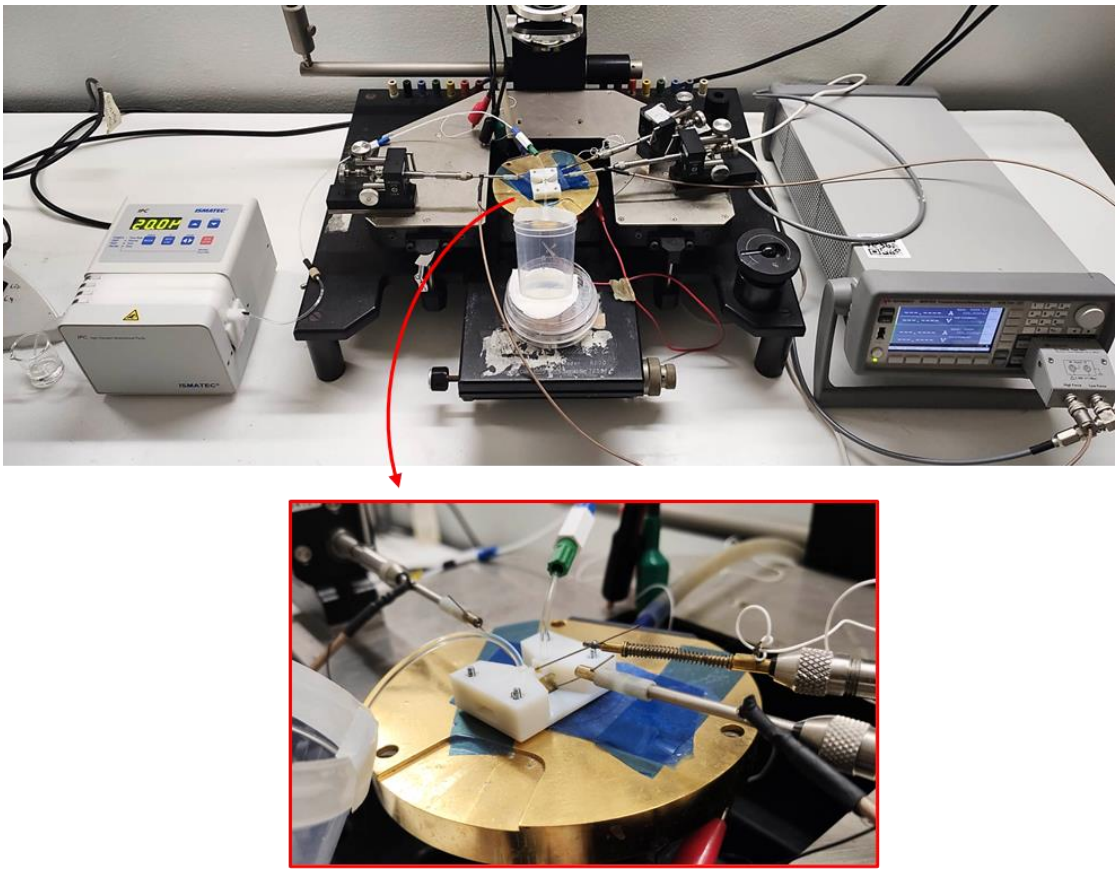

Figure 46 – Picture of the entire measurement set-up, with a detail of the EGOFET device

3.4 Electrical characterization

Preliminary electrical characterizations are executed to investigate the functionality and the performance of the individual devices.

- Transfer characteristic: this measure is performed on each of the five devices on the chip. The transfer curves are essential in order to extract some crucial figures of merit, namely the threshold voltage and the transconductance. Moreover, this procedure is helpful to identify any non-working device, and to find which one is most efficient, and so exploit it for the bio-detection measure.

The measures are performed applying a constant voltage on Channel 1 (usually V_{DS}=–0.5V) while on Channel 2 is applied a voltage sweep, usually V_{GS}=0.1V → − 0.8V and back, for five consecutive times (see figure 47).

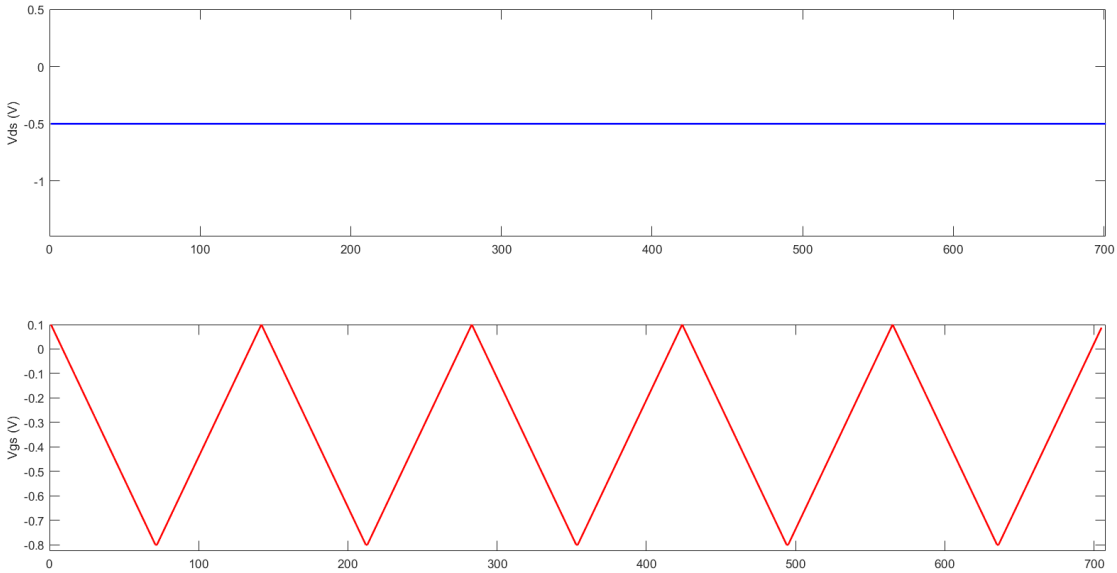

Figure 47 – The applied voltage on CH1 (drain electrode, in blue) and on CH2 (gate electrode, in red) during the transfer characteristics

The measured quantities are both I_{DS} and I_{GS} currents (Figure 48). As already said, each measure is repeated five times, and the curves are plotted together to point out the tendency of the current to drift when a sweeping voltage is applied. Furthermore, both the forth and back are displayed to evaluate the hysteresis, red flag for electrochemical doping behaviour. The gate current is monitored because its contribution should be as low as possible (high values of gate current may indicate the presence of short circuits between the electrodes).

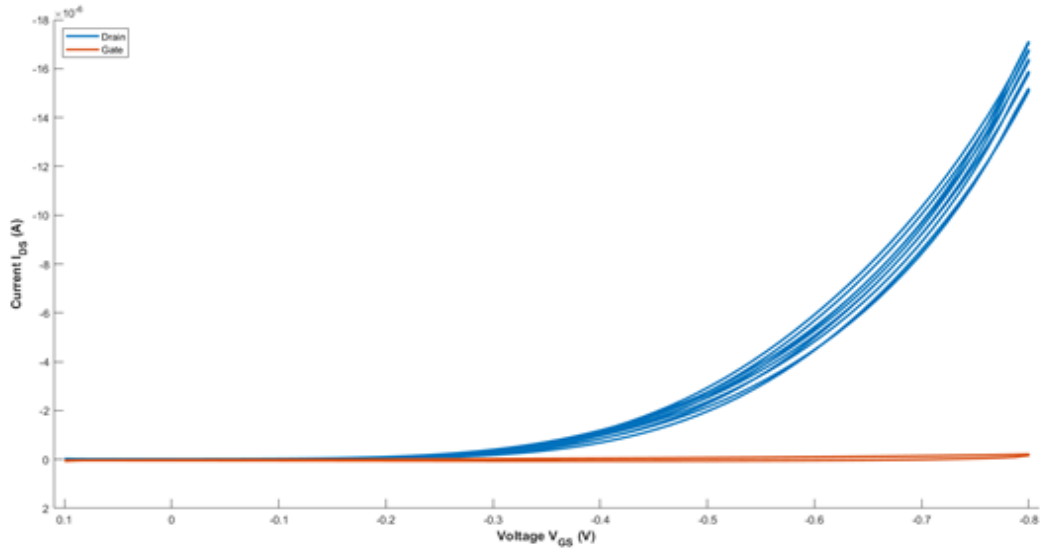

Figure 48 – The measured currents I_{DS} (drain electrode, in blue) and I_{GS} (gate electrode, in red) during the transfer characteristics. Each measure is repeated five times.

After each device has been characterized, an overall plot is displayed (figure 49), combining the last forth transfer curve of the five devices in order to compare them and decide which one will be used for the biosensing measures.

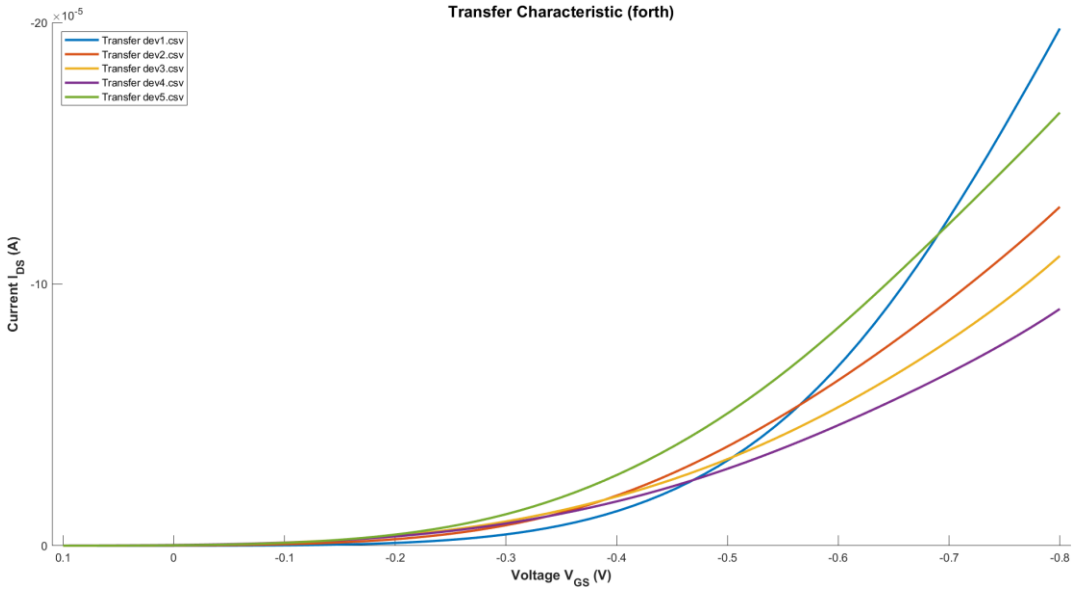

Figure 49 – Comparison between the last forth transfer curve of the individual devices.

From the transfer curves the values of the threshold voltage (V_t) and the maximum transconductance ($g_{m,max}$) are calculated, using a MATLAB script.

The main decisional parameters, along with low hysteresis and low drift during the repeated transfers, are:

- A high $g_{m,max}$, considering that it is a parameter related with the current amplification effect of the transistor, and thus on how well could be detected the sensing signal.
- A negative V_t, that means that the transistor (p-type) is working correctly.
- Low I_{off} currents, thanks to low I_{GS} contribution.
- The range of I_{DS}, in the order of tens or hundreds of μA, to have a consistent measure in long time

- Output characteristic: different output curves are obtained for different V_{GS} (from 0.1V, to –0,8V with step size of 0.1 V). On Channel 2 the several V_{GS} values are applied, and for each of them on Channel 1 a voltage sweep is applied, V_{DS}=0V → – 0.8V and back, for five consecutive times (Figure 50).

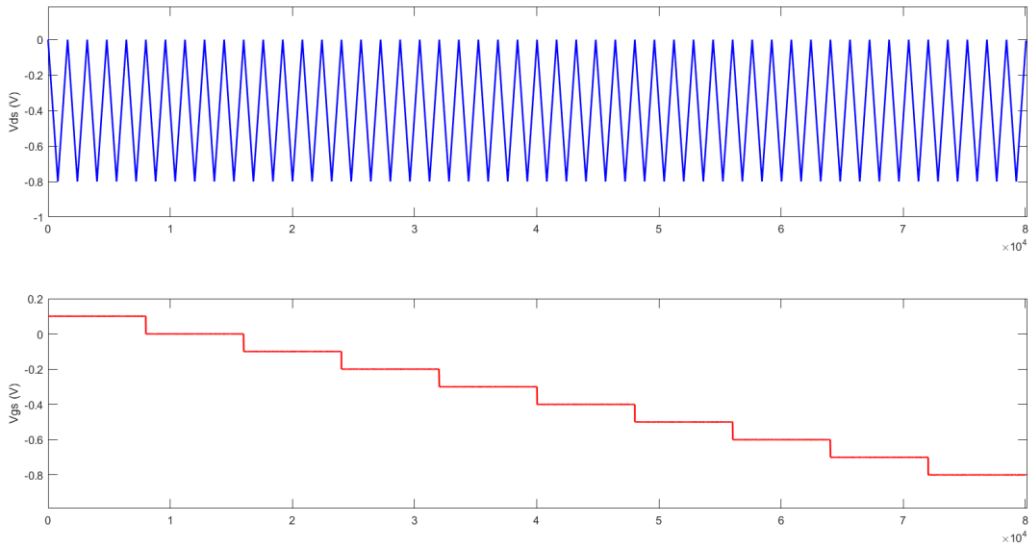

Figure 50 – The applied voltage on CH1 (drain electrode, in blue) and on CH2 (gate electrode, in red) during the output characteristics

The current measured is I_{DS}, and the repeated curves are displayed (Figure 51). Until the V_t is not reached, the transistor should be off. Once the transistor turns on, the conventional output curve should be clear, with the distinction of the linear and the saturation regions, and with an increase of the current for higher V_{GS}.

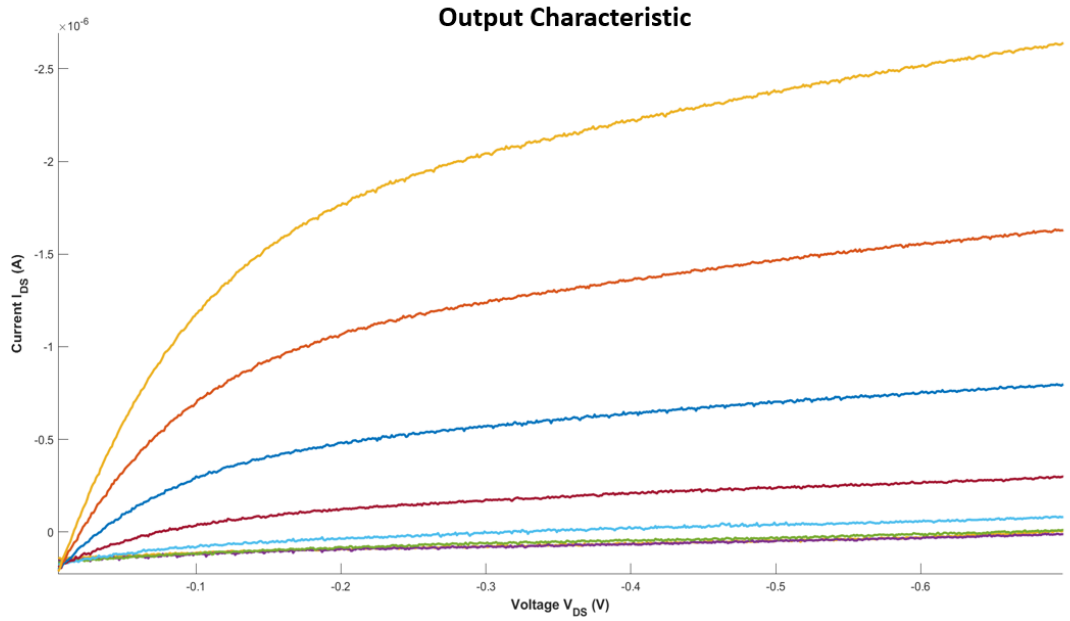

Figure 51 – Output characteristics obtained for different gate bias

- Gate Capacitance: a constant positive gate voltage is applied for 5 seconds on Channel 2, and the I_{GS} current on the same channel is monitored. This measure is repeated independently for V_{GS} pulses of increasing intensity, from 100 mV to 500 mV, with a step-size of 100 mV . The Channel 1 has V_{DS}=0.

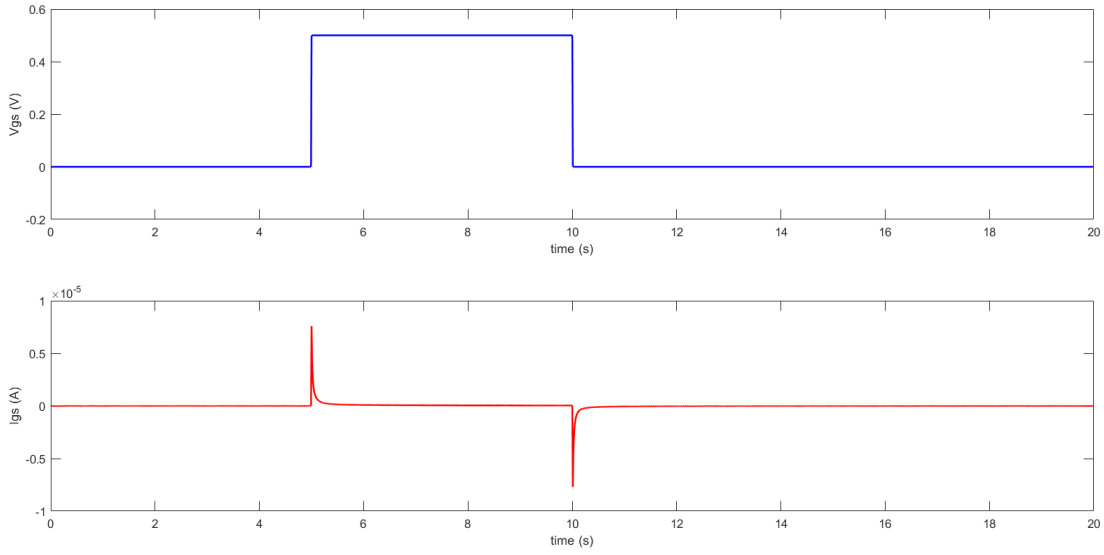

Figure 52 – Capacitance measurement: example with V_{GS}=+500 mV (in blue) and the I_{GS} response (in red)

The charge Q stored in the capacitance can be calculated as the area under the I_{GS} (Figure 52) curve. More precisely the area calculated is the between the

current curve and its linear fit of the last point before the second pulse (Figure 53). From the charge stored it is possible to calculate the capacitance (Formula (1)).

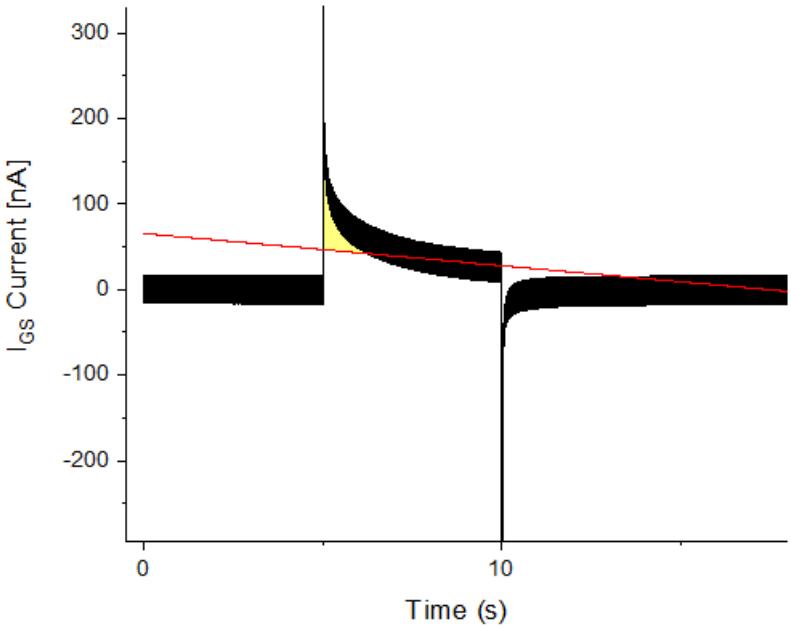

Figure 53 – The calculated area (filled in yellow) is the one between the I_{GS} curve (black) and the linear fit (red line) extrapolated considering the current points between second 8.5 and 10.

3.4.1 Real Time Measurement

In literature, in the majority of cases the detection of the target of interest is accomplished through the comparison between different electrical characterizations that are measured before and after the target exposure of the sensor. Above all, the transfer characteristic is exploited, and how the I_{DS} changes with different analyte concentrations is studied, in order to evaluate the response and the sensitivity of the device. Furthermore, from the transfer curve the transconductance and the threshold voltage are extracted and their values before and after the incubation with the target are compared.

In this work a different type of measure has been tested, namely a real time measurement, in which fixed values of V_{DS} and V_{GS} are applied (Channel 1 and Channel 2 respectively) on the EGOFET terminals, while monitoring in real time the I_{DS} trend over a long period, before, during and after the exposition of the sensor to the target. This method has been chosen in order to perform a measure as substantial

as possible, considering the instability of the device causes a strong drift in the baseline of the current. Indeed, just comparing the characterization of the device before and after the target injection, it may provide an inaccurate result about the real detection, because the signal drift may be misinterpreted as a sensing signal. Therefore tracking the bio-detection in real time could be crucial to better oversee the unpredictable evolution of the current. Anyhow it is important to point out a drawback of such typology of measure, which is the possibility to overstress the device with a prolonged imposition of a bias voltage.

A standard protocol has been followed in order to minimize variability in results, that comprises three main steps:

1. *Stabilization*: for 2 hours a blank buffer flows in the fluidic circuit. After a transient, the baseline usually becomes stable and maintains a definite trend.
2. *Sensing*: a solution of the same buffer used in the stabilization with the addition of the desired analyte is pumped into the chamber for 1 hour.
3. *Washing*: the buffer flows for 1 more hour, with the purpose of removing the adsorption of non-specific molecules of target.

Figure 54 – Flow diagram of the sensing measurement procedure.

The aim of the procedure is to identify the baseline that the current reaches during stabilization, then let the target flow into the sensor, and after the washing evaluate how the baseline has changed.

3.4.2 Transfer Real Time Measurement

Another real time measurement performed is the monitoring in time of the transfer characteristic. In this type of measure, the transfer curve is repeated 100 times, imposing a fixed V_{DS} while V_{GS} sweeps ($V_{GS} = 0.1V \rightarrow -0.8V$ and back).

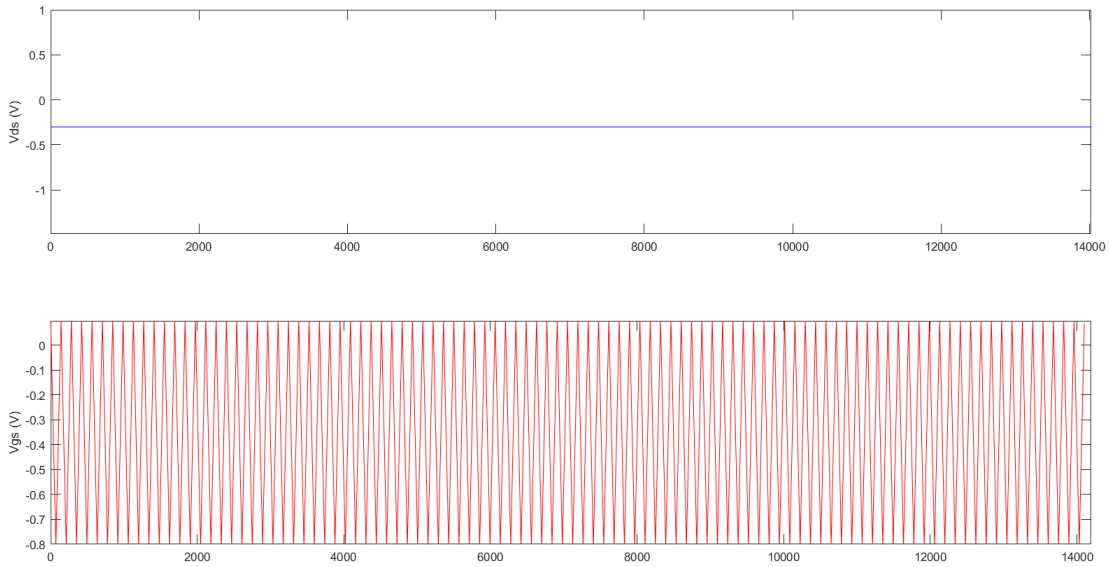

Figure 55 – Transfer real time measure: input voltages on CH1 (drain electrode, in blue) and on CH2 (gate electrode, in red)

Also in this case a fixed protocol has been followed:

1. *Stabilization*: for 20 minutes the buffer flows through the circuit.
2. *Sensing*: for 20 minutes the solution containing the target flows.
3. *Washing*: the buffer flows again for 20 minutes.

The purpose of this measure is to extract from the consecutive transfer curves the V_t and g_m values, and to monitor how their values change during the exposure to the target solution.

3.5 Measures performed

The measures have been performed in different conditions, both in terms of the target of interest and in terms of the configurations of the sensor.

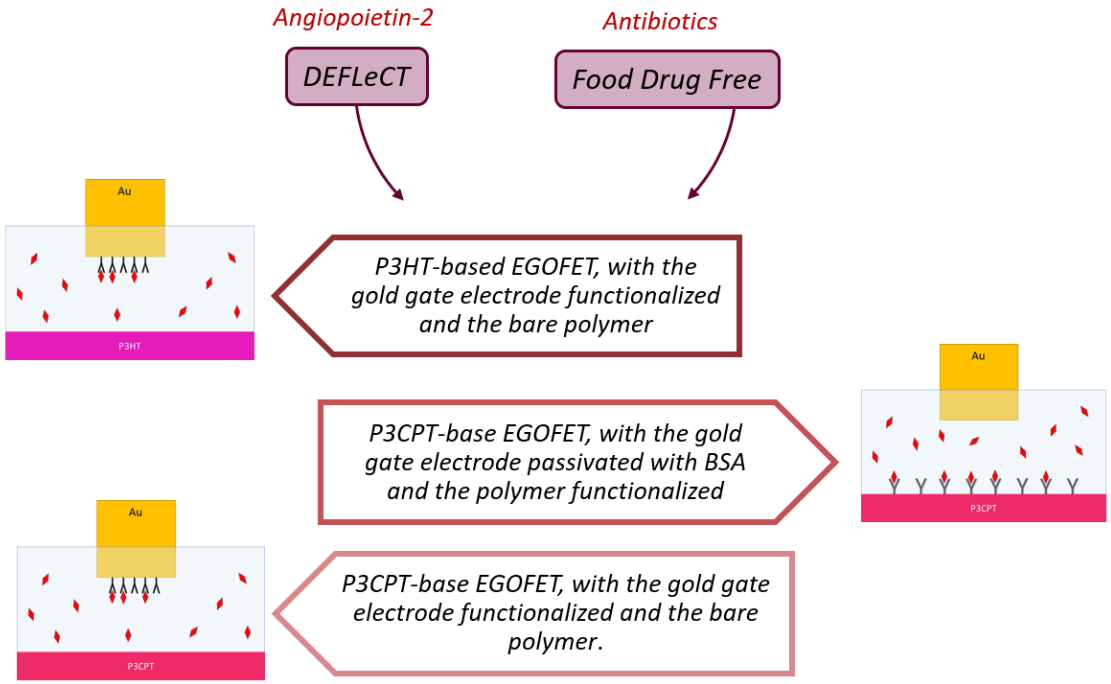

Figure 56 – Graphical abstract of the target of interest and the configuration employed.

When possible, a triplicate of each measure has been accomplished. The two major targets used in the experiments are:

- Proteins, mainly Angiopoietin-2. This research is inserted in a wider project, the *DEFLeCT* (Digital Technology for Lung Cancer Treatment). The aim of this project is to develop a technological platform for detection of lung cancer, in a prospective of enhance early diagnosis through the recognition of tumoral biomarker in low concentration.
- Antibiotics: Tetracycline. In the context of a *FDF* (Food Drug Free) project, an investigation of the performance of the device with an antibiotic solution as target has been carried on. The purpose of the project is the detection of the presence of drugs traces in food samples, considering that is an element that enhance the nowadays worldwide threat of antibiotic resistance [66]. The objective is to develop an easy to use and mobile detection platform.

Concerning the different types of configuration, the sensing mechanism will be deepened in the next paragraphs, still they are here quickly depicted:

1. *P3HT-based EGOFET, with the gold gate electrode functionalized and the bare polymer*. In order to have a specific biosensing, a functionalized surface is

needed, and in this combination the simplest way is to perform a SAM on the gold gate surface. In fact, P3HT without any surface modification does not expose any functional group.

2. *P3CPT-base EGOFET, with the gold gate electrode passivated with BSA and the polymer functionalized*. This configuration has been chosen considering the possibility of the P3CPT to be easily functionalized, thanks its external carboxyl groups. To avoid the participation of the gold gate surface in the sensing, the latter has been passivated with BSA.
3. *P3CPT-base EGOFET, with the gold gate electrode functionalized and the bare polymer*. About P3CPT polymer there are not enough information in literature about its capacitance with respect to the gold one. For this reason both configurations have been tested: with the functionalization on the polymer and bare gold, and with the functionalization on the gold surface and bare polymer.

In any case the basic principle is that when the target solution flows inside the chamber, the binding between the antigen and the receptor causes a change in the capacitance of the EDL, on the gate or on the OSC surface, depending which is the functionalized surface. The variation in the capacitance involves a change in the figure of merits of the EGOFET, and this effect could be monitored during the real time current measures, in which it manifests as a change in the I_{DS} current.

The aim of this measures is to obtain a specific sensing, and this should be expressed by a permanent change in the baseline of the current after the sensing of the target. The correlation between the change in the baseline and the specificity of the sensing relies on the assumption that the biorecognition element recognizes in a specific way the analyte, and the stable binding makes the baseline permanently change. That means that the I_{DS} baseline reached during the stabilization period should change during sensing and should not return back to the previous value after the washing. This behaviour is desirable because it implies that the washing did not effect a stable binding between the receptors and the analyte, and thus the capacitance of the active surface is firmly affected by the presence of the target molecules.

However, the difficulty in the fitting of the baseline in the I_{DS} trend during the stabilization period should not be underestimated. Considering the pronounced drift of the current, it is not always easy to have a fitting adherent to the current curve and

thus to be sure about the predicted trend. This is a limit for the extraction of the distance from the existing current, obtained when the sensor detects the target presence, and the predicted trend that the current should have followed in the case of no target solution seen by the sensor. Of course this lack in the quantification of the change in the baseline is an obstacle for an easy interpretation of the results.

The fit has been performed using the software Origin *(OriginLab Corporation)*, and when suitable the exploited fitting function is the "Double decreasing exponential".

3.6 Device functionalization

The selective biorecognition element (Figure 1) is the most critical component in the development of a biosensor because it lends the indispensable specificity required to detect an analyte of interest. In most cases during this work, the biosensing element to be immobilized was a protein, specifically an antibody, which could be exploited for the recognition of its target through the antigen-antibody interaction. As seen in the Chapter 2, different approaches can be adopted, as performing the bio-functionalization procedure on the surface of the gold gate electrode [19] or on the organic polymer semiconductor [20]. The surface of the device is commonly modified in order to expose a chemical functional group, such as carboxyl, hydroxyl, or amino groups, which can act as anchor points for the biorecognition elements, consisting of receptors or specific chemical moieties.

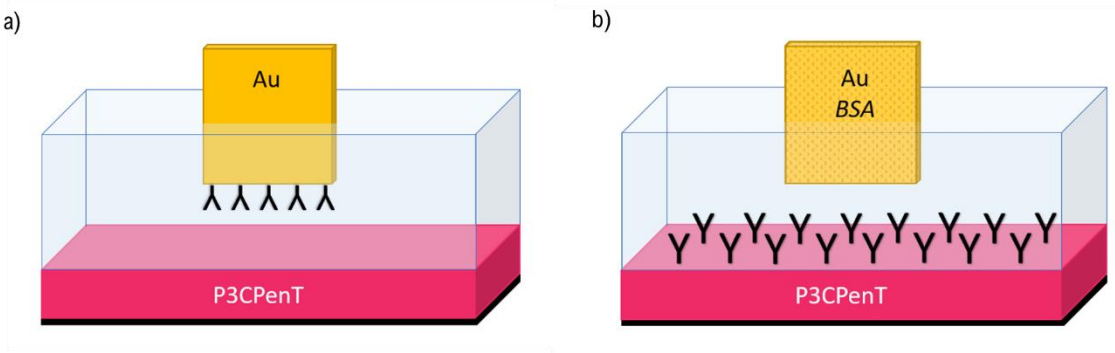

Figure 57 – Exemplificative pictures of the different types of bio-functionalization: on a) the gold gate electrode surface or b) the polymer surface.

3.6.1 Gold gate electrode functionalization

Concerning the functionalization of the gold gate electrode, the most widely used strategy is to form a Self-Assembled Monolayer (SAM) of thiols. SAMs represent a

versatile and simple method to arrange an organic monolayer on an inorganic substrate/surface [67]. They are nano-structured assemblies formed by a chemical functionality with high affinity with the substrate (ligand or headgroup), an alkyl chain (spacer) and a terminal functional group (Figure X) [68]. During the SAM formation, the molecules in solution are adsorbed onto the substrate and spontaneously self-assemble in crystalline or semicrystalline structures. The most common type of SAMs is the one formed from the adsorption of alkyl thiols on gold, thanks to the high affinity and strength of S-Au bonds [68].

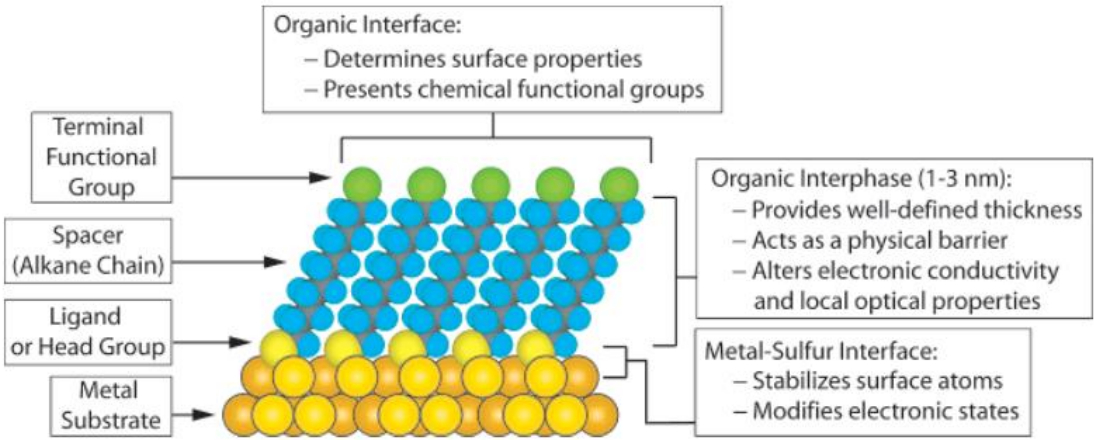

Figure 58 - Schematic illustration of an ideal SAM of alkyl thiols on a gold surface. Reprinted from [68]

Alkyl thiols (R-SH) are organic compounds characterized by the thiol (or sulfhydryl) functional group (-SH), bonded to an alkyl chain (R). In SAMs, the S-Au bonding is the adsorbent species, while the alkyl chains auto-assembly on the substrate, due to van der Waals interaction.

In this work, the organic compound used is 3-Mercaptopropionic acid, consisting of a thiol head group, a short carbon chain (2C) and a carboxyl end group. Thereby, the SAM obtained makes the surface covered by -COOH groups, available to further binding with receptors.

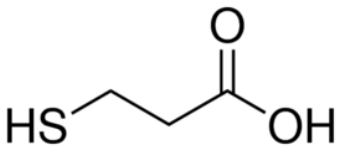

Figure 59 – Chemical structure of 3-Mercaptopropionic acid

The kinetic of the monolayers formation depends on several factors, some controllable, like temperature, solvent, concentration, chain length, and others related to the specific system, such as the rate of reaction with the surface and the reversibility of adsorption [69].

To prepare a SAM of thiols on gold, the most common protocol is represented by the immersion of the sample, in this case the gold electrode, in an ethanolic solution of thiols (1-10 mM) for about 12-18 hours, at room temperature [68]. In a brief period of time (milliseconds to minute), the exothermic adsorption of the anchoring groups occurs, while the ordered packing of the chains requires a longer period (on the order of several hours) [69].

In this work, for practical issues, for some experiments a shorter protocol for SAM formation has been accomplished, with an incubation time of 1 hour only. In other cases, a 48-72 hours incubation has been performed in an inert environment. The complete procedure pursued is the following:

- The gold samples are cleaned through immersion in acetone for about 5 minutes, and then dried with nitrogen.
- A 10 mM ethanolic solution of thiol is prepared, under a fume hood.
- The samples are incubated in a beaker or in a closed reactor by covering them with the thiol solution. Follows the incubation period (1 h or 48-72 h).
- The samples are cleaned through a serial immersion into two beakers of ethanol and one of deionized water. The samples are dried with nitrogen.

At this stage, the samples surface is supposed to be covered by a monolayer of thiols that expose carboxylic groups. The next step is the activation of these functional groups. This step is required to increase the -COOH reactivity to amino groups, to form an amide bond with the receptor and immobilize a layer of antibodies on the gold surface. A common technique is the conjugation through amide coupling [73]: in this reaction, the crosslinkers cause the direct conjugation of carboxylates to primary amines, but do not take part in the final chemical structure, thus are defined as zero-length carboxyl-to-amine crosslinkers [70].

The protocol adopted includes the use of 1-Ethyl-3-(3-dimethylaminopropyl)-carbodiimide hydrochloride (EDC) and N-hydroxy-sulfo succinimide sodium salt (Sulfo-NHS) [70]. EDC reacts with the -COOH forming an active O-acylisourea

intermediate, which is unstable. This compound may follow different paths (Figure 60):

- It could be displaced by nucleophilic attack by a primary amino group, which forms an amide bond with the original -COOH.
- EDC could couple the carboxyl to Sulfo-NHS, forming an amine-reactive Sulfo-NHS Ester, which is dry-stable (more stable intermediate compared to the O-acylisourea one); this intermediate allows the coupling with the primary amine of another molecule through the formation of an amide bond, resulting in a stable conjugate.
- Otherwise, the intermediate is displaced through hydrolysis and the carboxyl is regenerated.

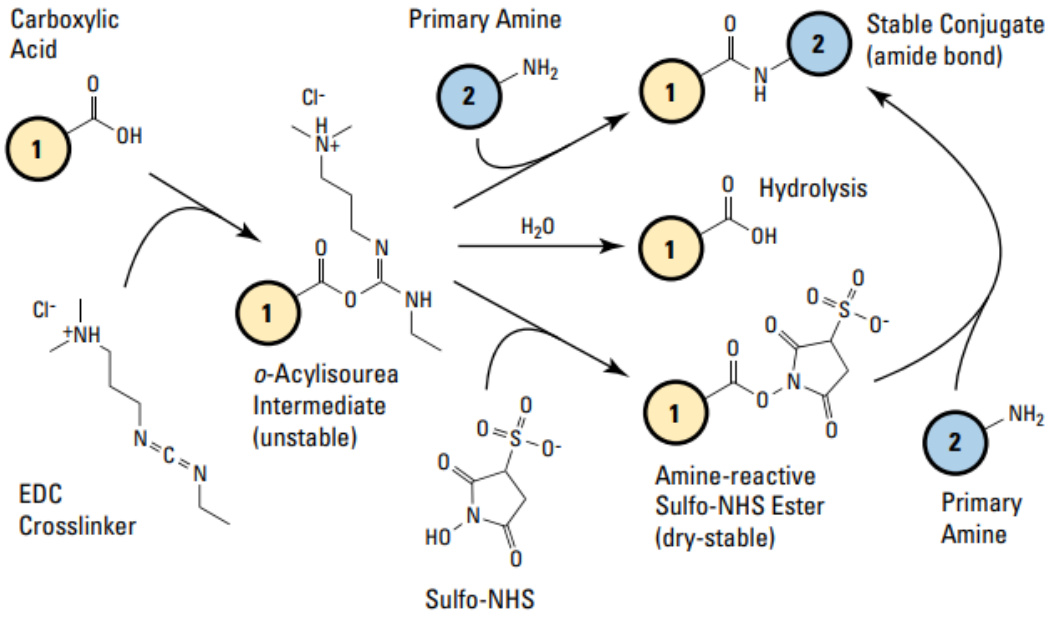

Figure 60 – Scheme of EDC (carbodiimide) and Sulfo-NHS crosslinking reaction. In this work the compound 1 is a thiol of the SAM exposing the carboxyl group; the compound 2 is the receptor. Reprinted from [70]

The procedure followed for the -COOH activation is:

- The samples are placed in a multiwell plate, in a MES buffer (4-morpholinoethanesulfonic acid, pH 4.8) for 15 minutes, in order to achieve the highest activation efficiency in acidic conditions.

- An EDC - Sulfo-NHS solution is prepared in MES buffer, by using 4 mM and 10 mM, respectively. The samples are kept in this solution for 15 minutes.
- The samples are washed in PBS 1x for 5 minutes. This step is repeated three times, changing the buffer. PBS is the buffer of choice because the efficiency of the bio-conjugation is highest when close to neutral pH.

For the detection of proteins, in particular Angiopoietin-2 (Ang2), the functionalization involved the Ang2 antibody. After the previous steps, the surface of the sample is ready for incubation with the antibodies. A droplet of solution containing anti-Ang2 antibodies (1 µg/ml) in PBS is carefully deposited on each sample and then placed at +4 °C, overnight. The day after, the samples are washed in PBS supplemented with 0.05% Tween-20 (PBS-tween) for 5 minutes on an orbital shaker (three times) and finally dried out with nitrogen.

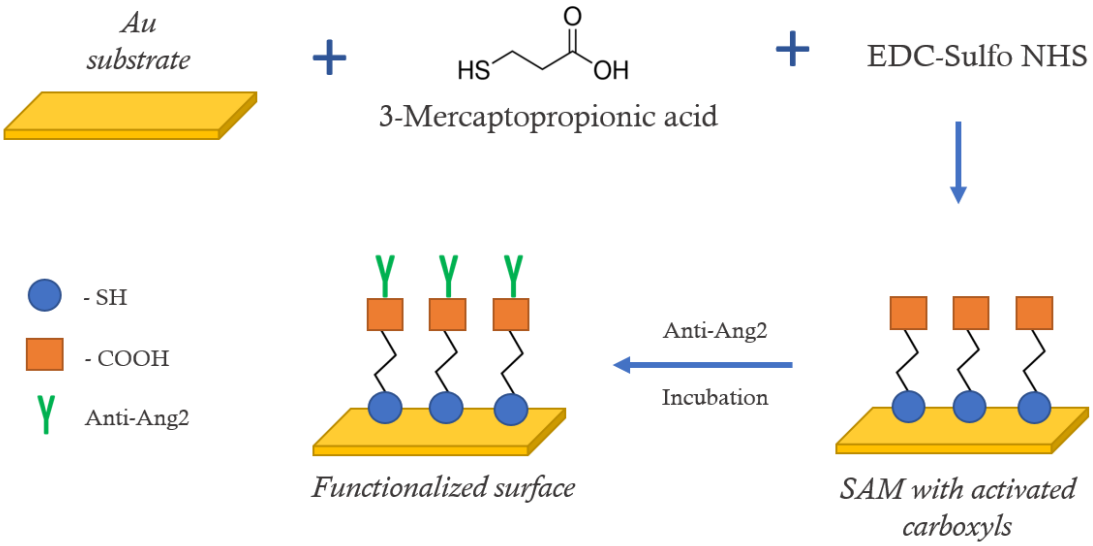

Figure 61 - Schematic illustration of the protocol used to obtain a functionalization with antibodies on the gold gate electrode surface.

In the case of the detection of antibiotics, a functionalization with aptamers has been used. Aptamers are single-stranded oligonucleotides, characterized by a precise 3D structure that allows a specific binding with the target molecule [71]. In this case, aptamers were designed to be able to recognize a specific target for antibiotics molecules, in particular Oxytetracycline hydrochloride, Tetracycline. The aptamers employed were eight bases long, selected from the literature [72]. Two modified versions have been used: the sequence ending with a thiol group (A8-NH_2, sequence:

5'-/5AmMC6/CGG TGG TG-3') and the one ending with an amino group (A8-NH_2, 5' Amino Modifier C6, sequence: 5'-/5AmMC6/CGG TGG TG-3').

3.6.2 Organic Semiconductor functionalization

The polymers used in this work are P3HT and P3CPT. P3HT does not expose any functional group and thus it is not used as a sensing surface in any test. Instead, its derivative P3CPT exposes a –COOH end group, and so it represents an interesting option as OSC in EGOFET application, allowing a direct functionalization without any surface treatment.

Regarding the activation of the carboxyl group on the P3CPT surface, the same process listed for the activation of the -COOH exposed by the SAM on the gold gate surface has been performed. This configuration has been used to detect Ang2. The antibodies immobilization procedure is the same cited in the case of the gold surface. Here the steps are resumed:

- The samples are cleaned in isopropyl alcohol.
- Activation of the carboxyl groups: EDC and Sulfo-NHS crosslinking reaction.
- Overnight incubation at +4°C with the solution of anti-Ang2 antibodies (1 µg/ml) in PBS
- Washing in PBS-tween.

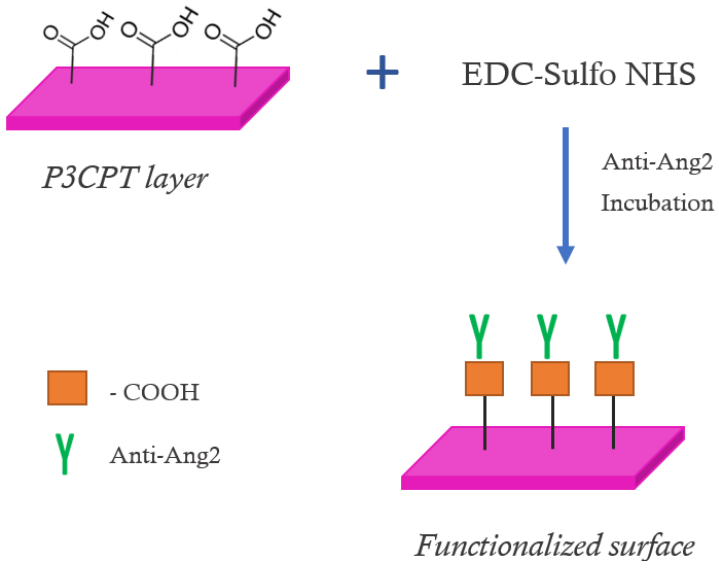

Figure 62 - Schematic illustration of the different steps to obtain a functionalization with antibodies on the layer of P3CPT deposited on the chip.

Chapter 4

Results and discussion

In this chapter the key results achieved during the experimental tests are shown. The outcome will be presented divided firstly on the basis of the different target molecules, and then on each type of configuration of the sensor. At the end of the chapter, some minor results concerning different configurations and targets will be exposed, too.

4.1 Angiopoietin-2

As already anticipated, to perform a specific biosensing it has been exploited as a probe on the active surface the Anti-Ang2. Antibody–antigen recognition process is at the basis of many biosensing devices, due to the high specificity of the binding.

The functionalization has been tested both on the polymer surface and the gold gate surface. In the following tests the target solution is Ang2 at concentration of 500 ng/ml diluted in PBS 0.01x, and the latter is the buffer solution used during stabilization and washing. Any exception will be declared.

4.1.1 P3HT-based EGOFET with gold gate electrode functionalized and bare polymer

The first configuration employed is the one in which the organic semiconductor of the EGOFET is P3HT, because this polymer was involved in previous studies [58][74]. In this case the functionalized surface is the gold gate electrode, on which a SAM of thiols is exploited to obtain a surface functionalized with the Anti-Ang2. After the stabilization period, in the EGOFET chamber flows the solution with the analyte, and the protein molecules bind with the antibody in a specific and solid way, but they also may be adsorbed on the polymer surface in a non-specific way.

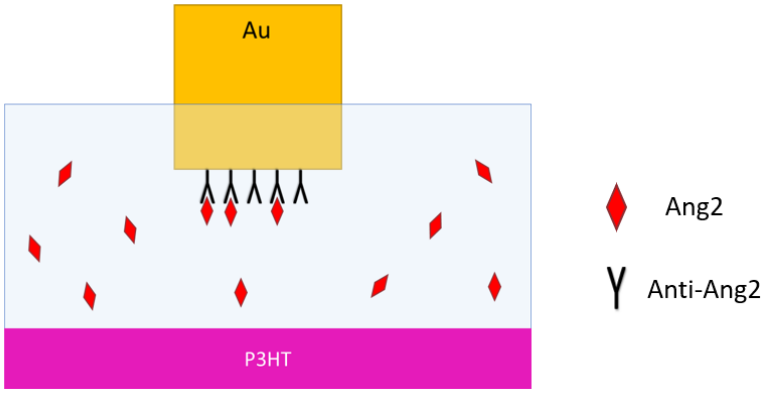

Figure 63 – Schematic picture of the P3HT-based device, with a simplified illustration of the functionalization with antibodies on the gold surface and the binding with the Ang2 molecule.

Experimental measurements in this configuration have shown that it has not reached a specific sensing (Figure 64).

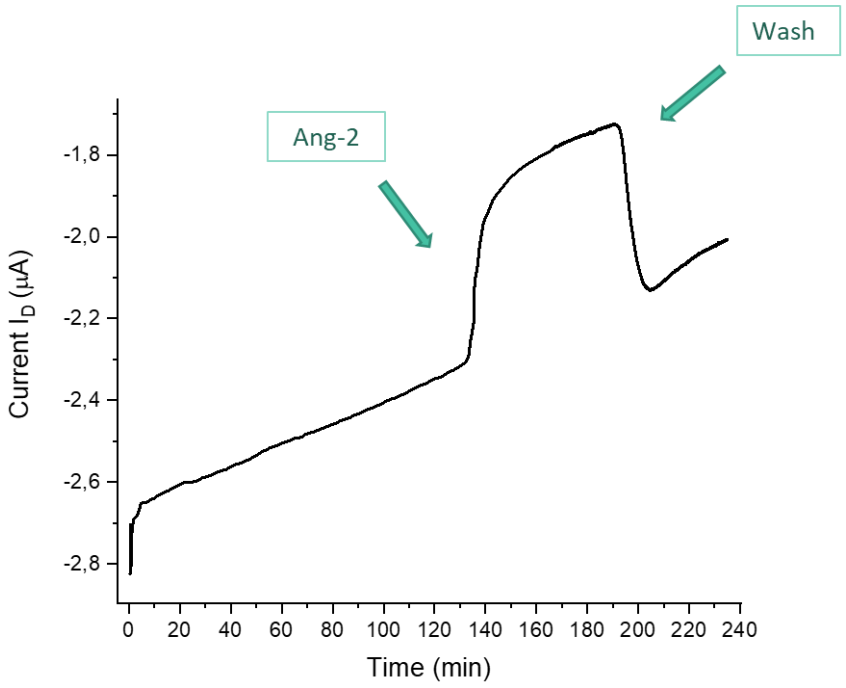

Figure 64 – Real time measurement (I_D current – time curve) of an experiment performed with P3HT-based EGOFET, with the functionalization on the gold electrode. Biosensing of 500 ng/ml of Ang2 diluted in PBS 0.01x.

The current during the exposition to the target significantly changes, with a variation of around 20%. Nevertheless, during the washing the current returns to the previous

baseline, and that means that the detected signal is not due a permanent binding with the biorecognition element.

An explanation may be that the EDL formed on P3HT interface exhibits a smaller capacitance than the EDL on the gold interface, and that means that in the harmonic series the prevailing capacitance is the one on the polymer:

$$\frac{1}{C_{tot}} = \frac{1}{C_{gate}} + \frac{1}{C_{OSC}}$$

$$if\ C_{gate} \gg C_{OSC} \rightarrow\ C_{tot} \cong C_{OSC}$$

Remembering the link between the current and the capacitance:

$$I_{DS} \propto (\mu C)\left(\frac{W}{L}\right)$$

it indicates that the main contribute in the changing of the channel current is due changes in the C_{OSC}. Basically this means it can be detected what happens on the polymer surface, rather than what happens on the gold one.

Therefore, it is possible that during the period in which n the electrolyte chamber flows the target solution, along with the Ang2 molecules captured by the antibodies, some molecules adsorb in a non-specific way on the surface of the polymer. During this sensing phase, it is observed a change in the measured I_{DS}, that reaches a new baseline. However, during the washing (the phase in which in the chamber flows only the buffer solution, without target molecules) the adsorbed molecules may be washed away, and that explains why the current trend comes back to the previous baseline.

The sensor clearly responds to a high quantity of target (500 ng/ml), but it has been tested also with lower concentration, and a response is detected until 5 ng/ml (data not shown).

4.1.2 P3CPT-based EGOFET with polymer functionalized and gold gate electrode passivated

Considering the above mentioned outcomes with the P3HT-based EGOFET, it has been decided to test the functionalization of the polymer surface, exploiting the P3CPT polymer, because its hydrocarbon chain exposes -COOH groups that allow

an easy functionalization. During the tests done in this configuration, in order to limit the adsorption of the protein on the surface of the gate electrode, the gold has been passivated in BSA.

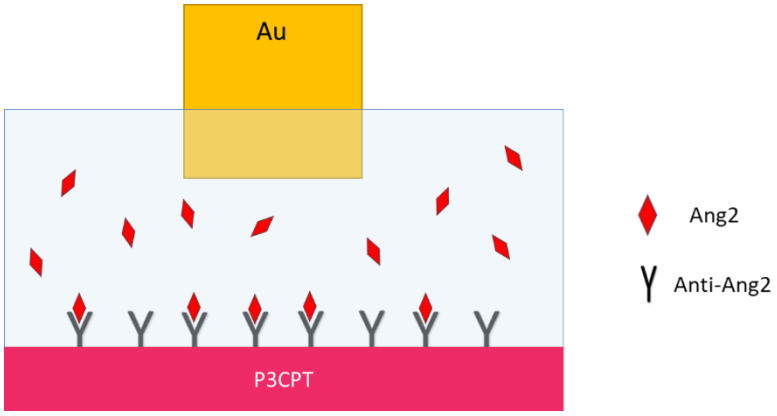

Figure 65 – Schematic picture of the P3CPT-based device, with a simplified illustration of the functionalization with antibodies on the polymer surface and the binding with the Ang2 molecule.

In this configuration only two tests have been accomplished, and the real time curves are here shown.

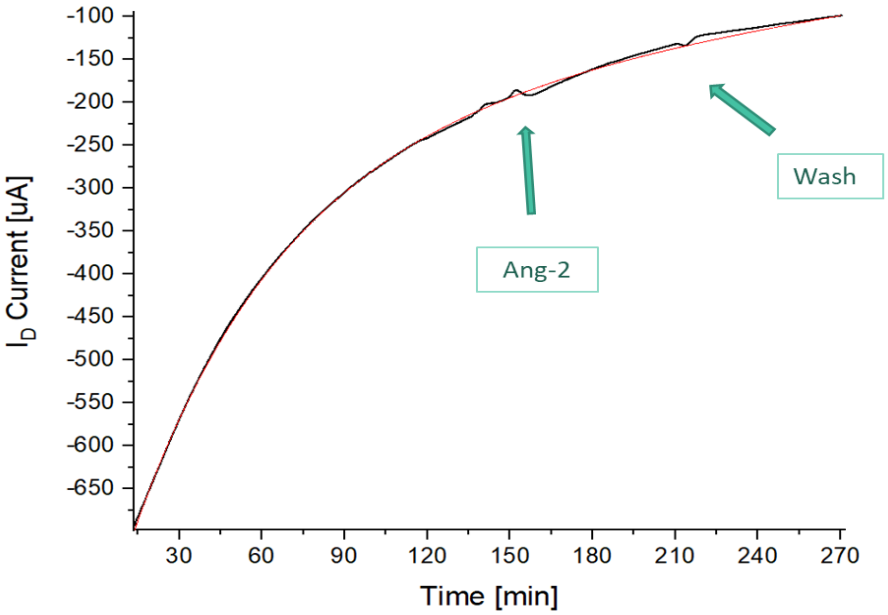

Figure 66 – *Test 1*, Real time measurement (I_D current – time curve) of an experiment performed with P3CPT-based EGOFET, with the functionalization on the polymer. Biosensing of 500 ng/ml of Ang2 diluted in PBS 0.01x. In red the baseline fitted during the stabilization, "Double decreasing exponential" fit.

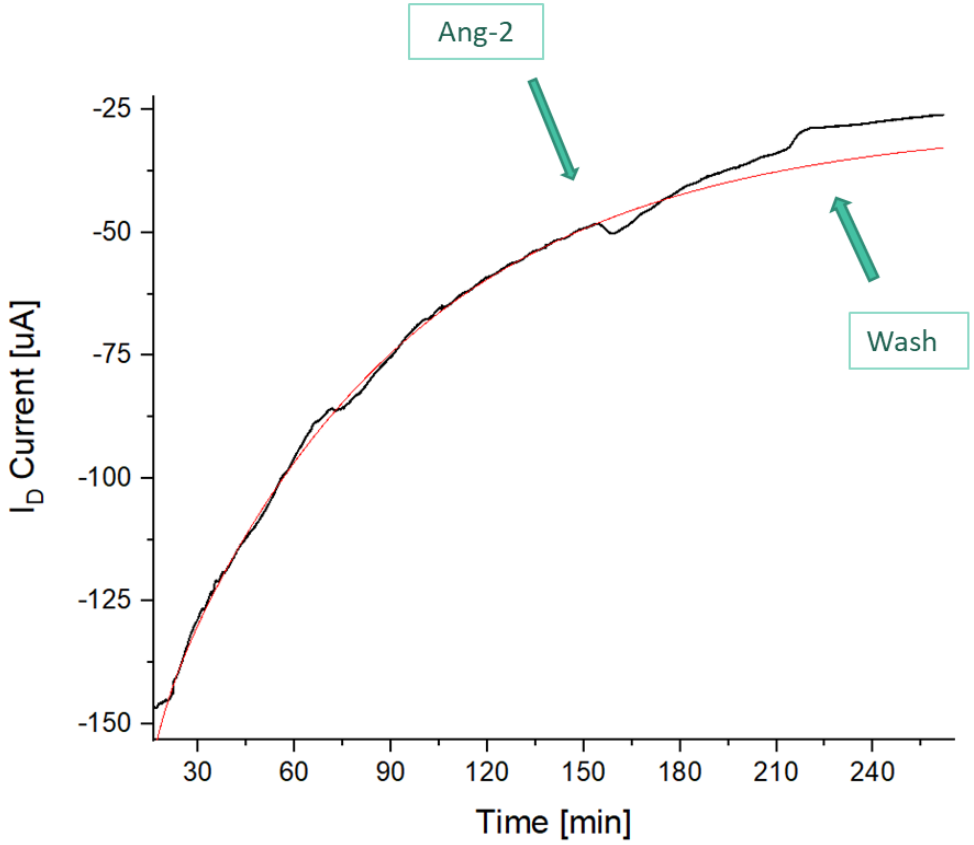

Figure 67 – *Test 2*, Real time measurement (I_D current – time curve) of an experiment performed with P3CPT-based EGOFET, with the functionalization on the polymer. Biosensing of 500 ng/ml of Ang2 diluted in PBS 0.01x. In red the baseline fitted during the stabilization, "Double decreasing exponential" fit.

In contradiction with the expectations, the obtained curves did not show a clear and unique result. In fact, in the *Test 1* (Figure 66) the baseline seems to get back to the stabilization value, while in the *Test 2* (Figure 67) the impediment in a precise fit of the curve makes hard to interpret the results as a specific sensing.

A possible explanation of the unsatisfactory results could be that does not take place a correct functionalization of the polymer surface or the correct protein-antibody binding. To remove any doubt, an ELISA (enzyme-linked immunosorbent assay) has been performed, and it has been proved a strong signal on the P3CPT surface (Figure 68). That means that the surface is actually functionalized with the antibodies, and that the binding with the protein does happen.

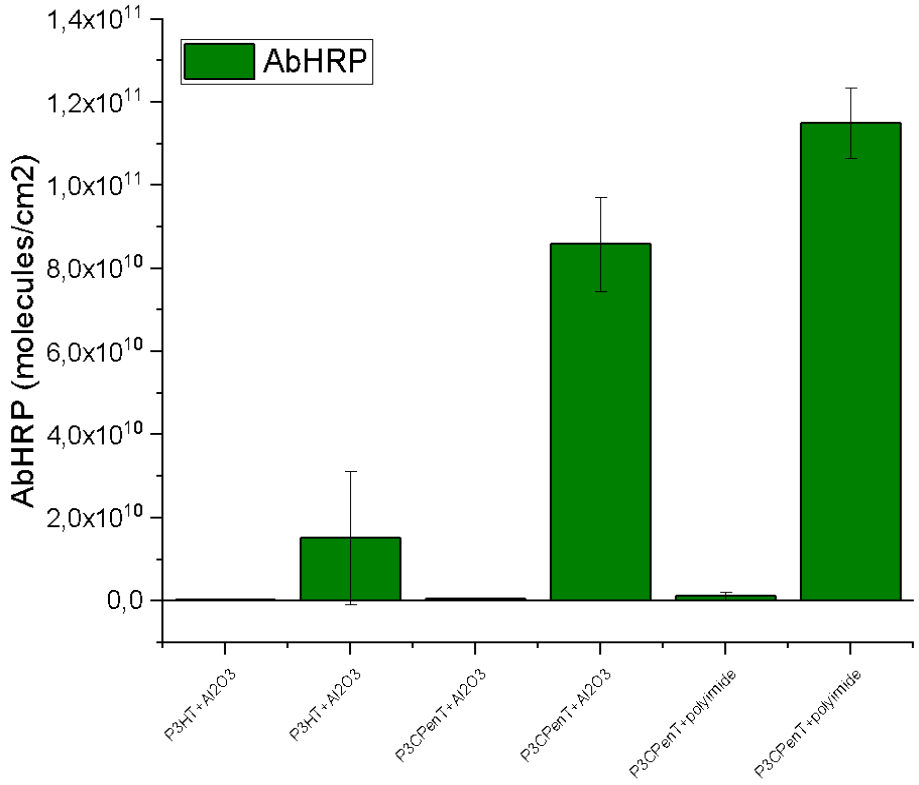

Figure 68- Results of an ELISA assay, both on P3HT and P3CPT. The result shows that the functionalization with antibodies worked on the P3CPT surface.

Excluded this hypothesis, it is possible that the P3CPT has a different behaviour with respect to P3HT, namely its EDL capacitance is not as low as in the previous case, and thus it is not the value that dominates in the capacitance series:

$$\frac{1}{C_{tot}} = \frac{1}{C_{gate}} + \frac{1}{C_{OSC}}$$

$$if\ C_{OSC} \gg C_{gate} \rightarrow\ C_{tot} \cong C_{gate}$$

This assumption is enhanced by the data in literature [40][75], according to which P3CPT shows higher C_{OSC} value compared to P3HT. Hence, although the advantage of the presence of carboxyl groups, this configuration may not be the best option to obtain a signal representing the specific sensing.

A table with key parameters extrapolated from the transfer characteristic of the chosen device (acquired before and after the sensing) of the two tests is presented.

		$\lvert I_{DS,max} \rvert$	V_{th}	Dev V_{th}	$g_{m,max}$
Test 1	Pre Sensing	5,26E-05	-4,22E-01	7,12E-03	2,74E-04
	After Sensing	6,22E-05	3,85E-01	6,37E-02	9,05E-05
Test 2	Pre Sensing	1,28E-04	-3,76E-01	4,24E-02	5,56E-04
	After Sensing	8,49E-05	-1,10E-01	3,30E-02	2,12E-04

In terms of figure of merits the two devices tested behaved in a similar way, with a decrease of the maximum drain current and a tendency of threshold voltage to positive values, features that may be due a degradation of the polymer for the electrical stress and the contact with the liquid electrolyte. The comparable pre-sensing transconductance value may be linked to the similar amplification of the sensing signal in the two cases.

Considering the low number of tests performed, this type of experiment needs to be repeated in future works in order to better evaluate the potentialities of the polymer functionalization.

4.1.3 P3CPT-based EGOFET with gold gate electrode functionalized and bare polymer

The previous considerations led to the choice of testing the configuration in which the OSC is P3CPT, and the functionalization is performed on the gold gate surface.

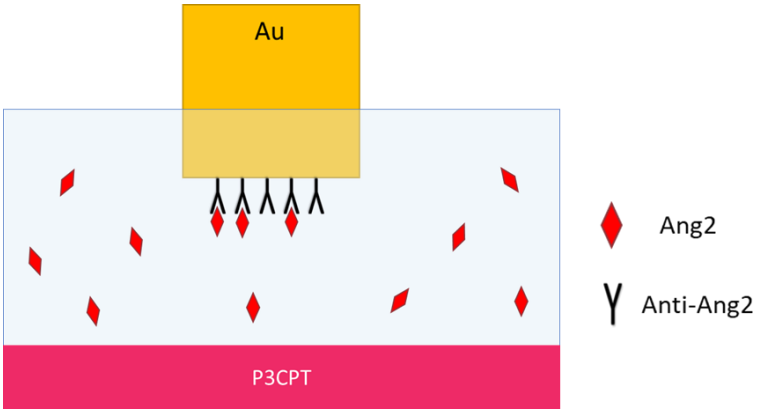

Figure 69 – Schematic picture of the P3CPT-based device, with a simplified illustration of the functionalization with antibodies on the gold surface and the binding with the Ang2 molecule.

This is the combination that has driven to the most promising outcomes (Figure 70).

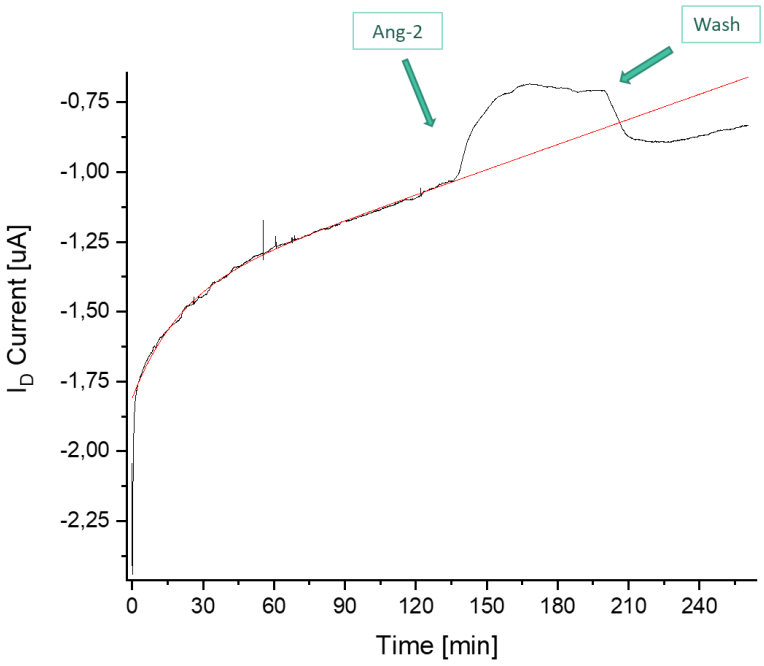

Figure 70– Real time measurement (I_D current – time curve) of an experiment performed with P3CPT-based EGOFET, with the functionalization on the gate. Biosensing of 500 ng/ml of Ang2 diluted in PBS 0.01x. In red the baseline fitted during the stabilization "Double decreasing exponential" fit.

A significant sensing signal is detected in this configuration, with a clear change in the baseline, that may be interpreted as a result of a permanent and specific binding between the antibody and the protein. The current decreased in absolute value during

the exposition to the analyte solution, and subsequently reaches a higher value compared to the predicted baseline. According to what has been previously said, the explanation for the proper functioning of this configuration may be that the capacitance of the EDL at the P3CPT interface is big enough to make the capacitance of the EDL at the gold interface dominates in the series:

$$\frac{1}{C_{tot}} = \frac{1}{C_{gate}} + \frac{1}{C_{OSC}}$$

$$if\ C_{OSC} \gg C_{gate} \rightarrow\ C_{tot} \cong C_{gate}$$

4.1.4 Angiopoietin-2: discussion

To sum up, with Ang2 as target and anti-Ang2 as molecules for the functionalization, the PH3T-based EGOFET did not show a specific sensing. That is probably due the low capacitance with respect to the gold surface, that did not allow the changes in the capacitance of the gold to be detected. A possible future step could be to downsize the gate electrode (the capacitance is inversely proportional to the dimension of the capacitor). As regards to the configuration with the P3CPT-based EGOFET, the functionalization on the polymer returned sensing signals low and difficult to interpret, while the functionalization on the gold gave the most interesting results. Both configurations should be tested in future experiments.

4.2 Antibiotics

In order to have a specific sensing, in this case the functionalization of the active surface has been done exploiting aptamers as recognition units. The aptamers employed for the tetracycline have 8 DNA bases.

Taking a cue from the outcome obtained with the protein detection, the configurations used comprise the functionalization of the gold surface, both with P3HT and P3CPT as semiconductor layer. A future investigation with the functionalization of the polymer will be useful to complete the picture.

4.2.1 P3CPT-based EGOFET with gold gate electrode functionalized and bare polymer

To enhance the binding between the antibiotic molecule and the aptamer, a suitable buffer is deionized water (ddH_2O). The first experiments involved this buffer and a solution of Tetracycline (concentration 20 or 200 ppm) in deionized water. It is important to mention that deionized water is not the better electrolyte for the device, considering the ultra-low concentration of ions has an effect on the EDL formation, and that has an effect on the EGOFET performances. In particular, it is possible to see that the transfer characteristics often present a much higher hysteresis with ddH_2O, compared to when PBS is employed.

The most significant results are displayed in the following pages.

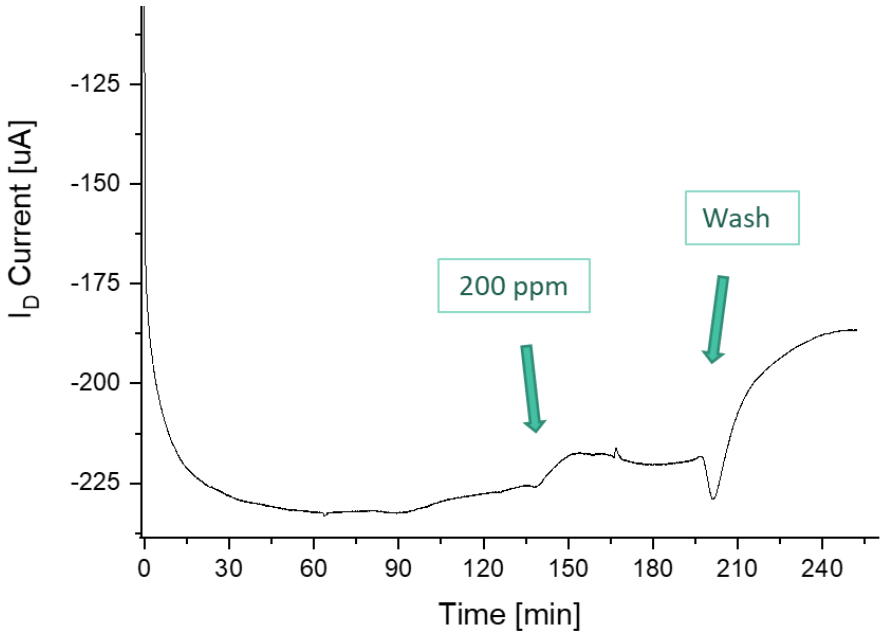

Figure 71 – *Test 1*, Real time measurement (I_D current – time curve) of an experiment performed with P3CPT-based EGOFET, with the functionalization on the gate. Biosensing of Tetracycline 200 ppm, diluted in deionized water.

In this case, after the exposition to the target solution, the sensor responds with a decrease of the current, while the washing of the target in excess causes a little spike (probably due to the pression of the pump turned off and back on for the change in the buffer) followed by a strong variation of the baseline.

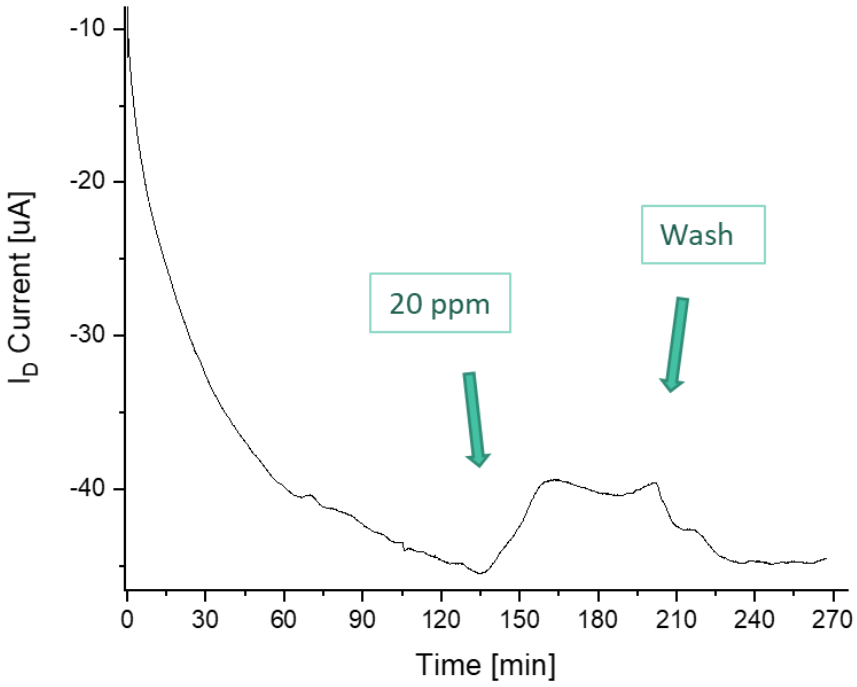

Figure 72 – *Test 2*, Real time measurement (I_D current – time curve) of an experiment performed with P3CPT-based EGOFET, with the functionalization on the gate. Biosensing of Tetracycline 20 ppm, diluted in deionized water.

Also in this case the sensor responds to the target with a significant variation of the current. Anyhow after the washing, the current increases again, but it seems to have a baseline different that during the stabilization. The unpredictable drift of the current affects the interpretation.

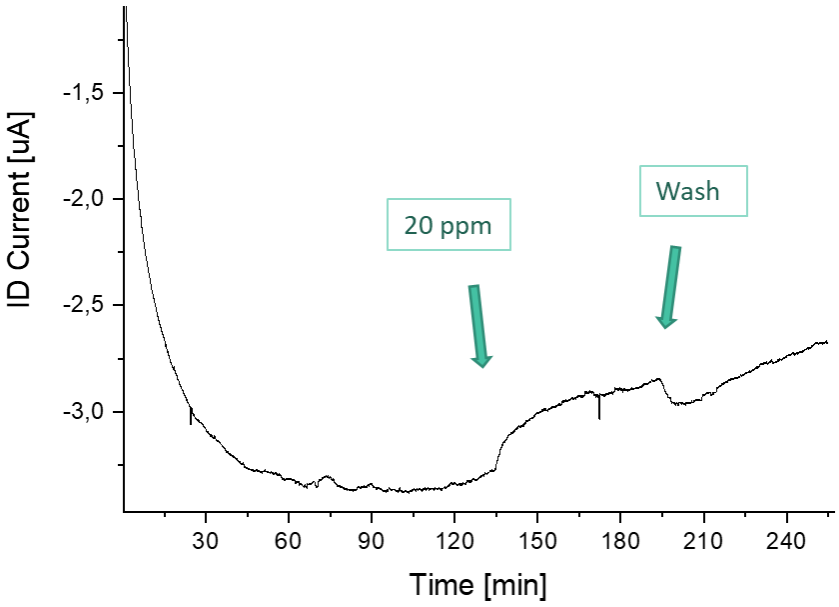

Figure 73 – *Test 3*, Real time measurement (I_D current – time curve) of an experiment performed with P3CPT-based EGOFET, with the functionalization on the gate. Biosensing of Tetracycline 20 ppm, diluted in deionized water. A consistent signal has been detected during sensing, but it seems non-specific, referring to the return to the baseline.

Finally, in this experiment, after a moderate sensing signal, the current seems to take back exactly the baseline.

About the shown curves, the main concern is clearly the non-repeatability of the results. In fact, even if in some cases a significative sensing signal has been detected, with a change in the baseline after the exposure to the target (*Test 1*), still in other cases in similar condition, a weak sensing has been sensed, with the current that returns to the stabilization baseline (*Test 2* and *3*). In any case, it is evident that in all three cases shown the unpredictable drift of the current does not allow to fit the baselines with a common fitting function, and that is, as for the previous cases, a limit in the interpretation and in the current method.

To compare these three tests, a table with the figure of merits is shown.

		$\lvert I_{DS,max} \rvert$	V_{th}	Dev V_{th}	$g_{m,max}$
Test 1	Pre Sensing	2,14E-04	7,24E-01	1,27E-02	2,79E-04
	After Sensing	2,45E-04	2,97E-01	2,54E-02	4,04E-04
Test 2	Pre Sensing	1,36E-05	-9,80E-02	2,85E-02	3,60E-05
	After Sensing	5,81E-05	5,77E-01	1,83E-02	8,24E-05
Test 3	Pre Sensing	2,55E-06	-2,62E-01	7,28E-03	9,37E-06
	After Sensing	5,29E-06	-1,01E-01	4,88E-03	1,44E-05

It is possible to observe that even if the devices are tested in the same condition, the ranges of current vary of one or two orders of magnitude between the three cases. The nature of this difference is still not clear, may be linked with the fabrication processes or with the functionalization procedure, that are both steps operator-dependent. From the table it is also possible to read that the third case, in which the signal detected was the weakest, is also the case with the lower transconductance.

A factor that must be taken into account is that during these experiments the short protocol of SAM formation on the gold surface has been exploited. To reduce the antagonist factors against a proper and repeatable measure, a longer and most correct procedure has been followed. So, a long incubation with the thiols has been accomplished, in inert environment. In these cases the NH_2-apamers have been employed, bonded to the -COOH groups exposed by the SAM. Despite this, still non uniform results have been obtained in the experiments, achieving some good and specific sensing (Figure 74), but also several tests in which no signal has been detected.

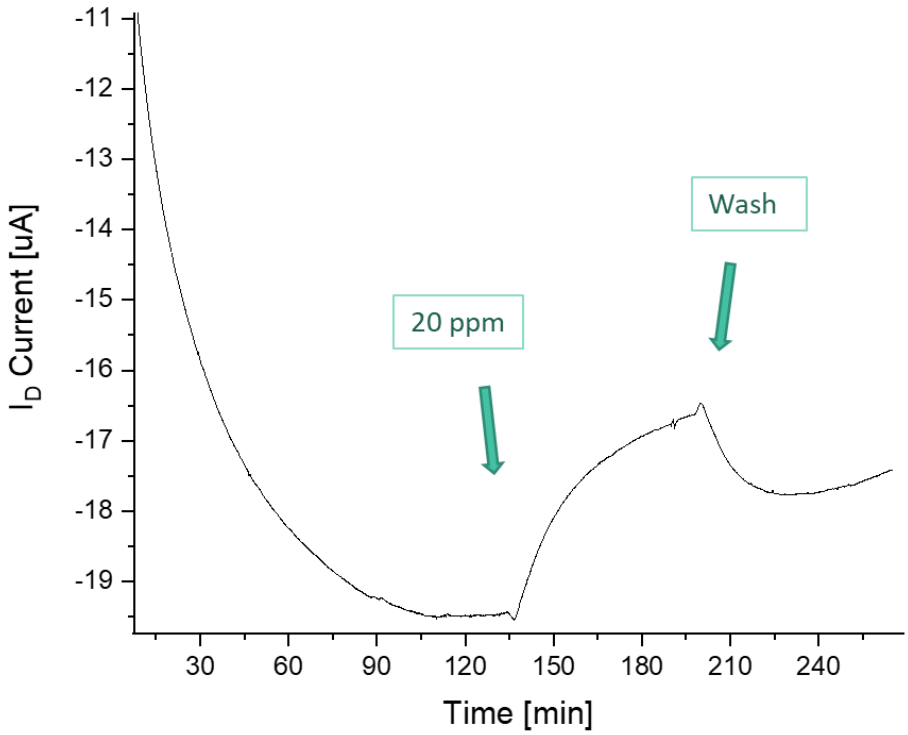

Figure 74 – Real time measurement (I_D current – time curve) of an experiment performed with P3CPT-based EGOFET, with the functionalization on the gate. Biosensing of Tetracycline 20 ppm, diluted in deionized water. A consistent specific signal has been detected during sensing.

In the experiment shown in Figure 74, the sensor detected a consistent signal, with the current that after the washing stabilizes on a baseline that appears different from the previous one.

Anyhow, a relevant factor that had a remarkable impact on the controversial results of these experiments is the low solubility of Tetracycline in water. In fact, after some tests it has been clear that the poor solubility of the drug in deionized water (even if the solution was shaken and sonicated) is an obstacle for a correct sensing. First of all, it is hard to be sure about the effective concentration of an aliquot taken from a not properly dispersed solution. Moreover, the molecules could be aggregated in clusters that do not correctly interact with the receptors.

To reduce this effect, a different version of the antibiotic has been chosen, namely the Oxytetracycline hydrochloride, which is easily soluble in water. Because of the presence of the hydrochloric acid, this solution has an acid pH (around 3.5 at 200 ppm). Considering that the sensor is sensitive to the pH changes, a phosphate buffer

has been used (Na_2HPO_4 5mM). This latter solution (Oxytetracycline HCl in phosphate buffer) appears clearer and more dispersed compared to the previous one (Tetracycline in ddH20), enhancing the suspect that the low performances in detection of the Tetracycline may be affected by this feature. The experiment accomplished in this condition is shown in the following figure.

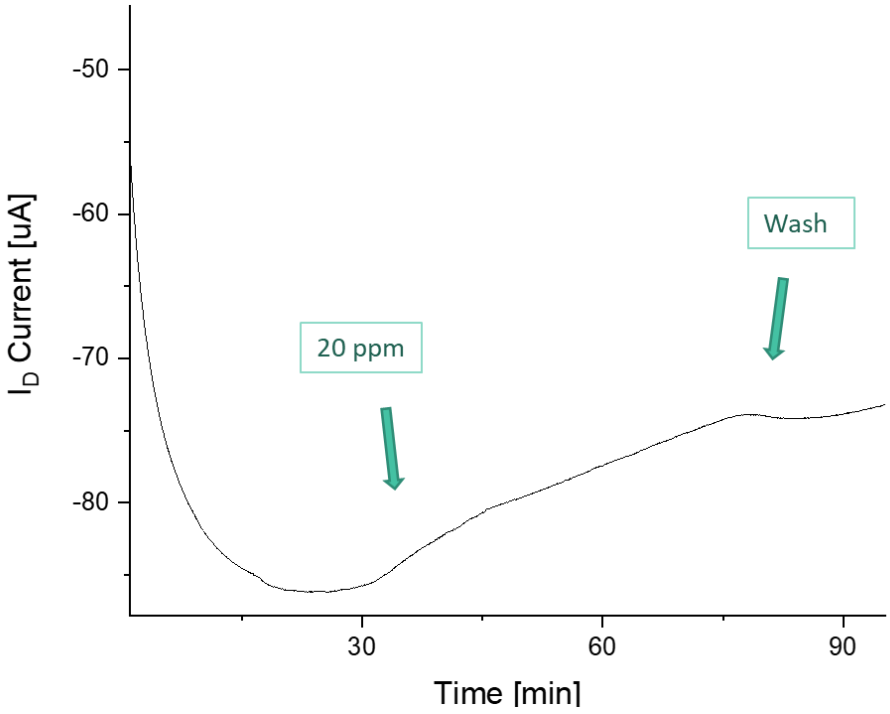

Figure 75 – Real time measurement (I_D current – time curve) of an experiment performed with P3CPT-based EGOFET, with the functionalization on the gate. Biosensing of Oxytetracycline HCl 20 ppm, diluted in sodium phosphate buffer. A weak signal has been detected during sensing.

From the curve it is evident that, even if the solubility issue may be resolved, the sensor detected a weak signal, with a slight deviation from the baseline.

4.2.2 P3HT-based EGOFET with gold gate electrode functionalized and bare polymer

In this configuration the antibiotics tested have been the Oxytetracycline hydrochloride and the Sulfadimethoxine. Sulfadimethoxine is soluble in methanol, thus the buffer employed has been PBS and a 10% of methanol. About the Oxytetracycline hydrochloride, PBS 1x has been used in order to buffer the acid pH

of the antibiotic solution. Also in this case the gold gate electrode has been functionalized with aptamers suitable for the binding with the drug molecule.

In this configuration, the response of the sensor to different concentrations of the analyte has been tested.

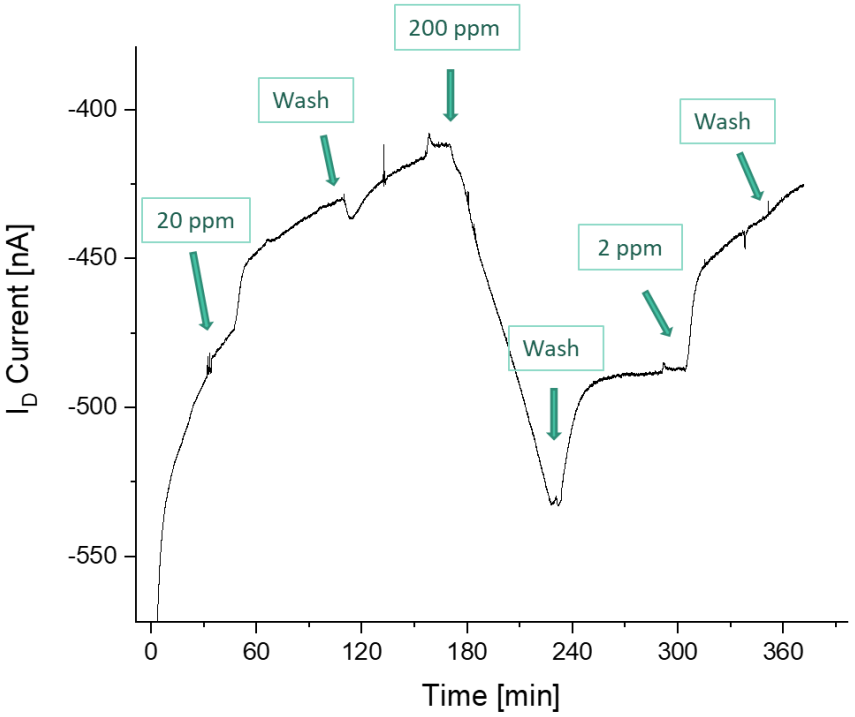

Figure 76 – Real time measurement (I_D current – time curve) of an experiment performed with P3HT-based EGOFET, with the functionalization on the gate. Biosensing of Oxytetracycline HCl (20, 200 and 2 ppm), diluted in PBS 1x.

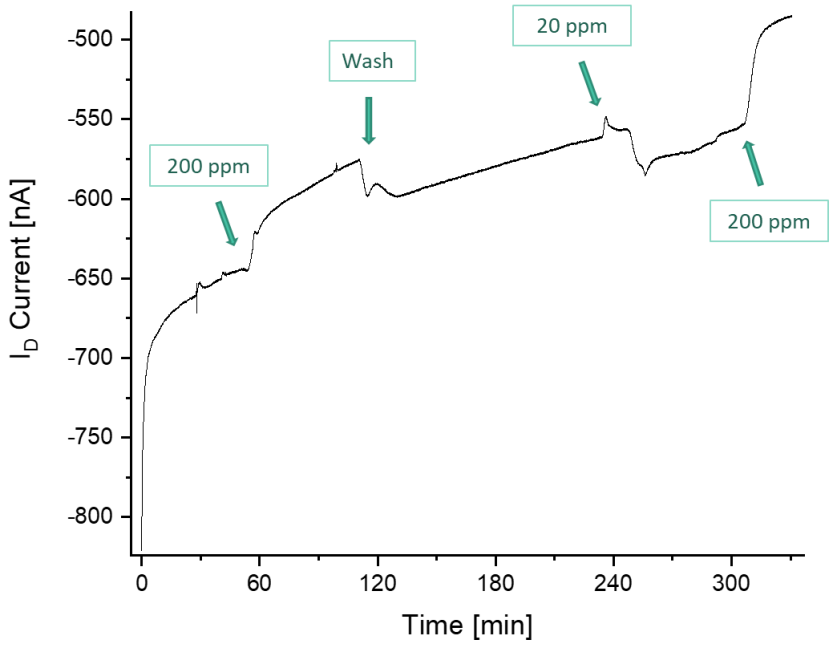

Figure 77 – Real time measurement (I_D current – time curve) of an experiment performed with P3HT-based EGOFET, with the functionalization on the gate. Biosensing of Sulfadimethoxine (200 and 20 ppm), diluted in 10% of methanol and PBS 1x.

During the experiments, the sensor always responded with a change in the baseline of the current, but not always in a coherent way. In fact, the current did not respond with a change in the trend proportional to the concentration of the target, but instead in an unpredictable way. This effect may be explained by the coexistence of antagonist phenomena, maybe linked with the pH changing, or with the presence of contaminants. Thus, further investigation is needed in order to better understand the different response to variable concentrations of target and the role of pH on the sensing.

4.2.3 Antibiotics: discussion

The P3CPT-based EGOFET with the gold functionalization with aptamers led to a not homogenous series of outcome. An interesting result is that with P3CPT and the functionalization of gold with aptamers, the baseline trend is different with respect to case of P3CPT with the functionalization with the antibodies for the protein detection. In the latter, the current during stabilization decreased in absolute value with a function that can be fitted with a double decreasing exponential. Instead, with

the gold gate functionalized with aptamers, the current increases in absolute value in the first period of the stabilization, and then apparently inverts the trend.

Further tests will be needed also in the case of P3HT-based EGOFET, a configuration that with antibiotics has not been studied methodically.

4.3 Other results

4.3.1 Transfer real time

As previously anticipated, the transfer real time measure consists of consecutive transfer characteristics (V_{DS}= − 0.5V, V_{GS}=0.1V → − 0.8V). To read the results it is convenient to display how the figures of merits (threshold voltage and transconductance) change during the repetitions, rather than plot just the several transfer characteristics. These parameters are calculated for each repeated transfer characteristics.

In the following graphs are presented the results of two distinct experiments, for each the V_{th} and g_m values are displayed both for the forth curves and for the back curves of the transfer characteristic.

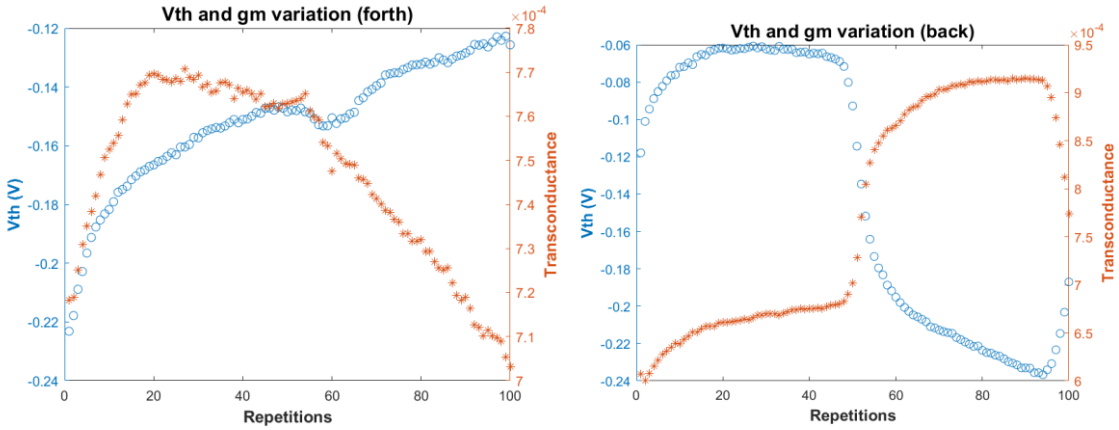

Figure 78 – Transfer real time measurement of an experiment performed with P3CPT-based EGOFET. Biosensing of 500 ng/ml of Ang2 diluted in PBS 0.01x. In blue are the values of the V_{th}, for each repetition, while in red the g_m, both for the fort curves and for the back curves of the transfer characteristics.

It is possible to see that the reaction of the sensor to the presence of the analyte manifests itself with a change in the value of these figures of merits. In the first experiment (Figure 78), the forth curves, gm seems to permanently change its trend

after the exposure to the analyte, while Vth recovers its baseline. In the back curves instead, both parameters change the trend, even if in the last repetition, during the washing, they are probably returning to the previous baseline. This latter behaviour is more noticeable in the second experiment (Figure 79).

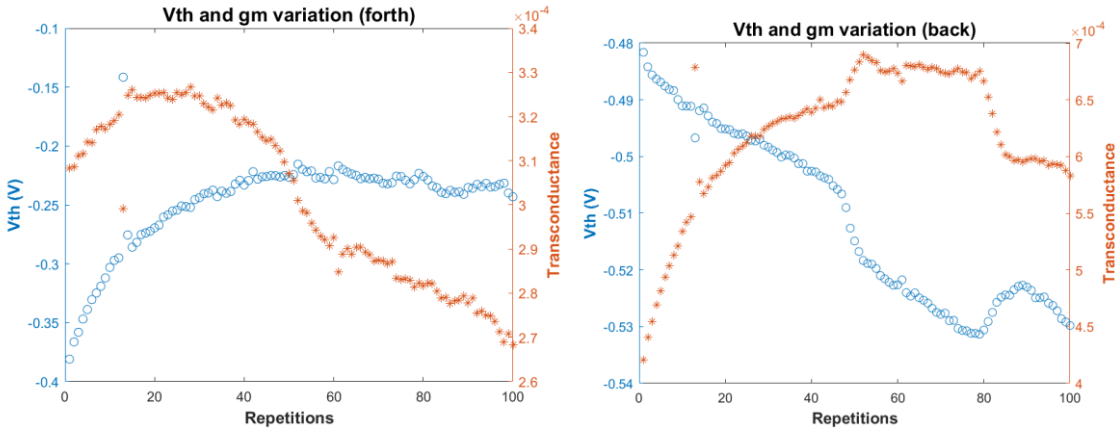

Figure 79 – Transfer real time measurement of an experiment performed with P3CPT-based EGOFET. Biosensing of 500 ng/ml of Ang2 diluted in PBS 0.01x. In blue are the values of the V_{th}, for each repetition, while in red the g_m, both for the fort curves and for the back curves of the transfer characteristics.

This type of measure needs to be repeated with a functionalized surface and for a longer period, in order to understand if it could represent a valid alternative to the real time measure with a fixed operating point, considering the advantage of being less stressful for the device.

4.3.2 Non-interdigitated S/D electrodes

In some experiments a different device architecture has been employed, characterized by the absence of an interdigitation between the source and drain electrodes. This configuration implies a change in the W/L ratio, that is about ten times lower than the interdigitated electrodes. The change in the W/L value has an effect on all the features of the EGOFET.

In this case, the tests have been executed without any functionalized surface, thus it is not relevant to reach a specific sensing. Instead, it is interesting that the current, during the stabilization period, quickly stabilizes in an almost constant value (Figure 80).

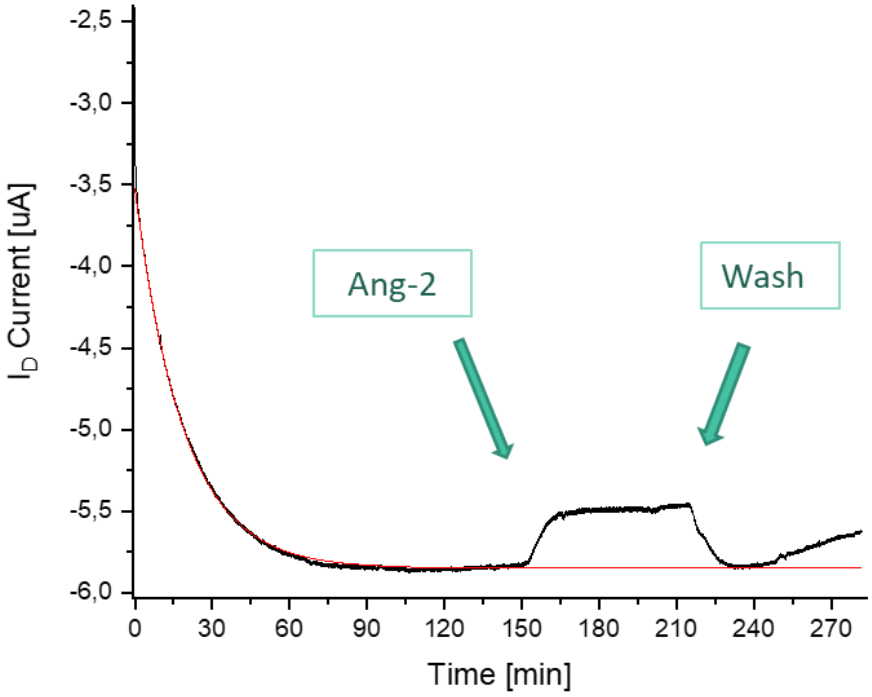

Figure 80 – Real time measurement (I_D current – time curve) of an experiment performed with P3CPT-based EGOFET. Biosensing of 500 ng/ml of Ang2 diluted in PBS 0.01x. In red the baseline fitted during the stabilization. A flat baseline and a good sensing are obtained.

That results may be linked with the fact that lower W/L ratio means lower amplification of the current signal, and thus a minor electrical stress to the polymer and a faster stabilization of the current at an almost flat baseline. Hence, this configuration deserves other tests in order to understand if it allows a lower drift in the current. That could be a clue feature to obtain a correct fitting of the baseline and a readable sensing signal.

4.3.3 Overnight measurements

As said in the previous paragraphs, one of the problems of the real time measures is the instability of the current during the stabilization period, representing an obstacle to a proper interpretation of the sensing signal. This drift makes it hard to correctly fit the trend of the current in order to compare the new baseline (achieved when the device is exposed to the target) and the predicted one (namely how the baseline should proceed without changing in the electrolyte).

To better understand the stability issue, some measures with a longer period of stabilization have been performed. This type of measures is executed similarly to the real time ones, with a fixed operation point (usually V_{DS}= -0.5 V and V_{GS}= -0.6 V), but prolonged all night long, so with around 12-16 hours of stabilization.

The outcomes of these measures can be useful in the definition of a fitting function over the long period, exploitable also in the shorter measure.

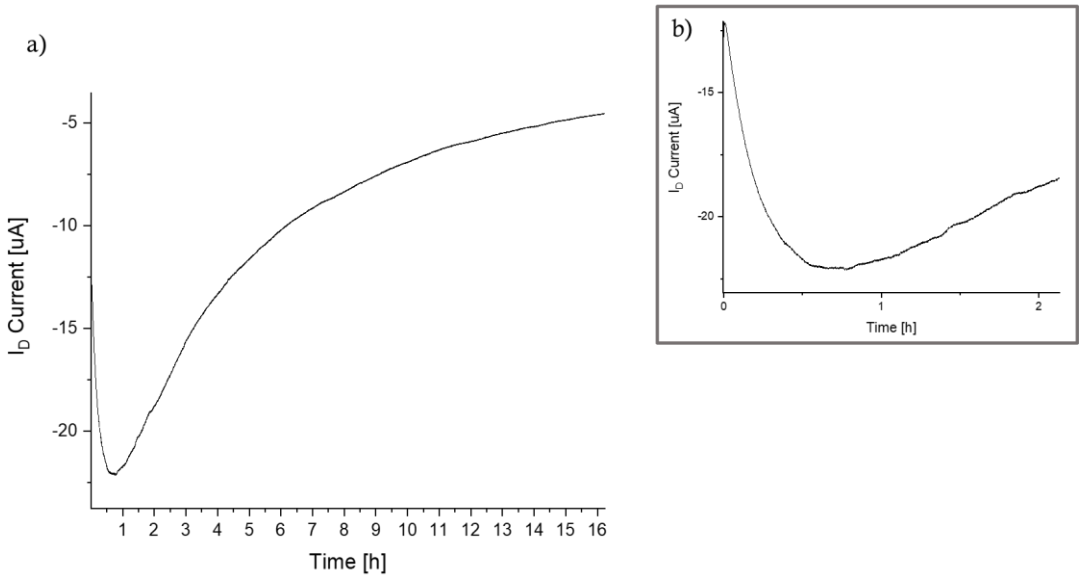

Figure 81 – Overnight real time measurement (I_D current – time curve) of a P3CPT-based EGOFET: a) the complete 16-hours measure, it is possible to see the logarithmic trend towards zero; b) a detail of the first hours: the current increases in absolute value with an exponential function.

From the outcomes, it seems that the better fitting solution is an exponential in the first 30 minutes/1 hour, followed by a logarithmic function in the next hours. That could mean that in the moment in which usually the target flows in the chamber, the baseline of the current is simultaneously changing its trend independently by the interaction of the device with the analyte.

It is important to notice that in the long period the trend of the current is toward zero, in fact the degradation of the polymer due to the stress caused by the applied bias and due to the contact with the liquid lead to the shutdown of the device. Comparing the transfer characteristic executed before and after the overnight measure, it is possible to observe a dramatic decrease in the device performance.

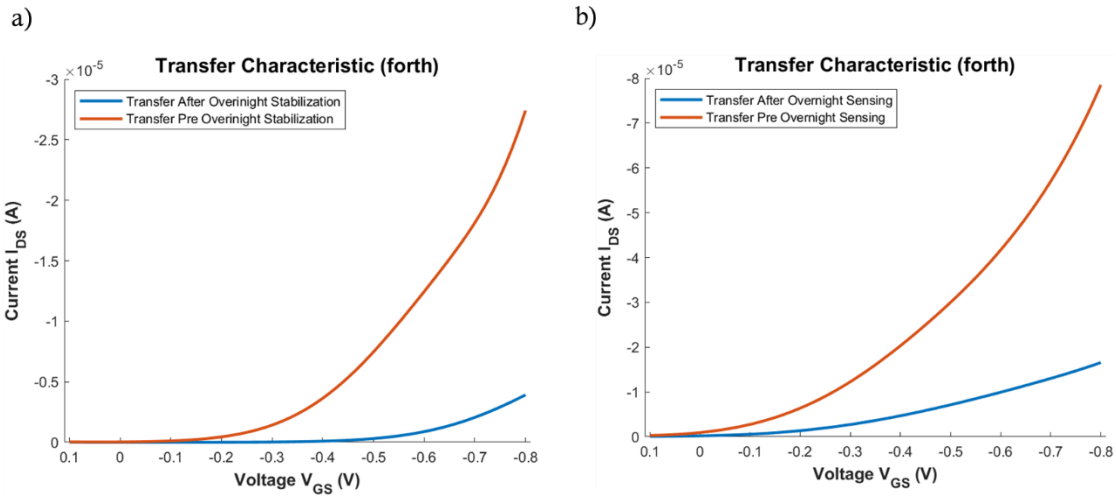

Figure 82 -Transfer characteristics of two distinct experiments (P3CPT-based EGOFET with bare polymer and passivated gold gate electrode), executed before (in red) and after (in blue) the overnight measure.

In these two tests the values of the figure of merit get worse, as it is possible to see in the following table:

a)	$\lvert I_{DS,max} \rvert$	V_{th}	Dev V_{th}	$g_{m,max}$
Pre overnight stabilization	2.7e-05	-0.36	0.026765	1.2e-05
After overnight stabilization	3.9e-06	-0.44	0.0066699	2.031e-05

b)	$\lvert I_{DS,max} \rvert$	V_{th}	Dev V_{th}	$g_{m,max}$
Pre overnight stabilization	7.8e-05	-0.149	0.019159	2.4e-04
After overnight stabilization	1.8e-05	0.090069	0.0246	3.9e-05

The overnight measure has been performed also on devices in which, during the fabrication, the polymer solution has been filtered before the spinning. This procedure has been tried with the aim of reducing the agglomerates of polymer on the surface, with the suspect they could interfere with the correct conduction and thus be a contributing factor of the strong drift of the current during the stabilization, along with affecting a uniform electrical behaviour of the different devices on the same chip.

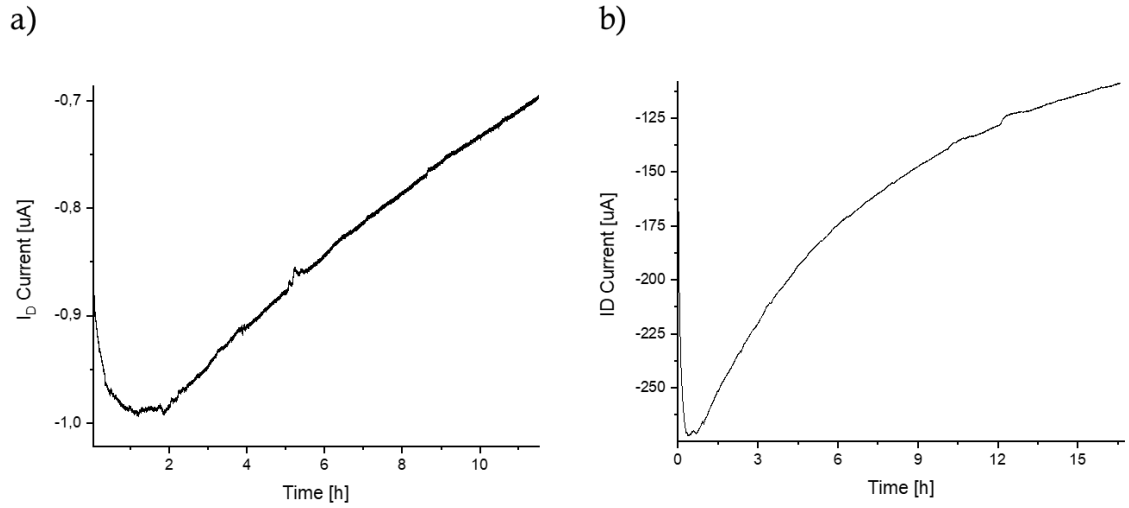

Figure 83 – Overnight real time measurement (I_D current – time curve) of a P3CPT-based EGOFET, with polymer solution filtered with filter dimension of a) 450 nm and b) 100 nm

The filtered solution deposited on the chips appears way more uniform and smoother, but in the electrical behaviour not much changed. In fact, the overnight measures showed that even with the filtered solution the current drift during the hours of stabilization was not reduced.

4.3.4 Ag/AgCl gate electrode

In some experiments the Ag/AgCl gate electrode has been used, in order to compare its performances with the gold one. The Ag/AgCl electrode is a non-polarizable electrode, thus does not take part in an exchange of charges with the electrolyte and no EDL formation occurs. The employed device was P3CPT-based, with no functionalized surface.

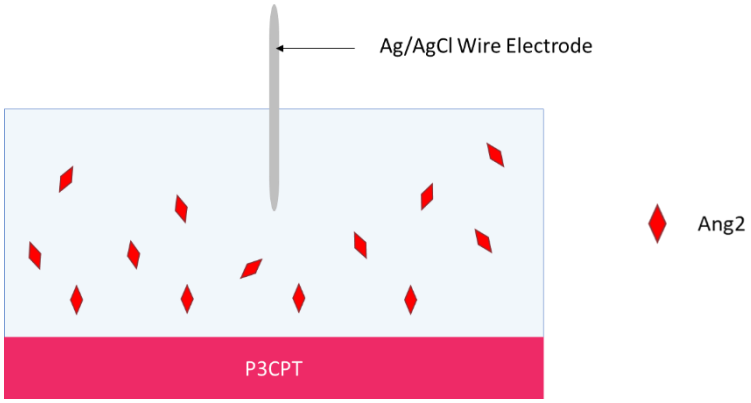

Figure 84 – Schematic picture of the P3CPT-based device with a Ag/AgCl wire electrode immersed in the electrolyte.

During the real time measures, a steep drop of the current occurs within the first hour, and also in the following hours the current proceeded towards zero, reaching few tens of nA of value. When the target solution flew in the chamber, the sensor responded with a slight signal, as is possible to see in the Figures 85 and 86 .

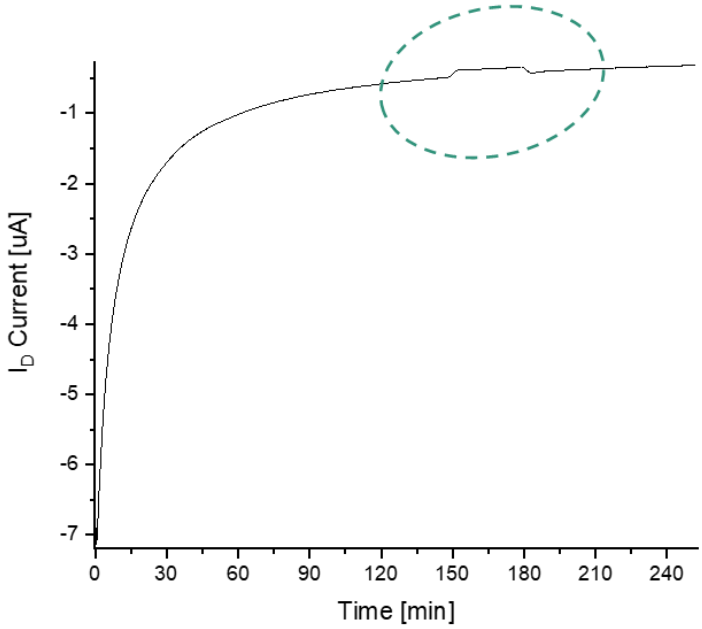

Figure 85 – Real time measurement (I_D current – time curve) of an experiment performed with P3CPT-based EGOFET and an Ag/AgCl gate electrode. The polymer solution was filtered (450 nm filter) before spinning. Biosensing of 500 ng/ml of Ang2 diluted in PBS 0.01x.

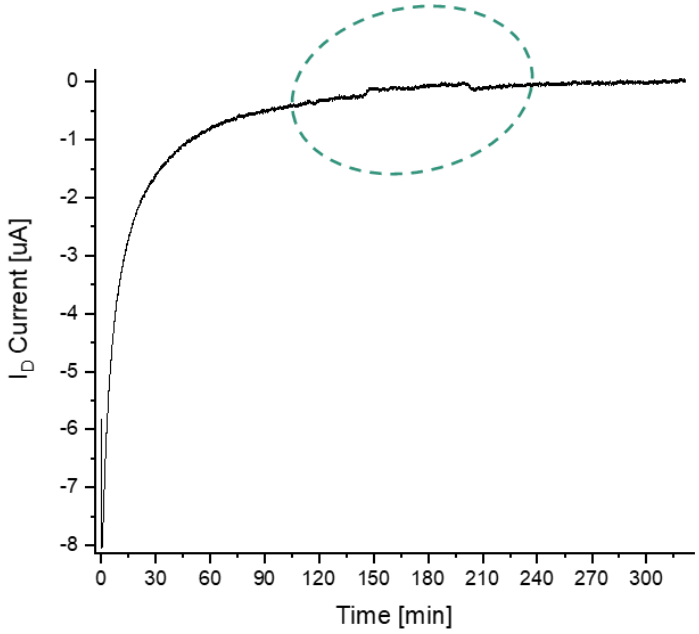

Figure 86 – Real time measurement (I_D current – time curve) of an experiment performed with P3CPT-based EGOFET and an Ag/AgCl gate electrode. The polymer solution was filtered (100 nm filter) before spinning. Biosensing of 500 ng/ml of Ang2 diluted in PBS 0.01x.

Referring to the obtained results, this configuration did not seem to be a better solution compared to the one that employs the gold gate, even if theoretically the non-polarizable electrode should be more stable. During the electrical characterization, in the transfer characteristics the devices showed way higher drain currents (from hundreds of μA to few mA), that could mean a higher electrical stress on the polymer, and thus a fast decline of the polymer performances.

Conclusions and future works

In this work an EGOFET-based sensor has been tested in several conditions in order to better understand the performances of the device. The two main target molecules detected are Angiopoietin-2 and Tetracycline. To obtain a specific biorecognition surface, the functionalization has been tested on the gold gate electrode and on the polymer surface. Furthermore, two polymers have been tested as organic semiconductors: P3HT and P3CPT.

The typology of measure investigated the most is a real time measure, in which fixed values of V_{DS} and V_{GS} are applied, and the channel current I_{DS} is recorded as the output signal. This measure allows monitoring in real time the current behaviour during all the phases of the protocol: stabilization, flux of the target solution, washing. The EGOFET is highly sensitive to the changes in the EDLs capacitance, and, considering the connection between current and capacitance in a FET, the binding between the target and the recognition element results in a current signal change.

The P3TH-based EGOFET has been tested with the functionalization on the gold gate, but resulted in non-specific sensing. This could be caused by an EDL capacitance on the gate too high to be detected, with respect to the equivalent on the polymer/electrolyte interface. In a future work this configuration may be tested with a smaller gate electrode.

The most remarkable results have been obtained with the P3CPT-based EGOFET and the functionalization on the gold gate. In fact, Angiopoietin-2 has been specifically detected, and also intriguing results have been obtained with antibiotics. This configuration is assumed to allow a specific sensing due to the higher capacitance of the P3CPT compared to P3HT, as reported in literature. Moreover, the employment of P3CPT permitted a direct functionalization of the polymer,

thanks to the exposed carboxyl group. On the other hand, the presence of this end group makes the polymer more hydrophilic and more prone to the electrochemical doping, which causes the degradation of the polymer in contact with the liquid electrolyte. Both configurations require further investigations to understand if employing P3CPT is worth it, or if the instability of the polymer is a too constrictive drawback.

The main concern of the real time measure is the presence of an unpredictable current drift during all the tests. This strongly affects the interpretation of the results, due the difficulty of fitting the current trend and thus of reading small differences between the current and the baseline, predicted during the stabilization. The drift is conceivably caused by the electrical stress imposed to the device for a long period of time in real time measurements. Future works must compare the pros and cons of this protocol with those of less stressful measures, as the transfer characteristic real time measure. An interesting outcome is that the drift has been discovered to depend on the type of the functionalization accomplished. This feature should be considered for the future experiments, in order to identify a correct function to fit the current trend.

A further future work that could improve the prospect of the sensor, is to accomplish an optimization of the fabrication processes, to identify a production protocol suitable for improving the device performances and obtaining repeatability in the performance of the devices.

References

[1] *IUPAC. Compendium of Chemical Terminology, 2nd ed*. (the "Gold Book"). Compiled by A. D. McNaught and A. Wilkinson. Blackwell Scientific Publications, Oxford (1997). Online version (2019-) created by S. J. Chalk. ISBN 0-9678550-9-8. https://doi.org/10.1351/goldbook.

[2] Daniel Thevenot, Klara Toth, Richard Durst, George Wilson. Electrochemical biosensors: recommended definitions and classification. *Biosensors and Bioelectronics*, Elsevier, 2001, 16, pp.121 - 131. ff10.1081/AL-100103209ff. ffhal-01084678f

[3] Serna Cock L, Zetty Arenas AM, Ayala Aponte A. Use of enzymatic biosensors as quality indices: A synopsis of present and future trends in the food industry. *Chil J Agric Res* 2009;69:270–280.

[4] Piro, B., & Reisberg, S. (2017). Recent Advances in Electrochemical Immunosensors. *Sensors (Basel, Switzerland)*, *17*(4), 794. https://doi.org/10.3390/s17040794

[5] Strehlitz B, Nikolaus N, Stoltenburg R. Protein Detection with Aptamer Biosensors. *Sensors (Basel).* 2008 Jul 23;8(7):4296-4307. doi: 10.3390/s8074296. PMID: 27879936; PMCID: PMC3697175.

[6] Vo-Dinh, T., Cullum, B. Biosensors and biochips: advances in biological and medical diagnostics. *Fresenius J Anal Chem* **366,** 540–551 (2000). https://doi.org/10.1007/s002160051549

[7] Monošík, R., Streďanský, M., & Šturdík, E. (2012). Biosensors - classification, characterization and new trends. *Acta Chimica Slovaca*, 5(1), 109–120. https://doi.org/10.2478/v10188-012-0017-z

[8] Rodriguez-Mozaz, S., Marco, M.-P., de Alda, M. J. Lopez and Barceló, D. "Biosensors for environmental applications: Future development trends" *Pure and Applied Chemistry*, vol. 76, no. 4, 2004, pp. 723-752. https://doi.org/10.1351/pac200476040723

[9] R. Monošík, P. Magdolen, M. Streďanský, E. Šturdík, Monitoring of monosaccharides, oligosaccharides, ethanol and glycerol during wort fermentation by biosensors, HPLC and spectrophotometry, *Food Chemistry*, Volume 138, Issue 1, 2013, Pages 220-226, ISSN 0308-8146, https://doi.org/10.1016/j.foodchem.2012.10.039.

[10] Bhalla, N., Jolly, P., Formisano, N., & Estrela, P. (2016). Introduction to biosensors. *Essays in biochemistry*, *60*(1), 1–8. https://doi.org/10.1042/EBC20150001

[11] Kost, Gerald J., *1.* Goals, guidelines and principles for point-of-care testing, in Principles & practice of point-of-care testing, Hagerstwon, MD, Lippincott Williams & Wilkins, 2002, pp. 3–12, ISBN 0-7817-3156-9.

[12] Liu, N., Chen, R., & Wan, Q. (2019). Recent advances in electric double-layer transistors for bio-chemical sensing applications. *Sensors* (Switzerland), *19*(15). https://doi.org/10.3390/s19153425

[13] Sedra, A. S.,. Smith, K. C. Microelectronic Circuits, 2011, 6° ed. Oxford University Press, Inc.

[14] Kergoat, L., Piro, B., Berggren, M., Horowitz, G., & Pham, M. C. (2012). Advances in organic transistor-based biosensors: From organic electrochemical transistors to electrolyte-gated organic field-effect transistors. *Analytical and Bioanalytical Chemistry*, 402(5), 1813–1826. https://doi.org/10.1007/s00216-011-5363-y

[15] Sokolov, A. N., Roberts, M. E., & Bao, Z. (2009). Fabrication of low-cost electronic biosensors. *Materials Today*, 12(9), 12–20. https://doi.org/10.1016/S1369-7021(09)70247-0

[16] Wang, D., Noël, V., & Piro, B. (2016). Electrolytic gated organic field-effect transistors for application in biosensors—A review. *Electronics*, 5(1). https://doi.org/10.3390/electronics5010009

[17] Tang, W., Huang, Y., Han, L., Liu, R., Su, Y., Guo, X., & Yan, F. (2019). Recent progress in printable organic field effect transistors. *Journal of Materials Chemistry* C, 7(4), 790–808. https://doi.org/10.1039/c8tc05485a

[18] Kergoat L, Herlogsson L, Braga D, Piro B, Pham MC, Crispin X, Berggren M, Horowitz G (2010) A water-gate organic field-effect transistor. *Adv Mater* 22(23):2565–2569

[19] Mulla, M.Y.; Tuccori, E.; Magliulo, M.; Lattanzi, G.; Palazzo, G.; Persaud, K.; Torsi, L. Capacitance-modulated transistor detects odorant binding protein chiral interactions. *Nat. Commun*. 2015, 6.

[20] Magliulo, M., Pistillo, B. R., Mulla, M. Y., Cotrone, S., Ditaranto, N., Cioffi, N., Favia, P., & Torsi, L. (2013). PE-CVD of hydrophilic-COOH functionalized coatings on electrolyte gated field-effect transistor electronic layers. *Plasma Processes and Polymers*, *10*(2), 102–109. https://doi.org/10.1002/ppap.201200080

[21] J.J. Liou, A. Ortiz-Conde, F.J. García Sánchez Analysis and design of MOSFETs: modeling, simulation and parameter extraction, Kluwer Academic Publishers, New York, USA (1998)

[22] Zaumseil, J., & Sirringhaus, H. (2007). Electron and ambipolar transport in organic field-effect transistors. *Chemical Reviews*, *107*(4), 1296–1323. https://doi.org/10.1021/cr0501543

[23] Torsi, L., Magliulo, M., Manoli, K., & Palazzo, G. (2013). Organic field-effect transistor sensors: A tutorial review. *Chemical Society Reviews*, 42(22), 8612–8628. https://doi.org/10.1039/c3cs60127g

[24] Kim, Y.-B. (2010). Challenges for Nanoscale MOSFETs and Emerging Nanoelectronics. *Transactions on Electrical and Electronic Materials*, 11(3), 93–105. https://doi.org/10.4313/teem.2010.11.3.093

[25] Università Degli Studi Di Modena E Reggio Emilia, PhD Program in Molecular and Regenerative Medicine XXXI cycle, Vitaliy Parkula - *Organic Electronic Transistors For Biosensing*

[26] Du, H., Lin, X., Xu, Z., & Chu, D. (2015*).* Electric double-layer transistors: a review of recent progress. *In Journal of Materials Science* (Vol. 50, Issue 17). Springer US. https://doi.org/10.1007/s10853-015-9121-y

[27] "The electrical double layer". 2011. Archived from the original on 31 May 2011.

[28] Adam Marcus Namisnyk. "A survey of electrochemical supercapacitor technology" (PDF). Archived from the original on 2014-12-22.

[29] Zhang, L., & Zhao, X. S. (2009). Carbon-based materials as supercapacitor electrodes. *Chemical Society Review*s, *38*(9), 2520–2531. https://doi.org/10.1039/b813846j

[30] Kim, S. H., Hong, K., Xie, W., Lee, K. H., Zhang, S., Lodge, T. P., & Frisbie, C. D. (2013). Electrolyte-gated transistors for organic and printed electronics. *Advanced Materials*, *25*(13), 1822–1846. https://doi.org/10.1002/adma.201202790

[31] Min, Y., Akbulut, M., Sangoro, J. R., Kremer, F., Prud'homme, R. K., & Israelachvili, J. (2009). Measurement of forces across room temperature ionic liquids between mica surfaces. *Journal of Physical Chemistry C*, 113(37), 16445–16449. https://doi.org/10.1021/jp904629b

[32] Lin, S. P., Pan, C. Y., Tseng, K. C., Lin, M. C., Chen, C. D., Tsai, C. C., Yu, S. H., Sun, Y. C., Lin, T. W., & Chen, Y. T. (2009). A reversible surface functionalized nanowire transistor to study protein-protein interactions. *Nano Today*, 4(3), 235–243. https://doi.org/10.1016/j.nantod.2009.04.005

[33] Chen, K. I., Li, B. R., & Chen, Y. T. (2011). Silicon nanowire field-effect transistor-based biosensors for biomedical diagnosis and cellular recording investigation. *Nano Today*, *6*(2), 131–154. https://doi.org/10.1016/j.nantod.2011.02.001

[34] Palazzo, G., De Tullio, D., Magliulo, M., Mallardi, A., Intranuovo, F., Mulla, M. Y., Favia, P., Vikholm-Lundin, I., & Torsi, L. (2015). Detection beyond Debye's length with an electrolyte-gated organic field-effect transistor. *Advanced Materials*, *27*(5), 911–916. https://doi.org/10.1002/adma.201403541

[35] Gelinck GH, Huitema HE, van Veenendaal E, Cantatore E, Schrijnemakers L, van der Putten JB, Geuns TC, Beenhakkers M, Giesbers JB, Huisman BH, Meijer EJ, Benito EM, Touwslager FJ, Marsman AW, van Rens BJ, de Leeuw DM. Flexible active-matrix displays and shift registers based on solution-processed organic transistors. *Nat Mater.* 2004 Feb;3(2):106-10. doi: 10.1038/nmat1061. Epub 2004 Jan 25. PMID: 14743215.

[36] Kaake LG. Towards the Organic Double Heterojunction Solar Cell. *Chem Rec.* 2019 Jun;19(6):1131-1141. doi: 10.1002/tcr.201800180. Epub 2019 Apr 4. PMID: 30946526.

[37] Liao, C., & Yan, F. (2013*).* Organic semiconductors in organic thin-film transistor-based chemical and biological sensors. *Polymer Reviews*, 53(3), 352–406. https://doi.org/10.1080/15583724.2013.808665

[38] Shirakawa, H.; Louis, E. J.; MacDiarmid, A. G.; Chiang, C. K.; Heeger, A. J. Synthesis of Electrically Conducting Organic Polymers: Halogen Derivatives of Polyacetylene, (CH)x. J. Chem. Soc. Chem. Commun. 1977, 578–580.

[39] Köhler A., Bässler H*.,* Electronic Processes in Organic Semiconductors - An Introduction. 2015 Wiley-VCH Verlag GmbH & Co. KGaA, Boschstr. 12, 69469 Weinheim, Germany

[40] Laiho, A., Herlogsson, L., Forchheimer, R., Crispin, X., & Berggren, M. (2011*).* Controlling the dimensionality of charge transport in organic thin-film transistors. Proceedings of the National Academy of Sciences of the United States of America, *108*(37), 15069–15073. https://doi.org/10.1073/pnas.1107063108

[41] *OpenStax, Chemistry*. OpenStax CNX. Jun 20, 2016 http://cnx.org/contents/85abf193-2bd2-4908-8563-90b8

[42] Chen, F. C. (2018). *Organic semiconductors*. *Encyclopedia of Modern Optics*, *1–5*, 220–231. https://doi.org/10.1016/B978-0-12-803581-8.09538-2

[43] Reynolds, J.R., Thompson, B.C., & Skotheim, T.A. (2019). *Conjugated Polymers: Properties, Processing, and Applications* (4th ed.). CRC Press. https://doi.org/10.1201/9780429190520

[44] Sirringhaus, H., Brown, P. J., Friend, R. H., Nielsen, M. M., Bechgaard, K., Langeveld-Voss, B. M. W., … de Leeuw, D. M. (1999). Two-dimensional charge transport in self-organized, high-mobility conjugated polymers. *Nature*, 401(6754), 685–688. doi:10.1038/44359

[45] Duarte, A., Pu, K. Y., Liu, B., & Bazan, G. C. (2011). Recent advances in conjugated polyelectrolytes for emerging optoelectronic applications. *Chemistry of Materials,* 23(3), 501–515. https://doi.org/10.1021/cm102196t

[46] Zeglio, E., & Inganäs, O. (2018). Active Materials for Organic Electrochemical Transistors. 1800941, 1–18. https://doi.org/10.1002/adma.201800941

[47] Akwii, R. G., Sajib, M. S., Zahra, F. T., & Mikelis, C. M. (2019*).* Role of Angiopoietin-2 in Vascular Physiology and Pathophysiology. *Cells*, 8(5), 471. https://doi.org/10.3390/cells8050471

[48] Thurston, G., & Daly, C. (2012). The complex role of angiopoietin-2 in the angiopoietin-Tie signaling pathway. Cold Spring Harbor Perspectives in Medicine, 2(9), 1–14. https://doi.org/10.1101/cshperspect.a006650

[49] Fiedler U, Reiss Y, Scharpfenecker M, Grunow V, Koidl S, Thurston G, Gale NW, Witzenrath M, Rosseau S, Suttorp N, et al. 2006. Angiopoietin-2 sensitizes endothelial cells to TNF-a and has a crucial role in the induction of inflammation. *Nat Med* 12: 235–239

[50] Mandriota SJ, Pepper MS. 1998. Regulation of angiopoietin2 mRNA levels in bovine microvascular endothelial cells by cytokines and hypoxia. *Circ Res* 83: 852–859

[51] Hu, B.; Cheng, S.Y. Angiopoietin-2: Development of inhibitors for cancer therapy. *Curr. Oncol. Rep*. 2009, 11, 111–116.

[52] Chopra I, Roberts M (June 2001). "Tetracycline antibiotics: mode of action, applications, molecular biology, and epidemiology of bacterial resistance*". Microbiology and Molecular Biology Reviews*. 65 (2): 232–60, second page, table of contents. doi:10.1128/MMBR.65.2.232-260.2001. PMC 99026. PMID 11381101.

[53] Britannica, The Editors of Encyclopaedia. "Tetracycline". *Encyclopedia Britannica*, Invalid Date, https://www.britannica.com/science/tetracycline. Accessed 23 February 2021.

[54] National Center for Biotechnology Information (2021). PubChem Compound Summary for CID 5323, Sulfadimethoxine. Retrieved February 24, 2021 from https://pubchem.ncbi.nlm.nih.gov/compound/Sulfadimethoxine.

[55] https://engineeringtutorial.com/power-mosfet/

[56] https://www.electronics-tutorials.ws/amplifier/mosfet-amplifier.html

[57] MERCAT Cleanrooms. Cleanroom classification https://www.mecart-cleanrooms.com/learning-center/cleanroom-classifications-iso-8-iso-7-iso-6-iso-5/

[58] Parmeggiani, M. (2021). Liquid gated organic devices for sensing applications : from transistors to single molecule break junctions. *PhD Thesis.*

[59] Demelas, M., Lai, S., Spanu, A., Martinoia, S., Cosseddu, P., Barbaro, M., & Bonfiglio, A. (2013). Charge sensing by organic charge-modulated field effect transistors: Application to the detection of bio-related effects. *Journal of Materials Chemistry* B, 1(31), 3811–3819. https://doi.org/10.1039/c3tb20237b

[60] Myers, J. D., & Xue, J. (2012). Organic semiconductors and their applications in photovoltaic devices. *Polymer Reviews*, 52(1), 1–37. https://doi.org/10.1080/15583724.2011.644368

[61] Sinno, H., Nguyen, H. T., Hägerström, A., Fahlman, M., Lindell, L., Coulembier, O., Dubois, P., Crispin, X., Engquist, I., & Berggren, M. (2013). Amphiphilic semiconducting copolymer as compatibility layer for printing polyelectrolyte-gated OFETs. *Organic Electronics*, 14(3), 790–796. https://doi.org/10.1016/j.orgel.2012.12.031

[62] Thiemann, S., Sachnov, S. J., Gruber, M., Gannott, F., Spallek, S., Schweiger, M., Krückel, J., Kaschta, J., Spiecker, E., Wasserscheid, P., & Zaumseil, J. (2014). Spray-coatable ionogels based on silane-ionic liquids for low voltage, flexible, electrolyte-gated organic transistors. *Journal of Materials Chemistry* C, 2(13), 2423–2430. https://doi.org/10.1039/c3tc32465f

[63] Das, R., & Chanda, A. (2016). Fabrication and Properties of Spin-Coated Polymer Films. *Nano-Size Polymers, 283–306.* doi:10.1007/978-3-319-39715-3_10

[64] Sallucci, L. (2019) Process optimization and experimental measurements of organic electrochemical transistors for in liquid biosensing. Politecnico Di Torino*, Master ' s Degree in Biomedical Engineering*

[65] https://www.debem.com/it/funzionamento-pompa-peristaltica/

[66] Marianne Frieri, Krishan Kumar, and Anthony Boutin. "Antibiotic resistance." In: *J. Infect. Public Health* 10.4 (July 2017), pp. 369–378. issn: 18760341. doi: 10. 1016/j.jiph.2016.08.007. url: https://linkinghub.elsevier. com/retrieve/pii/S1876034116301277.

[67] Ulman, A. (1996). Formation and Structure of Self-Assembled Monolayers.

[68] Love, J. C., Estroff, L. A., Kriebel, J. K., Nuzzo, R. G., & Whitesides, G. M. (2005). Self-assembled monolayers of thiolates on metals as a form of nanotechnolog*y*. In *Chemical Reviews* (Vol. 105, Issue 4). https://doi.org/10.1021/cr0300789

[69] Bain, C. D., Troughton, E. B., Tao, Y. T., Evall, J., Whitesides, G. M., & Nuzzo, R. G. (1989). Formation of Monolayer Films by the Spontaneous Assembly of Organic Thiols from Solution onto Gold. *Journal of the American Chemical Society*, 111(1), 321–335. https://doi.org/10.1021/ja00183a049

[70] ThermoFisher Scientific - Easy molecular bonding: crosslinking technology. Reactivity chemistries, applications, and structure references

[71] Meng, H. M., Liu, H., Kuai, H., Peng, R., Mo, L., & Zhang, X. B. (2016). Aptamer-integrated DNA nanostructures for biosensing, bioimaging and cancer therapy. *Chemical Society Reviews*, 45(9), 2583–2602. https://doi.org/10.1039/c5cs00645g

[72] Kwon, Y. S., Ahmad Raston, N. H., & Gu, M. B. (2014). An ultra-sensitive colorimetric detection of tetracyclines using the shortest aptamer with highly enhanced affinity. *Chemical Communications*, 50(1), 40–42. https://doi.org/10.1039/c3cc47108j

[73] Chiadò, A., Palmara, G., Ricciardi, S., Frascella, F., Castellino, M., Tortello, M., Ricciardi, C., & Rivolo, P. (2016). Optimization and characterization of a homogeneous carboxylic surface functionalization for silicon-based biosensing. *Colloids and Surfaces B:Biointerfaces*,143,252–259. https://doi.org/10.1016/j.colsurfb.2016.03.048

[74] Parmeggiani, M., Verna, A., Ballesio, A., Cocuzza, M., Piatti, E., Fra, V., Pirri, C. F., & Marasso, S. L. (2019). P3HT processing study for in-liquid EGOFET biosensors: Effects of the solvent and the surface. *Sensors (Switzerland),* 19(20), 1–12. https://doi.org/10.3390/s19204497

[75] Toss, H., Suspène, C., Piro, B., Yassar, A., Crispin, X., Kergoat, L., Pham, M. C., & Berggren, M. (2014). On the mode of operation in electrolyte-gated thin film transistors based on different substituted polythiophenes. *Organic Electronics*, 15(10), 2420–2427. https://doi.org/10.1016/j.orgel.2014.06.017

A Tommi e a Nonna Liliana

Ringrazio i miei genitori, perché a loro devo tutto.
Ringrazio i miei fratelli, che sono per me sostegno perenne. E Jane, ovviamente, per aspettarmi ogni volta con pazienza.

Ringrazio la mia stupenda, enorme, pazza famiglia, ormai piena di marmocchi adorabili, per essere un'inesauribile fonte di energia.

Ringrazio le mie amiche, per essere sempre al mio fianco, da sempre.

Ringrazio Marco, per essere stato il miglior compagno che potessi desiderare per questi assurdi e meravigliosi anni.